DOT/FAA/AR-97/88

Office of Aviation Research
Washington, D.C. 20591

Crack Growth-Based Predictive Methodology for the Maintenance of the Structural Integrity of Repaired and Nonrepaired Aging Engine Stationary Components

April 1999

Final Report

This document is available to the U.S. public through the National Technical Information Service (NTIS), Springfield, Virginia 22161.

U.S. Department of Transportation
Federal Aviation Administration

NOTICE

This document is disseminated under the sponsorship of the U.S. Department of Transportation in the interest of information exchange. The United States Government assumes no liability for the contents or use thereof. The United States Government does not endorse products or manufacturers. Trade or manufacturer's names appear herein solely because they are considered essential to the objective of this report. This document does not constitute FAA certification policy. Consult your local FAA aircraft certification office as to its use.

This report is available at the Federal Aviation Administration William J. Hughes Technical Center's Full-Text Technical Reports page: www.tc.faa.gov/its/act141/reportpage.html in Adobe Acrobat portable document format (PDF).

Technical Report Documentation Page

1. Report No.	2. Government Accession No.	3. Recipient's Catalog No.
DOT/FAA/AR-97/88		

4. Title and Subtitle	5. Report Date
CRACK GROWTH-BASED PREDICTIVE METHODOLOGY FOR THE MAINTENANCE OF THE STRUCTURAL INTEGRITY OF REPAIRED AND NONREPAIRED AGING ENGINE STATIONARY COMPONENTS	April 1999
	6. Performing Organization Code

7. Author(s)	8. Performing Organization Report No.
Michael L. Barron	

9. Performing Organization Name and Address	10. Work Unit No. (TRAIS)
GE Aircraft Engines One Neumann Way Cincinnati, Ohio 45215	11. Contract or Grant No. DTFA03-94-C-00066

12. Sponsoring Agency Name and Address	13. Type of Report and Period Covered
U.S. Department of Transportation Federal Aviation Administration Office of Aviation Research Washington, DC 20591	Final Report
	14. Sponsoring Agency Code ANE-110

15. Supplementary Notes

Significant contribution was made by the Edison Welding Institute and Ohio State University under subcontract to GE Aircraft Engines. The FAA William J. Hughes Technical Center COTR is Mr. Richard Micklos.

16. Abstract

This report contains the description and results of work conducted by General Electric Aircraft Engines (GEAE) between October 1994 and April 1997 under the Federal Aviation Administration (FAA) contract to study aging engine issues relative to stationary components. Specifically, the FAA's goal was to develop "Crack Growth-Based Predictive Methodologies for the Maintenance of the Structural Integrity of Repaired and Nonrepaired Aging Engine Stationary Components." GEAE's project in support of this goal was to study specific components, combustion casings, and compressor rear frames in service on older GEAE engines to determine if periodic inspections are warranted and to develop the tools necessary to conduct effective inspections should the data support a proactive need.

The project was originally scheduled to cover a 5-year period but was prematurely curtailed due to funding priorities. A detail description of the planned work scope along with results for that portion of the work that was completed are reported herein.

17. Key Words		18. Distribution Statement
Aging Engine	Periodic Inspection	This document is available to the public through the National Technical Information Service (NTIS) Springfield, Virginia 22161.
Structural Integrity	Material Properties	
Crack Growth	Combustion Casings	
Weldability	Repair	

19. Security Classif. (of this report)	20. Security Classif. (of this page)	21. No. of Pages	22. Price
Unclassified	Unclassified	105	

TABLE OF CONTENTS

LIST OF FIGURES

LIST OF TABLES

LIST OF ABBREVIATIONS AND TERMS

Compressor Rear Frame (CRF)—A jet engine part.

Cooling Time (CT)—In the varestraint test, the cooling time is the minimum time between when the arc is extinguished and when the sample is bent that results in no liquation cracking. Higher values of CT represent a material's lower resistance to liquation cracking.

Crack-Susceptible Region (CSR)—In the varestraint test, the crack-susceptible region is the measurement of the farthest distance that liquation cracks extend into the heat-affected zone from the edge of weld pool. Large CSR values represent a material's lower resistance to liquation cracking.

Ductility Recovery Temperature (DRT)—After the test sample is heated to peak temperature during hot-ductility testing, the ductility recovery temperature is the temperature on cooling at which the sample begins to exhibit ductility when it is fractured.

Fatigue Crack Growth (FCG)—Progressive growth of a crack due to fatigue loading as opposed to a monotonic tensile load.

Heat-Affected Zone (HAZ)—The base material adjacent to the weld that has been structurally altered during the welding.

Hot Isostatic Pressed (HIP)—A thermal and pressure treatment commonly used to close internal pores or voids in castings for improved material integrity.

Hot-Ductility Testing—Weldability test in which material samples are fractured at various temperatures along the heating and cooling portions of a weld thermal cycle: The ductility of the sample is measured by its reduction in area.

Inconel 718—(IN718)

K_b Specimen—A rectangular cross section test specimen used for crack growth testing which best represents geometry and stress levels in aircraft engine components.

Nil Ductility Temperature (NDT)—During heating in the hot-ductility test, the nil ductility temperature is the temperature at which the test sample exhibits zero ductility when it is fractured.

Nil Strength Temperature (NST)—During heating in the hot-ductility test, the nil strength temperature is the temperature at which the test sample exhibits zero strength. This temperature is generally higher then the nil ductility temperature.

Peak Temperature (T_p)—In hot-ductility testing, the test sample is first heated to a peak temperature and then allowed to cool in order to perform on-cooling tests.

Varestraint Testing—Weldability test in which a weld is made on a test sample and then bent to produce cracks from the weld pool into the heat-affected zone.

EXECUTIVE SUMMARY

Combustion casings and compressor rear frames (having integral combustion casings) are considered the most critical stationary components on General Electric Aircraft Engines (GEAE) engines. Concern over the possible aging effects due to loss in material properties with time as a result of multiple repair cycles and long service exposure led to some preliminary work at GEAE in 1991 and early 1992. Recommendations from the team that conducted this preliminary work formed the basis for a follow-on project in support of the Federal Aviation Administration's (FAA's) goal to develop "crack growth-based predictive methodologies for the maintenance of the structural integrity of repaired and nonrepaired aging engine stationary components."

It is important to point out that effective field control programs are in place for these critical components. Experience has shown that once a specific problem area is identified it can be effectively managed in the field. The objective of this project was to determine on a proactive basis if periodic inspections would be beneficial in avoiding future failure modes due to currently unknown aging effects. Additionally, if weldability degradation was occurring due to multiple repairs and thermal exposures, could a rejuvenation heat treatment be defined which would restore weldability and, consequently, improve the general quality level and consistency of repaired parts going back into service?

Although the project was terminated early, sufficient material property data was generated to conclude that only moderate degradation in fatigue and crack growth rate properties occur with time and with multiple-repair heat treatment exposures. This result suggests no reason why the components studied should not remain safe while being maintained to the approved service manual limits, repairs, and GEAE recommended field management programs. Retirement of these components, therefore, becomes an economic issue. Unfortunately we were unable to identify an effective rejuvenation heat treatment cycle to improve weldability within known temperature restraints.

1. INTRODUCTION.

General Electric Aircraft Engines (GEAE) undertook a 5-year project in support of the Federal Aviation Administration's (FAA's) goal to develop "crack growth-based predictive methodologies for the maintenance of the structural integrity of repaired and nonrepaired aging engine stationary components." The effort began in October 1994 and was concluded prematurely in April 1997 due to funding priority issues. The original workscope included completion of five major tasks as shown below and was focused on GEAE mature engine model combustion casings and compressor rear frames (CRF). Figures 1 and 2 are views showing these typical components.

Task I: Crack Growth Predictions and Verification
Task II: Material Property Testing
Task III: Weldability Improvements
Task IV: Field Inspection Data and Periodic Inspection Determination
Task V: Periodic Inspection Plan

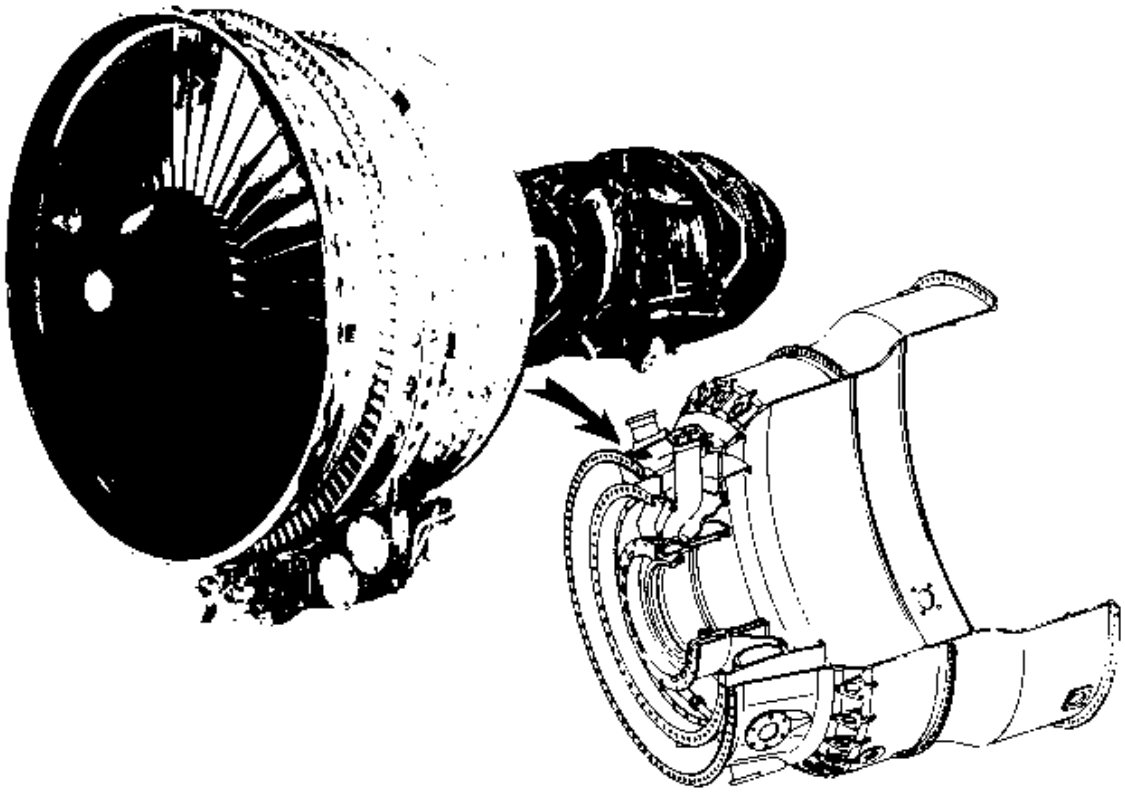

FIGURE 1. CF6-50 HIGH-BYPASS TURBOFAN

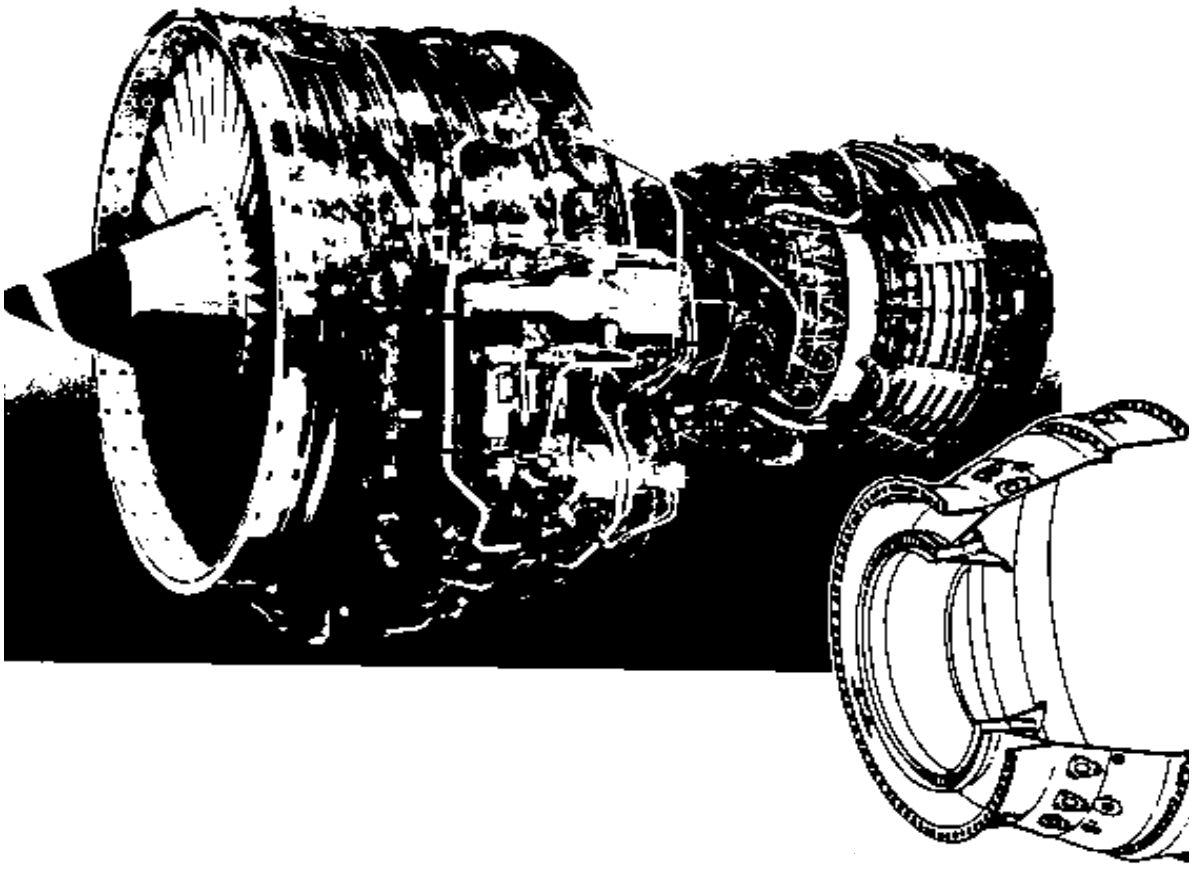

FIGURE 2. CFM56-3 HIGH-BYPASS TURBOFAN

One of the primary objectives of the project was to define a periodic inspection plan for the specific components being studied should such an inspection be deemed necessary based on the data results. It was expected that the general approach and methodology developed could be applied to other static components along with the generic portion of the data generated. Although the project was terminated prematurely, Task II: Material Property Testing and Task III: Weldability Improvements, were completed along with portions of Task I, Crack Growth Predictions and Verifications. Useful data are presented in this report along with conclusions and recommendations to the extent possible.

As background information, there has been no requirement to track operating time or flight cycles on the mature engine stationary components. Some airlines attempt to keep flight-hour and cycle records on certain static components, but experience has shown that, even when these data are available, accuracy can be poor. This makes it nearly impossible to determine how much life has been used and how much is remaining at any particular point in time.

Fortunately, engine stationary components have two important characteristics that allow a reasonable approach to maintaining structural integrity.

- Based on the long-time history of large commercial turbofans, there are very few stationary components with failure modes that could jeopardize the safety of flight.

- Major stationary components usually have good damage tolerance with relatively long residual lives.

The latter of these characteristics makes the objective of being able to predict the remaining life of stationary components based on crack growth a viable (and possibly the only) option. The fact that only a few stationary components could fail in such a way as to pose a safety concern limits the breadth of the necessary effort and can be used to set work priorities.

One obvious question is how much, if any, do key material properties degrade with time? In particular, do low-cycle fatigue and, more importantly, crack growth rate properties change after long time service exposure? Also, do these properties change as a result of weld repairs and repeated postweld repair heat treatments?

A GEAE engineering team performed limited work during 1991 to review experience and evaluate our aging engine compressor rear frames and combustion casings. This effort produced some limited material property data and weldability results. In addition to follow-on work in these areas, the team recommended other work tasks which together formed the foundation for this project.

Work in 1991 included getting a high-time/high-cycle CF6 CRF from the field for microstructure evaluation and material testing. Attempts to resurrect repair history on any one of several candidate frames proved futile. In order to assess material property degradation due to exposure to multiple repair heat treatment cycles, test samples were taken from common heats of material. The samples were fully heat treated and then subjected to 15 and 30 simulated repair heat treatment cycles. The number of repair heat treatment cycles selected was based on judgment after discussions with operators and GE Field Service personnel—with 30 cycles being the upper bound. Based on microstructure comparison, the high-time part studied had been exposed to about 15 heat treatment cycles. This early mechanical property data showed a tendency toward reduced tensile properties with multiple-repair heat treatment cycles but little degradation in low-cycle fatigue or crack growth behavior.

Some work was accomplished in 1991 by the Edison Welding Institute under GEAE contract to look at weldability of wrought and cast Inconel 718 (IN718) material after exposure to the aforementioned 15 and 30 simulated repair heat treatment cycles. This limited work used test coupons and showed a tendency toward increased cracking (poorer weldability) with the multiple-repair heat treatment cycles for cast material. Follow-on work by the Edison Welding Institute was conducted under this project to understand, characterize, and improve IN718 repair weldability. The objective of Task III: Weldability Improvements, was to develop weld techniques and a postweld heat treatment that would reduce the propensity of IN718 aged material to crack during the repair process. The benefits for improved weldability would be to reduce the number of repair cycles required during any particular shop visit and to minimize the possibility of undetected cracks being returned to service.

As discussed earlier, the project workscope included five major tasks. Completion of the first four of these tasks was considered essential by GEAE in order to develop the data needed (1) to determine if a periodic inspection would be beneficial for the components studied and (2) to define the details of such an inspection plan. In order to accomplish the end objective with realistic and practical results, many relevant issues needed to be investigated and considerable data needed to be generated. Obviously, periodic inspections are added expense for the airline operators and care must be taken to assure that they are necessary, effective in finding the size cracks being sought, and can be reasonably accomplished with personnel, facilities, and processes available at the inspection site.

There are two situations that may result in distinctly different approaches to the problem. One is where a significant failure database exists and, as a result, a statistical approach to defining an inspection interval can be used to avoid future failures. The other is where a significant number of failures have not occurred but there is a desire to prevent future failures by taking proactive action through the introduction of an inspection interval. The latter was GEAE's approach with, of course, the key question being is proactive action necessary.

The GEAE approach requires detailed knowledge of component operating temperatures, stress levels, and the flight mission. Since the engine components being studied were designed before sophisticated finite element structural analysis had evolved, the first order of business was to upgrade the thermal and stress analyses for the components being studied. Once the temperatures and stresses were calculated, residual lives based on crack propagation from an inspectable flaw size needed to be calculated. Here it was recognized that the classical GEAE fracture mechanics approach using stress-intensity (K) solutions for load-controlled boundary conditions may result in very conservative crack growth predictions. Typical engine frames and casings are thermally loaded and/or structurally redundant as well as mechanically loaded. For these type components, displacement-controlled boundary condition solutions or a combination of load and displacement boundary condition solutions are needed to predict more realistic crack growth rates.

In order to understand GEAE's approach to this project, an overview discussion of the work scope included in each of the first four tasks is provided as follows.

Task I of the project was to construct modern finite element models of the components under study and to complete detailed thermal and stress analyses at several key flight mission points. In order to predict accurate crack growth lives, the goal was to define and verify a robust process that could be used to calculate stress intensities for arbitrary boundary conditions and component geometries.

Task II of the project was to develop all the material property data needed to assess degradation due to multiple repairs and aging. Any degradation effects would need to be considered in predicting useful remaining residual lives for the aged components studied. A secondary goal for Task II was to verify that any new heat treatment developed to improve weldability would not degrade important material properties.

Task III, to develop improved weldability, involved continued work by the Edison Welding Institute (EWI). As indicated earlier, aged components entering the service shops for overhaul may have an unknown history in terms of flight cycles, flight hours, number of times repaired, and types of repairs accomplished. In order to set a future inspection interval, it was necessary to be able to select any aged component at random, accomplish a refurbishment repair, and have confidence that it could be returned to service for a number of flight cycles or a time period independent of its prior history. The GEAE position was that the repaired component returning to service must be put in a consistent material condition and repair quality level (i.e., a known baseline condition). EWI's work effort was to quantify the current situation and then develop and successfully demonstrate the refurbishment process.

Task IV consisted of three subtasks related to inspection. The first was a controlled experiment to evaluate the effectiveness of several cleaning techniques and nondestructive testing methods for finding cracks with simulated engine run conditions (i.e., typical oxidized surfaces and contaminated dirty surfaces). This subtask has been reassigned to Iowa State University and results should be available in the future.

The second subtask was to conduct field inspections on a statistically significant number of high-time components from several engine models at identified peak stress locations to help verify the analytical stress predictions. Finally, a subtask was included to develop the necessary inspection probes which would be required to perform "assembled condition" inspections on the components studied should a periodic inspection be deemed necessary. The number, type, and detail design of these probes were to be decided pending the results of the prior tasks.

2. RESULTS AND DISCUSSION.

Detailed results from the work tasks completed or partially completed are provided by task. From an overall standpoint, the fatigue crack growth test results are encouraging in that only moderate degradation appears to occur with long-time service exposure and multiple repair cycles for the components studied. This result, of course, is likely to be different for IN718 material components which operate at higher temperatures or for components made from different materials.

Under the weldability task, it was disappointing that EWI was unable to identify an effective rejuvenation heat treatment. Unfortunately, this means that, as the weldability of these components becomes more difficult with time, the components will become uneconomical to repair. The only option the operators have is to retire these expensive parts. There is not always sufficient data available to know when to make a good economically driven decision and, consequently, the tendency is to continue to repair. On the bright side, there is no reason why the components studied should not remain safe provided that the service manual limits, approved repairs, and currently recommended field management programs are properly followed.

2.1 TASK I: CRACK GROWTH PREDICTIONS AND VERIFICATION.

One subtask under this part of the project was to update the stress and life analyses on the components selected using the latest finite element modeling methods, available data, and

procedures. The CF6-50, CF6-6, and CF6-80A CRF's are three different configurations. The analysis plan was broken into four parts which include (1) model generation, (2) heat transfer analysis, (3) stress analysis, and (4) mission life analysis. The approach was to use three-dimensional (3D) finite element sector models with engine data as model inputs where possible. The results from the models were to be compared to CF6 CRF field experience.

The model generation was executed by Tata Consultancy Services. They used the part drawings to generate a Unigraphic (UG) solid model. The solid models were then used to create finite element meshes. Tata completed the UG modeling of the three CRF configurations. They also created fine- and coarse-mesh models of each configuration resulting in a total of six finite element models. Figures 3 through 10 show the Unigraphics solid models and coarse- and fine-mesh finite element models for each of the three configurations. Volvo was to perform the heat transfer, stress, and mission life analyses under GEAE guidance. GE and Volvo were in the process of gathering boundary condition data for input to these models at the time the project was terminated. Similar work on the CFM56 combustion case was deleted from the project earlier in order to reduce cost.

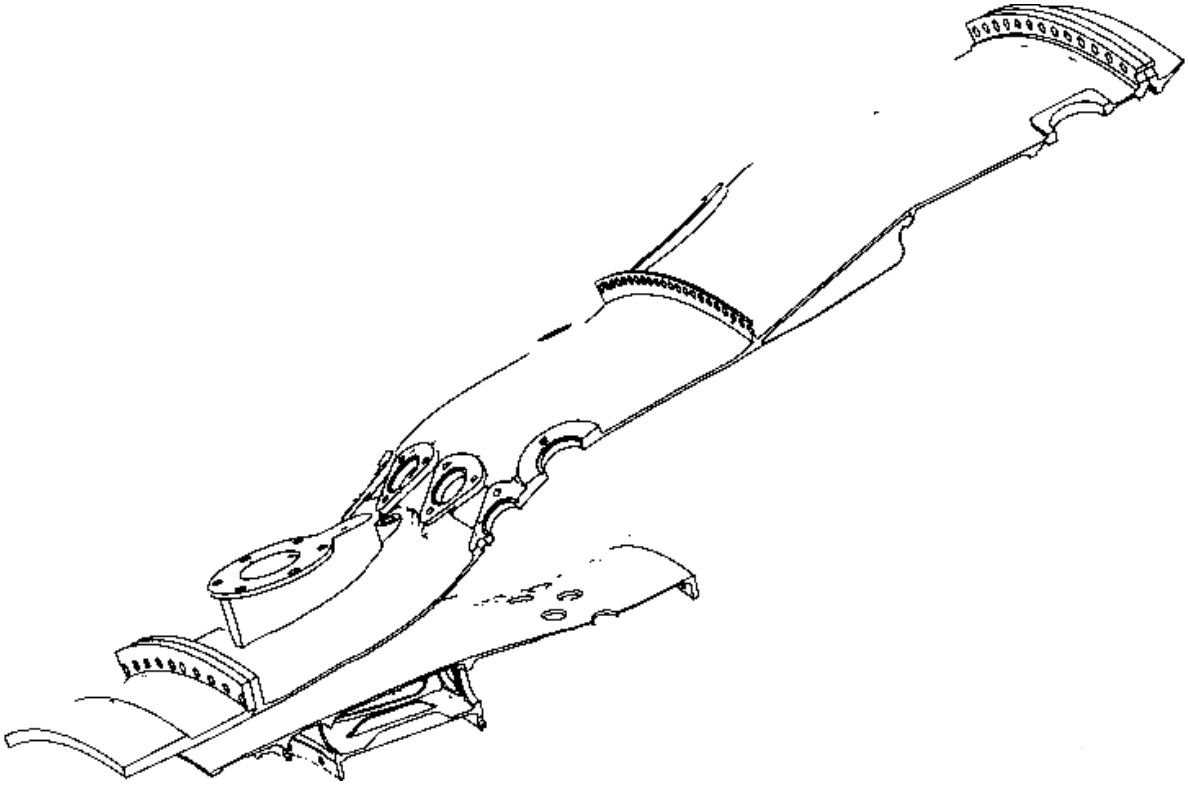

FIGURE 3. CF6-6 COMPRESSOR REAR FRAME UNIGRAPHIC MODEL

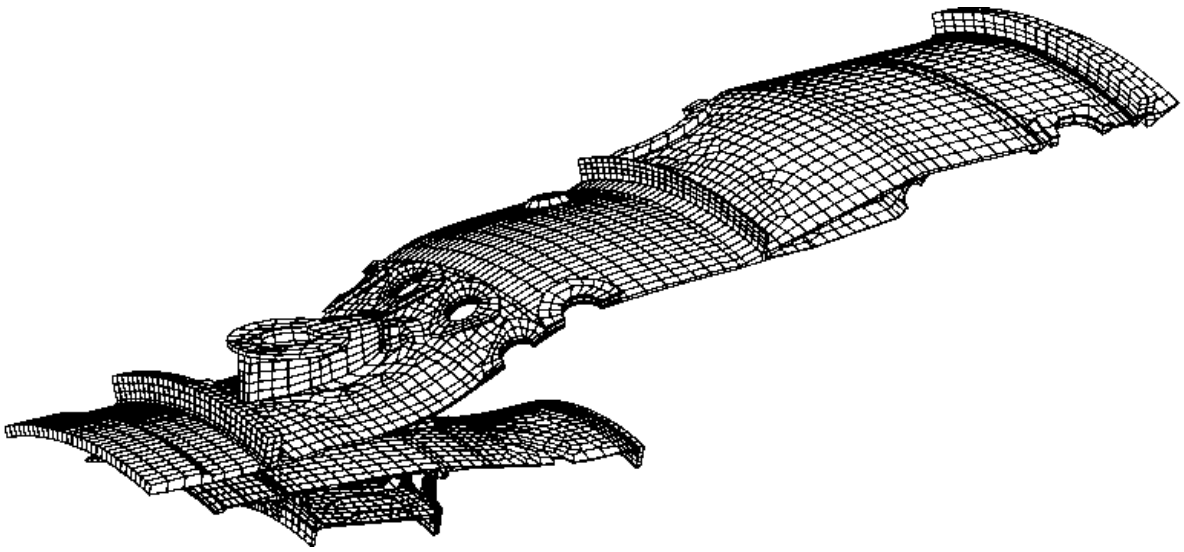

FIGURE 4. CF6-6 COARSE-MESH MODEL

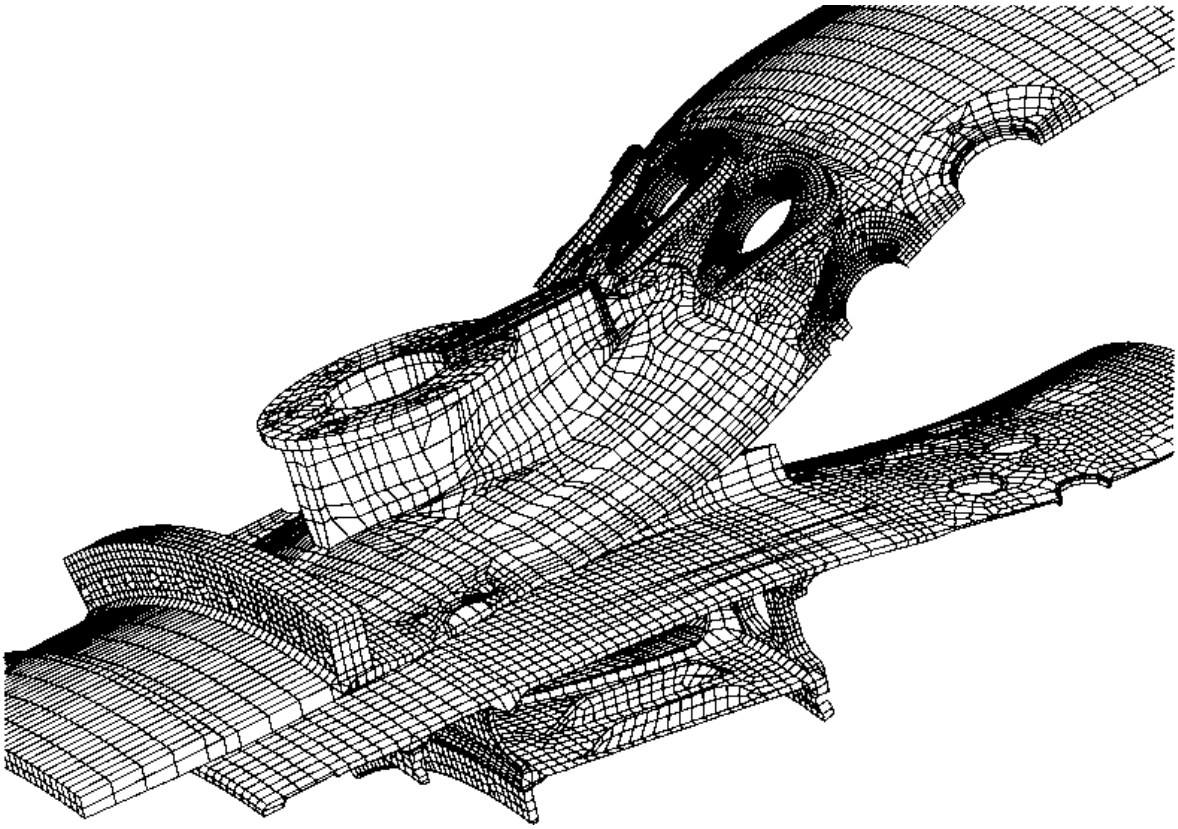

FIGURE 5. CF6-6 COMPRESSOR REAR FRAME FINE-MESH MODEL

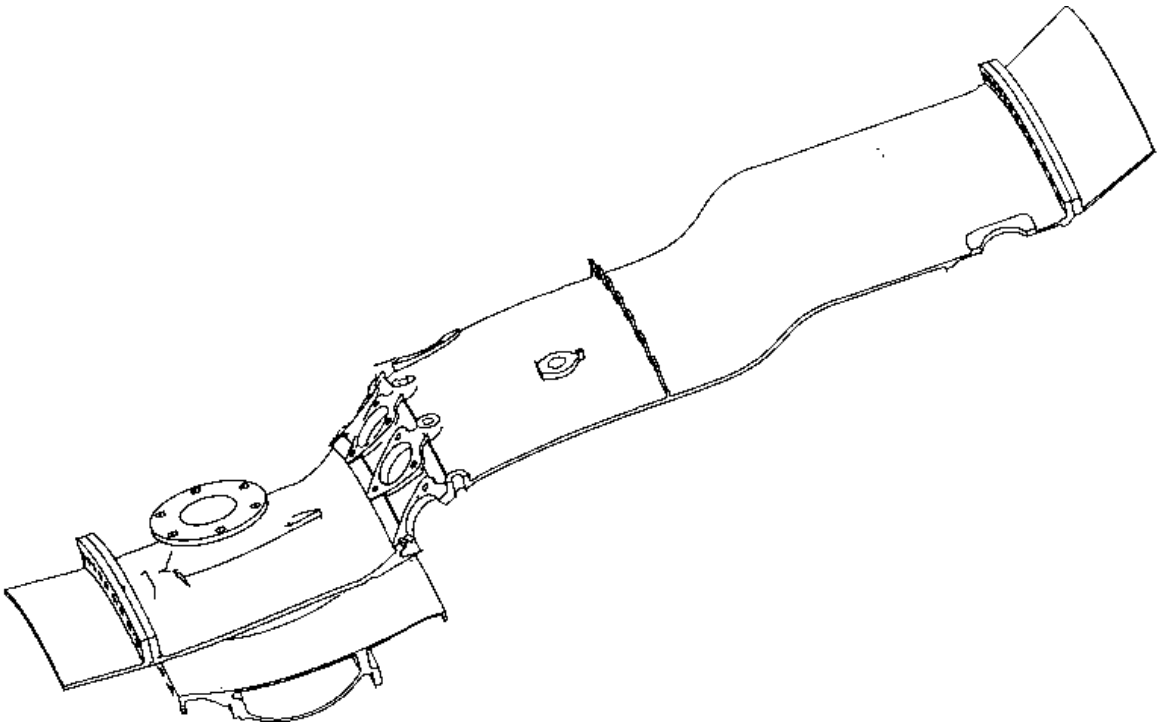

FIGURE 6. CF6-50 UNIGRAPHIC MODEL

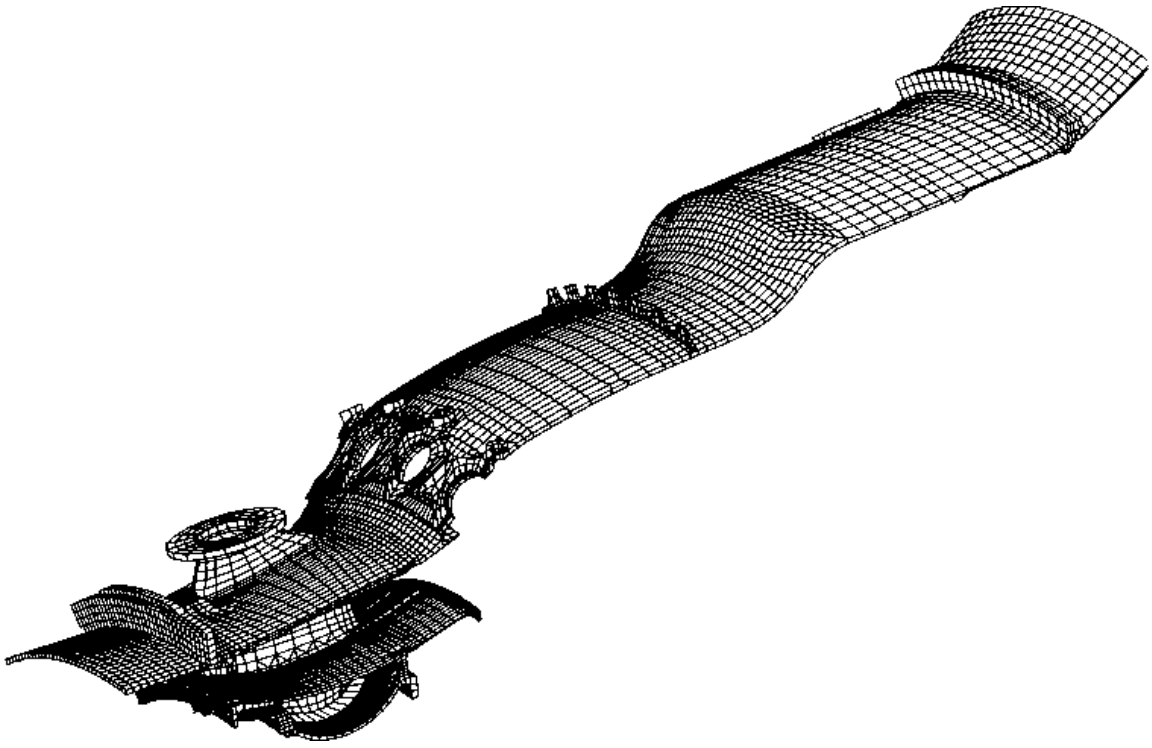

FIGURE 7. CF6-50 COMPRESSOR REAR FRAME COARSE-MESH MODEL

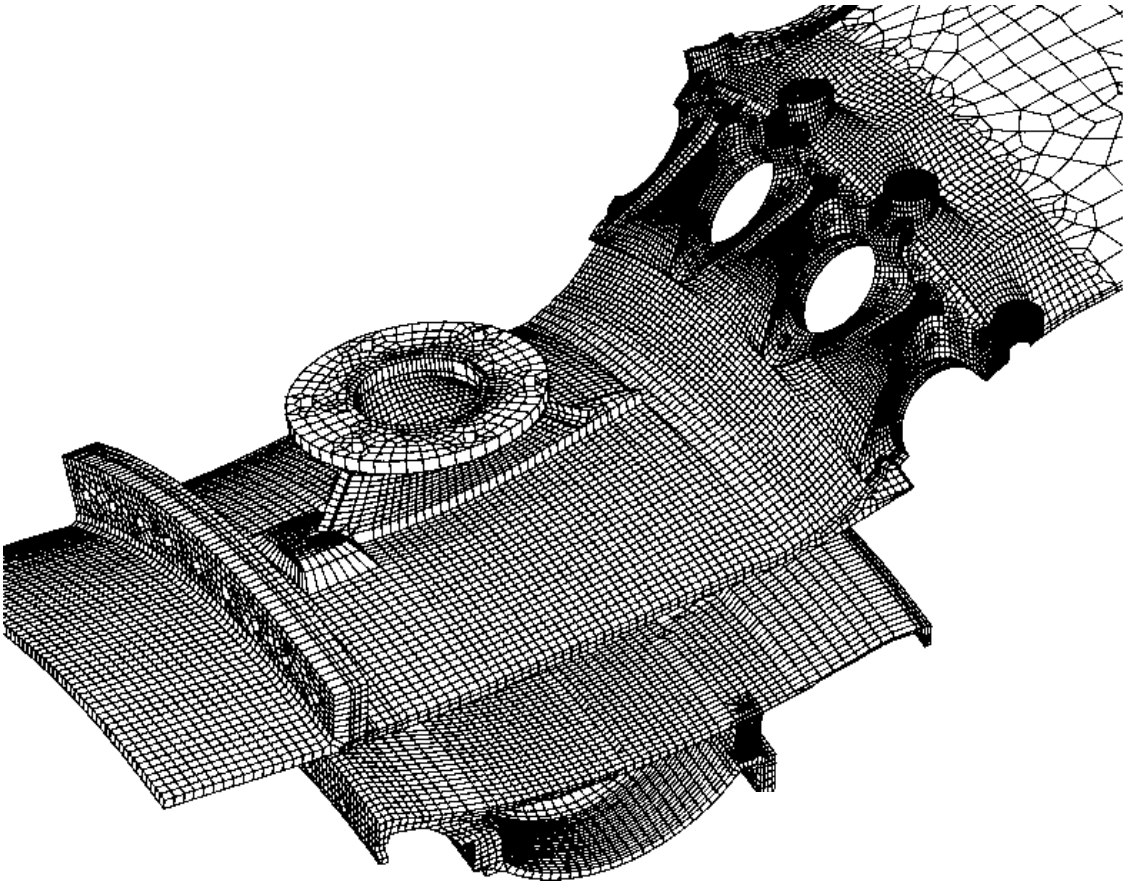

FIGURE 8. CF6-50 COMPRESSOR REAR FRAME FINE-MESH MODEL

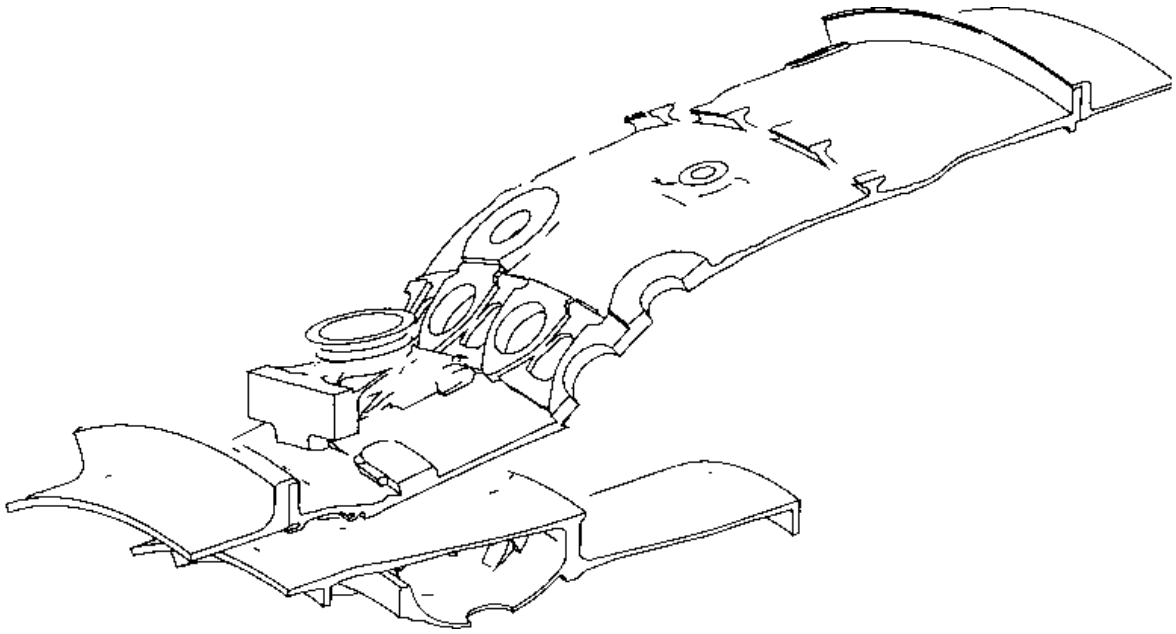

FIGURE 9. CF6-80A COMPRESSOR REAR FRAME UNIGRAPHIC SOLID MODEL

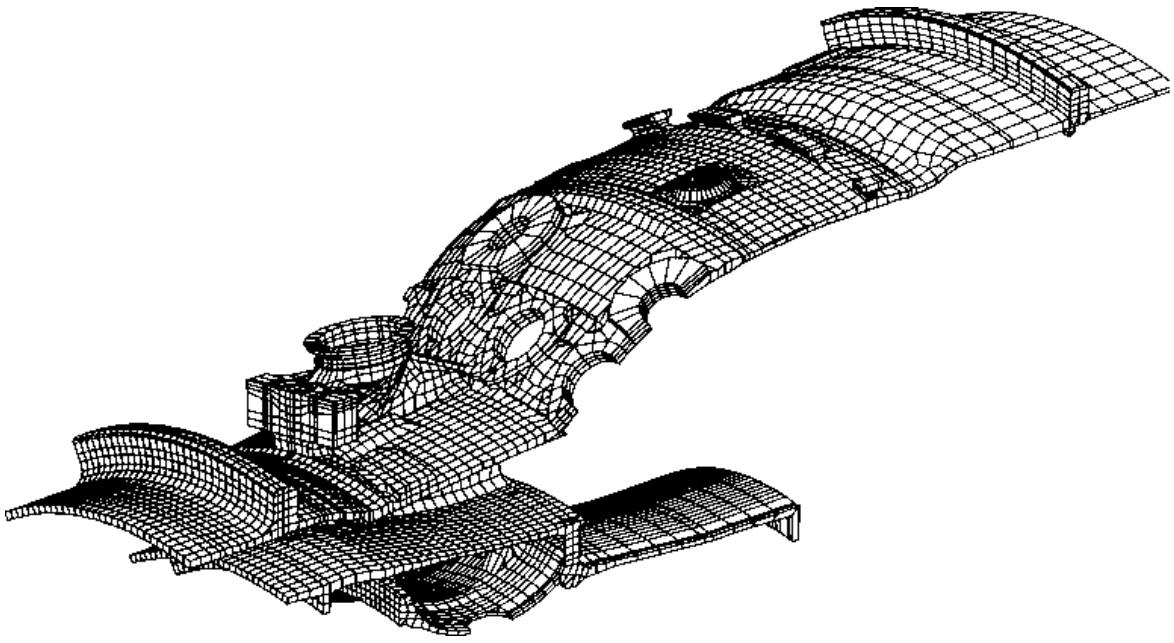

FIGURE 10. CF6-80A COMPRESSOR REAR FRAME COARSE-MESH MODEL

A second subtask under this part of the project was looking at analytical fracture mechanics methods to establish a robust process which could be used to calculate accurate stress intensities for arbitrary boundary conditions and complex component geometries. Thermally loaded structures such as frames and engine casings are better described with displacement or mixed-mode (load and displacement) boundary conditions. Initial work completed by Kemal Arin and Joseph Canha at the Department of Transportation Volpe Center showed favorable comparisons between the structural analysis codes ANSYS, BEASY, and known solutions for two-dimensional (2D) simple component geometries. ANSYS was chosen for ongoing analytical efforts since it is heavily used within GEAE and throughout industry worldwide.

The analysis approach used was to first select Mode I Stress-Intensity (K) solutions available in handbooks for relatively simple geometries and with well-defined load control boundary conditions and compare them with ANSYS models and then to progress toward more complex geometry and loading.

Mode I K can be obtained for an isotropic material from the crack opening displacements (δ) near the crack tip with Paris and Sih displacement fields as

$$\frac{\delta}{\sqrt{r}} = \frac{K}{2G}\frac{(1+\kappa)}{\sqrt{2\pi}} \tag{1}$$

where r is the distance from the crack tip, G is the shear modulus, and κ is equal to (3-4ν), ν is Poisson's ratio for plane strain or [(3-ν)/(1+ν)] for plane stress. Since δ/√r is not defined at the

crack tip to calculate K, crack opening displacements from nodes near the tip are defined with equation 2

$$\frac{\delta}{\sqrt{r}} = A + Br \tag{2}$$

where A and B are fit from nodal crack opening displacements near the crack tip for the problem of interest. The ANSYS KCALC command calculates K with equation 1 for a plane stress or plane strain stress state with the crack opening displacements assuming $\delta/\sqrt{r} = A$ as $r \rightarrow 0$ (ANSYS User's Manual).

2.1.1 Two-Dimensional Center-Cracked Panel Geometry—One-Dimensional Applied Load.

A center-cracked panel was used to check K-solution predictions for a simple 2D geometry. The theoretical stress-intensity solution used for comparison was developed by Tada. (H. Tada, PC Paris, and GR Irwin, The Stress Analysis of Cracks Handbook, Del Research Corporation, Hellertown, PA, 1973.)

$$\frac{K_{Tada}}{\sigma\sqrt{\pi a}} = Y_{Tada} = \left[1 - 0.025\left(2a/W\right)^2 + 0.06\left(2a/W\right)^4\right]\sqrt{\sec\left(\pi a/W\right)} \tag{3}$$

where

2a is the total crack length,
W is the total specimen width, and
σ is the far-field uniaxial stress.

One-quarter of the centered through-crack panel geometry was modeled with ANSYS assuming symmetry. K values were calculated with a uniform applied pressure of 1 ksi. The model dimensions were W/2 = 1 inch and H/2 = 3 inches where H is the total specimen height. The crack tip element sizes were approximately 0.1a with the crack along the local and global x axis. Differences between K calculated with the ANSYS KCALC command and the theoretical solutions are given as a function of 2a/W in figure 11. Predicted K values are within 0.35 percent of the theoretical solution confirming the initial work by Kemal Arin and Joseph Canha for 2D problems. Calculated K is insensitive to the plane stress/plane strain assumption since $A/(1+\kappa)$ remain essentially constant for a given 2a/W and specimen geometry.

2.1.2 Three-Dimensional Center-Cracked Panel Geometry Under a Uniaxial Applied Stress.

The 3D center-cracked panel geometry was extruded from a 2D model. Due to symmetry, only half of the specimen total thickness was modeled with through-thickness elements. The element thickness was weighted toward the outside surface to capture variations in K where plane stress conditions prevail. Ten elements were used through the thickness with the elements skewed so that the element at the surface of the specimen is one-quarter of the thickness of the element at

the center. Short-crack models were skewed more toward the surface to ensure plane stress was obtained in the surface elements. Preliminary mesh sensitivity studies have concluded the mesh sizes used produce converged solutions for the cases examined. Future studies were to determine a more rigorous mesh size criterion for typical problems. Predicted K at the center of the specimen, normalized by the Tada solution, is given as a function of the specimen thickness for 2a/W = 0.2 in figure 12. Since the KCALC command in ANSYS requires a plane stress or plane strain assumption, the predictions are given with both options. For B ≥ 2 inches, ANSYS prediction at the center element matches the theoretical solution using the plane strain option, which is reasonable for thick plates. For thin plates, plane strain is not achieved at the center of the specimen, and K is overpredicted by almost 6 percent for B = 0.2 inch.

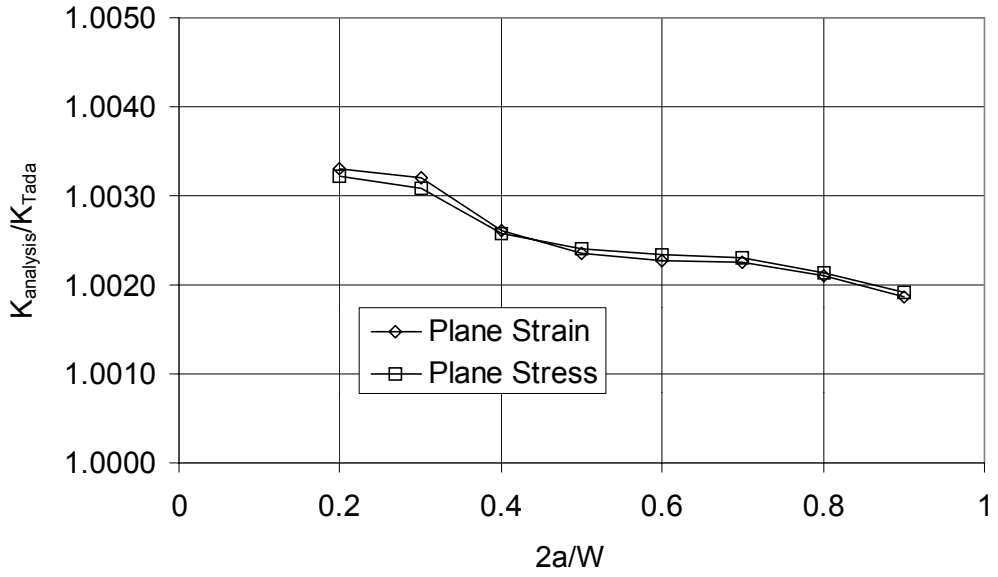

FIGURE 11. TWO-DIMENSIONAL CENTER-CRACKED PANEL

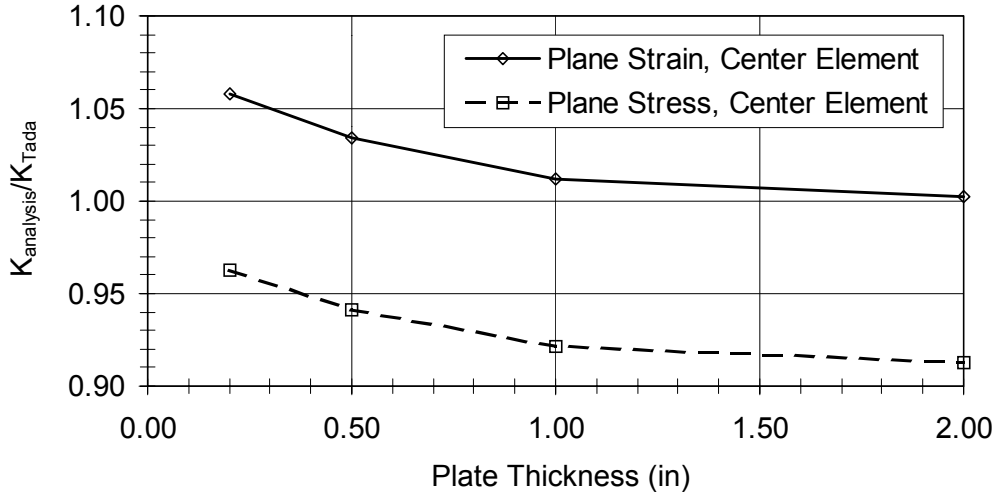

FIGURE 12. THREE-DIMENSIONAL CENTER-CRACKED PANEL, ONE-DIMENSIONAL APPLIED LOAD, SURFACE-WEIGHTED MESH, 2a/W = 0.2

Reformulating equation 1 for an arbitrary out-of-plane stress state is nontrivial, but a realistic K can be obtained by interpolating between predicted K using the ANSYS plane stress and plane strain results.

$$K = (1-\beta)K_{plane\sigma} + \beta K_{plane\varepsilon} \tag{4}$$

where β is equal to 0.0 for plane stress and 1.0 for plane strain. An interpolation factor with the necessary attributes is (personal communications with Horst deLorenzi at GE Corporate R&D 1996).

$$\beta = \frac{\sigma_z}{\nu(\sigma_x + \sigma_y)} \tag{5}$$

where σ_z is the through-thickness stress, and σ_x and σ_y are the in-plane stresses. β is obtained for cracking problems from the stress state at the node just ahead of the crack tip. K values through the specimen thickness using plane stress option, plane strain option, and constraint factor interpolation are shown in figures 13 and 14. Predicted K with the constraint factor varies smoothly through the thickness, is below the Tada solution near the surface of the specimen, and is above the Tada solution near the center of the specimen. Average predicted K using the ANSYS results with and without the constraint factor technique is given figure 15. (Note average K is weighted based on the thickness of each element.) The inferior prediction in figure 15 assumes plane strain for all interior elements and plane stress at the surface element. This approach consistently overpredicts average K by 4.7 percent for B = 0.2 inch and 2.0 percent for B = 2.0 inches as compared to the reference solution at 2a/W = 0.2. Interpolating between the plane stress/plane strain results with the constraint factor more accurately represents the crack tip stress state and reduces the errors in average K to less than 2 percent ($0.1 \le B/W \le 1$, 2a/W = 0.2).

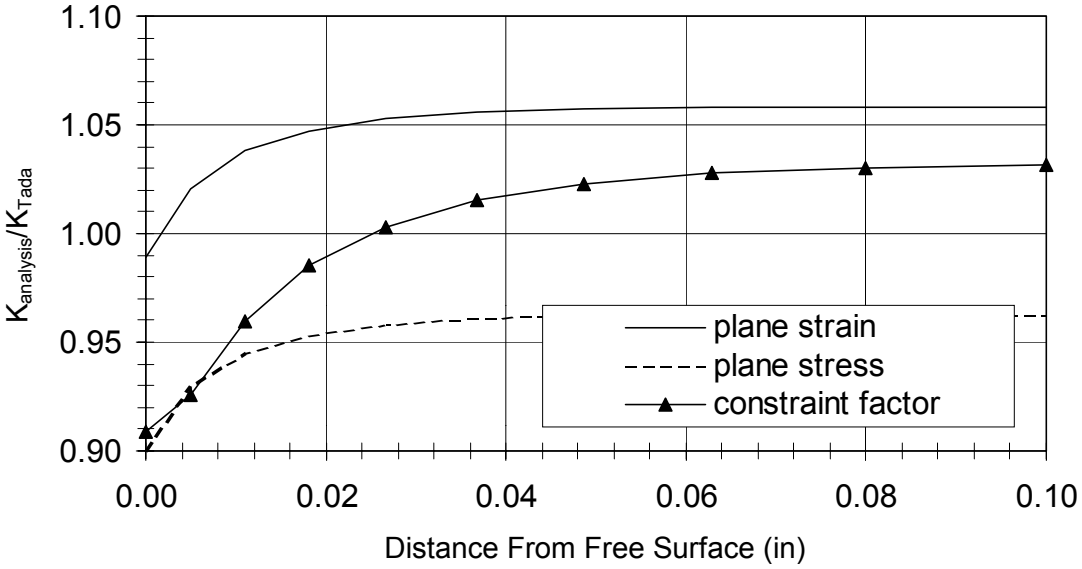

FIGURE 13. CENTER-CRACKED PANEL, ONE-DIMENSIONAL LOAD SURFACE-WEIGHTED MESH, B/W = 0.1, 2a/W = 0.2

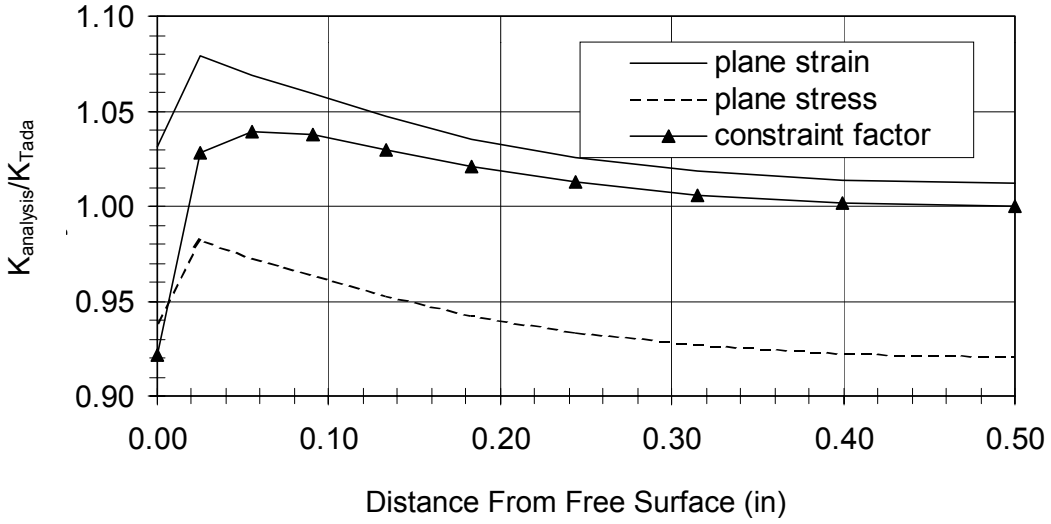

FIGURE 14. CENTER-CRACKED PANEL, ONE-DIMENSIONAL LOAD SURFACE-WEIGHTED MESH, B/W = 0.5, 2a/W = 0.2

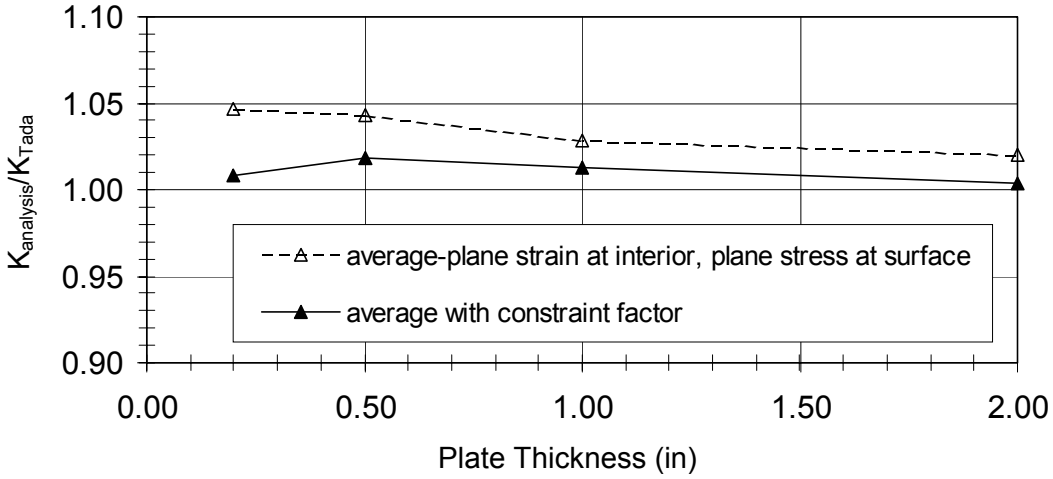

FIGURE 15. AVERAGE K FOR A THREE-DIMENSIONAL CENTER-CRACKED PANEL, ONE-DIMENSIONAL APPLIED LOAD, 2a/W = 0.2

2.1.3 Three-Dimensional Center-Cracked Panel Geometry With Crack Lengths and Applied Multiaxial Loads.

K for the 3D center-cracked panel was next evaluated for a wide range of crack lengths and applied stress states. The constraint factor needs to accurately predict K in stress fields ranging from biaxial tension to biaxial tension/compression. Finite width reference solutions for plates in a biaxial stress field are not available in the literature, but it has been experimentally confirmed that applied stresses parallel to the crack do not substantially influence da/dN and therefore K. (AF Liu, JE Allision, DF Dittmer, and JR Yamane, ASTM STP 677, pp. 5-22, 1979). Predicted Ks normalized by the Tada solution for biaxial stress at 2a/W = 0.2 are given in figures 16

and 17. The applied loads parallel to the crack had no impact on the crack opening displacement (δ in equations 1 and 2) and a small but reasonable impact on the constraint interpolation factor to influence K. Differences between average K calculated with the constraint factor and the Tada solution are examined for crack lengths ranging from 2a/W = 0.001 that is representative of machining damage to 2a/W = 0.5 (figures 18 and 19). Calculating average K with the constraint factor (a) is superior to K calculated with the plane strain options at all crack lengths except very short cracks where the constraint approach is only slightly inferior but still matches the Tada solution to within 2.2 percent for $0.001 \leq 2a/W \leq 0.5$ and (b) predicts loads parallel to the crack have a small influence of less than ± 3.6 percent on average K compared to reference solutions with a uniaxial far-field load. K calculated with the constraint factor closely matches the 2D reference solutions and is reasonable for complex stress fields where explicit reference solutions are not available.

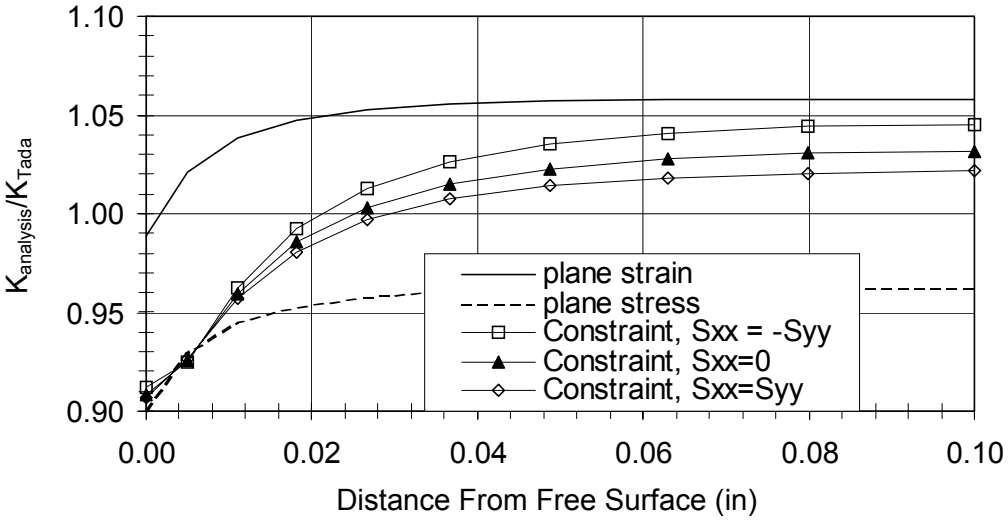

FIGURE 16. CENTER-CRACKED PANEL, 2a/W = 0.2, B/W = 0.1

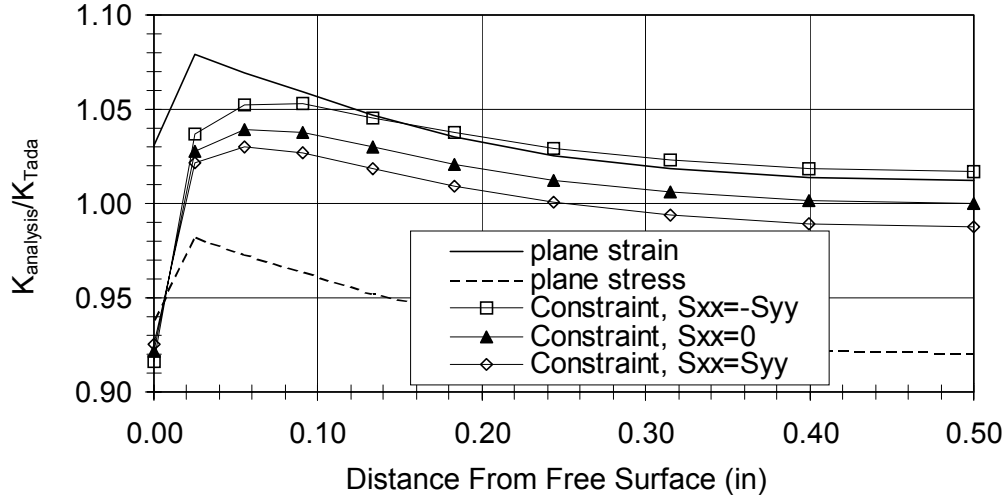

FIGURE 17. CENTER-CRACKED PANEL, 2a/W = 0.2, B/W = 0.5

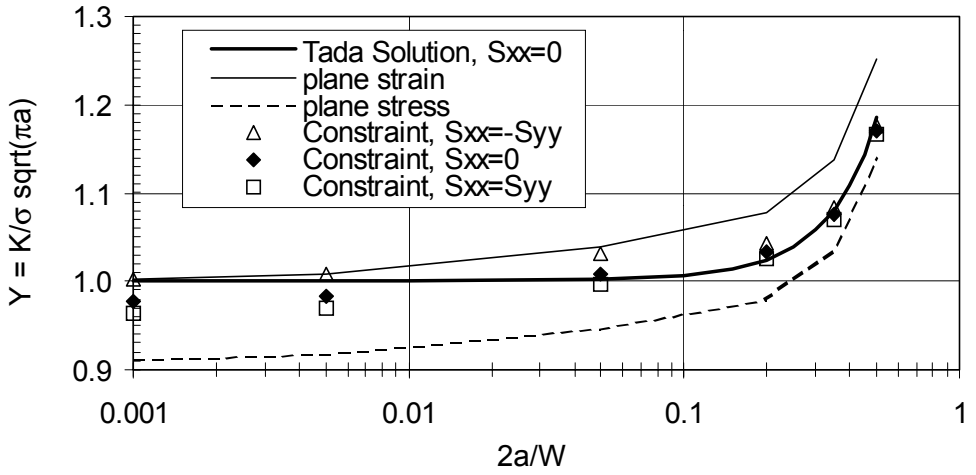

FIGURE 18. WEIGHTED AVERAGE K MULTIAXIAL APPLIED LOAD, B/W = 0.2

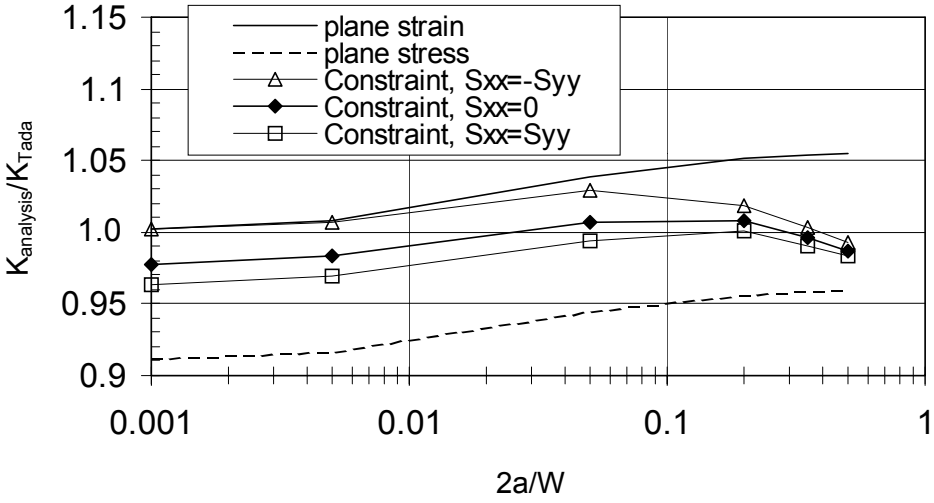

FIGURE 19. WEIGHTED AVERAGE K MULTIAXIAL APPLIED LOAD, B/W = 0.2

2.1.4 Localized Plasticity With Elastic Cycling for a Two-Dimensional Plate With a Hole.

Components with stress concentrations can experience initial localized plasticity on the first reversal when cracks are small or nonexistent followed by elastic cycling. The GEAE code PROPLIFE accurately correlates the experimental life of feature tests with localized plasticity using a Bueckner weight function approach that is based on the elastic and elastic/plastic stress gradients at the maximum load point. It is not clear how to similarly model localized plasticity with linear elastic analytical fracture mechanics techniques. An approach that combines a residual stress profile due to initial plasticity followed by subsequent elastic behavior can be used to predict K without the difficulties of a combined elastic-plastic/crack tip analysis. The residual stress approach first requires an elastic/plastic analysis of the uncracked component at the maximum load condition. The analysis is then unloaded to obtain a residual stress gradient in the component without external applied loads. The crack tip elements can then be placed in the

model with the applied loads added through the boundary conditions. The residual stress profile with the subsequent linear-elastic analysis of the cracked body can then be used to calculate K_{max} from the crack tip displacements using ANSYS in the usual manner. This approach is computationally efficient since an elastic-plastic analysis with the crack geometry is not required and the method can be easily applied for 2D and 3D component geometries.

A preliminary 2D test case was established to confirm the accuracy of this approach. The model considered was a symmetric crack from a 0.5-inch-diameter round hole in a 2.0-inch-wide plate. One-quarter of the geometry was modeled due to symmetry with the stress state set to plane stress. The bilinear stress-strain curve employed to obtain the residual stress in the uncracked geometry was representative of a nickel-base alloy with an elastic modulus was 30,000 ksi, an elastic Poisson's ratio of 0.3, a yield stress of 135 ksi, a plastic modulus of 3,000 ksi, and a plastic Poisson's ratio of 0.5. Calculated K as a function of the applied load up to maximum remote applied stresses of 40 ksi and 75 ksi are given for 2a/W = 0.25 in figure 20. K is proportional to the applied stress when either no notch tip plasticity occurs for the uncracked component ($S_{applied} \leq 40$ ksi) or no plasticity is permitted (linear elastic reference solution established by JC Newman, Report NASA TN D-6376, 1971). When the maximum load is increased so that notch tip plasticity is significant ($S_{applied} = 75$ ksi in figure 20), K_{max} established with the ANSYS residual stress technique (a) agrees with the Bueckner weight function approach used in PROPLIFE and (b) is substantially less than K_{max} calculated without initial notch tip plasticity affects. Localized plasticity with elastic cycling at a notch can substantially impact K and, therefore, should be included in an analysis to obtain accurate life predictions. Additional work was planned to verify the residual stress approach for localized plasticity as a function of the crack lengths, load level, and specimen thickness.

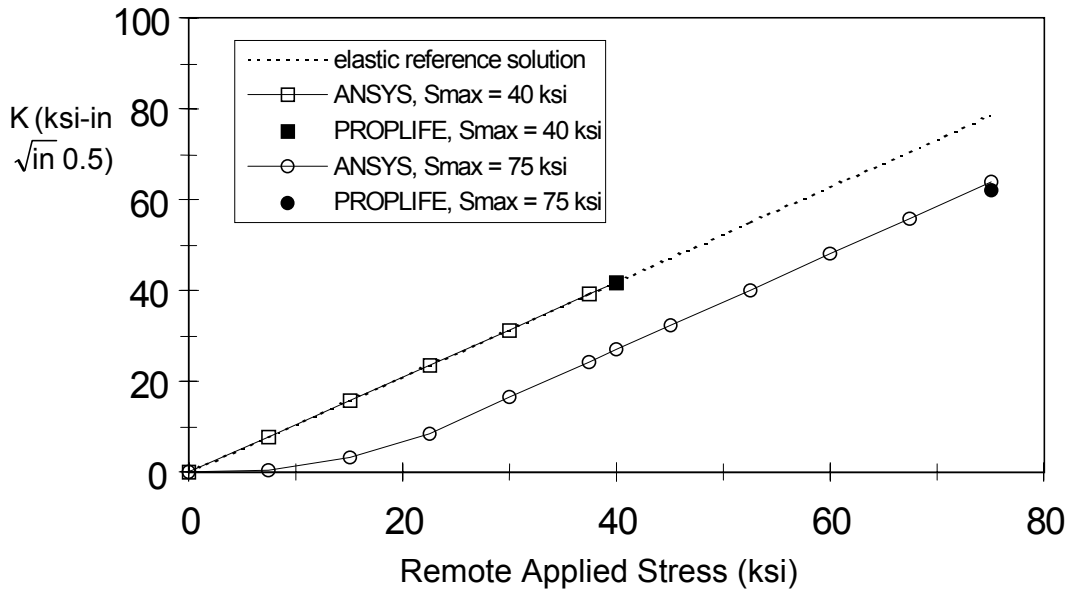

FIGURE 20. RESIDUAL STRESS METHOD, PLATE WITH A HOLE 2R/W = 0.25, 2a/W = 0.3, PLANE STRESS

2.2 TASK II: MATERIAL PROPERTY TESTING.

The possible mechanical property degradation of aging compressor discharge pressure vessels (e.g., casings, frames) due to prolonged engine operation and exposure to numerous repair cycles has been a concern. Limited work at GEAE in 1991 showed both wrought and cast+HIP IN718 casing material to have reduced yield and ultimate tensile strengths due to the overaging effect of multiple stress relief (~1700°F) cycles. Conversely, low-cycle fatigue (LCF) initiation, crack propagation, and threshold data at 800°F (which is the approximate temperature of concern for most GEAE casings) did not indicate a significant change in behavior (e.g., lower initiation, faster fatigue crack growth rate (FCGR)). Concerns about a lack of crack growth rate data at higher stress intensities (e.g., near-critical stress intensity) are addressed by subtask I.

Tungsten inert gas (TIG) welds and their adjoining heat affected zone (HAZ) are an integral feature of casings which are typically exposed to several stress relief cycles over time. Subtask II was to determine if these multiple thermal treatments have significantly affected the crack growth behavior of these welds and the HAZ areas.

Subtask III testing was conducted to support the Edison Welding Institute (EWI) weldability improvement studies discussed later in the report. The original subtask III plan called for crack growth rate testing to substantiate the weldability improvement of the heat treatment cycle determined by EWI. The plan was altered to add tensile, stress rupture, and LCF testing on one chemistry variation of each material.

Subtask IV was to develop a 300°F crack growth rate curve and Walker exponent on cast+HIP IN718 to expand the existing database. This was required for the task I life analyses and modeling of selected features.

Subtask V provided test data to EWI on the effect of multiple thermal cycles (1700°F) on tensile, stress rupture, and LCF properties of three different chemistries (Nb, B, and variations) of wrought and cast IN718. This material was used for their weldability studies.

Materials for subtasks I and II investigations of multiple repair cycle effects on crack growth rate of parent metal and weld areas included a new CF6-80 low-pressure turbine (LPT) case forging, a new CFM56 combustion case casting, and a high-time CF6-6 CRF field case representing both wrought IN718 and cast IN718 material. The test plan originally also required a CFM56 combustion case for the field exposed casting; however, it was difficult finding a retired casing. The CFM56 combustion case rarely requires weld repair.

Chemistries as recorded on material certification reports are listed in tables 1 and 2, respectively.

TABLE 1. CHEMISTRY OF CF6-80 LPT CASE USED FOR WROUGHT IN718 CRACK GROWTH TESTING

Fe	Si	Mn	Co	Nb	B	Al
20.8	0.12	0.07	0.32	5.08	0.004	0.52
Ti	Ni	Mo	S	P	C	Cr
0.96	52.21	3.04	<0.005	0.011	0.04	18.4

TABLE 2. CHEMISTRY OF CFM56 COMBUSTION CASE USED FOR CAST IN718 CRACK GROWTH TESTING

Fe	Si	Mn	Co	Nb	B	Al
Bal	0.09	0.04	0.09	5.14	0.002	0.49
Ti	Ni	Mo	S	P	C	Cr
0.9	52.6	2.96	<0.005	0.01	0.06	18.3

The CF6-80 LPT forging was acquired from a production lot processed by Carmel Forge per GEAE specification B50TF15 and utilized a Carpenter Technology heat of IN718. The CFM56 combustion case casting originated from a Certified Alloys chemistry (Heat No. 33948) and was cast by Precision Castparts to GEAE specification B50TF16. Standard heat treatment condition for these parts are as follows:

Wrought IN718 (CF6-80 LPT Case)

1775°F for 1 hour, OQ

+

1325°F for 8 hours, furnace cool at 100°F/hr to 1150°F,
Hold at 1150°F for 8 hours

Cast+HIP IN718 (CFM56 Combustion Case)

2050°F HIP/15 psi

+

1925°F for 1 hour, furnace cool to 1200°F w/in 23 min

1750°F for 1 hour, furnace cool to 1100°F w/in 23 min

1400°F for 5 hours, furnace cool at 100°F/hr to 1200°F,
Hold at 1200°F for 1 hour

Test specimens for the 300°F cast+HIP IN718 crack growth rate curve generated in subtask IV were machined from the new CFM56 combustion case.

Material for subtasks III and V was supplied by EWI. Three different chemistries of wrought IN718 were provided as 0.3- to 0.4-inch-thick plates. Chemistries were varied within the IN718 specification limits for niobium and boron content due to their effect on weldability. Target contents were as follows:

Heat Designation	Percent Nb	Percent B
997	4.5	0.003
995	5.0	0.0045
996	5.5	0.006

All materials were exposed to their standard heat treatment cycle as previously listed. Subtasks I, II, IV, and V utilized a simulated repair cycle that included a 1700°F stress relief followed by an age of 1400°F for 2 hours, furnace cooled at 100°F per hour to 1150°F, and then held for 5 hours. During actual casing repairs, the 1700°F stress relief may be used several times prior to the final age.

Compact tension (CT) specimens, used for most of the crack growth testing, met ASTM E647 minimum requirements. They were machined from casing walls or from welded blanks that originated from these walls. A single-edge notch K_b specimen was the crack growth geometry required for generating a threshold value for the 300°F cast+HIP IN718 curve in subtask IV. Fatigue crack growth rate (FCGR) testing performed in the GEAE laboratory utilized the direct current (DC) potential drop technique for crack length monitoring and a box furnace and an induction coil for temperature control.

Tensile, stress rupture, and LCF specimens for the EWI study were machined in the rolling direction after heat treatments had been completed.

Room temperature tensile and 1200°F stress rupture testing ran at approved vendors to ASTM E8 and E139 standards. Low-cycle fatigue specimens were cycled in strain control per GEAE specification E50TF148, at an R = 0 and a triangular wave form. Test frequency was 0.5 Hz to failure or, after 2 days, was switched to load control and increased to 5 Hz using the same minimum and maximum loads recorded after the second day.

2.2.1 Subtask I: Crack Growth Testing to Verify Regions II and III for Aged Material.

The 800°F FCGR data from the wrought case (new) with and without multiple thermal treatments and from the field case are plotted as da/dn (in/cycle) versus ΔK (KSI$\sqrt{}$in) in figure 21. The new case shows a slight acceleration of about 1.2-1.5X, depending upon ΔK range, in crack growth rate after exposure to 30 repair treatments. The field case has a FCGR similar to the exposed material at the lowest ΔK's but shows a slight acceleration with increasing ΔK's. Differences in FCGR between the two casings may be due to the finer grain size (ASTM 7.5) and heavier delta (Ni_3Cb) precipitation in the field case versus the exposed new forging (ASTM 5.0).

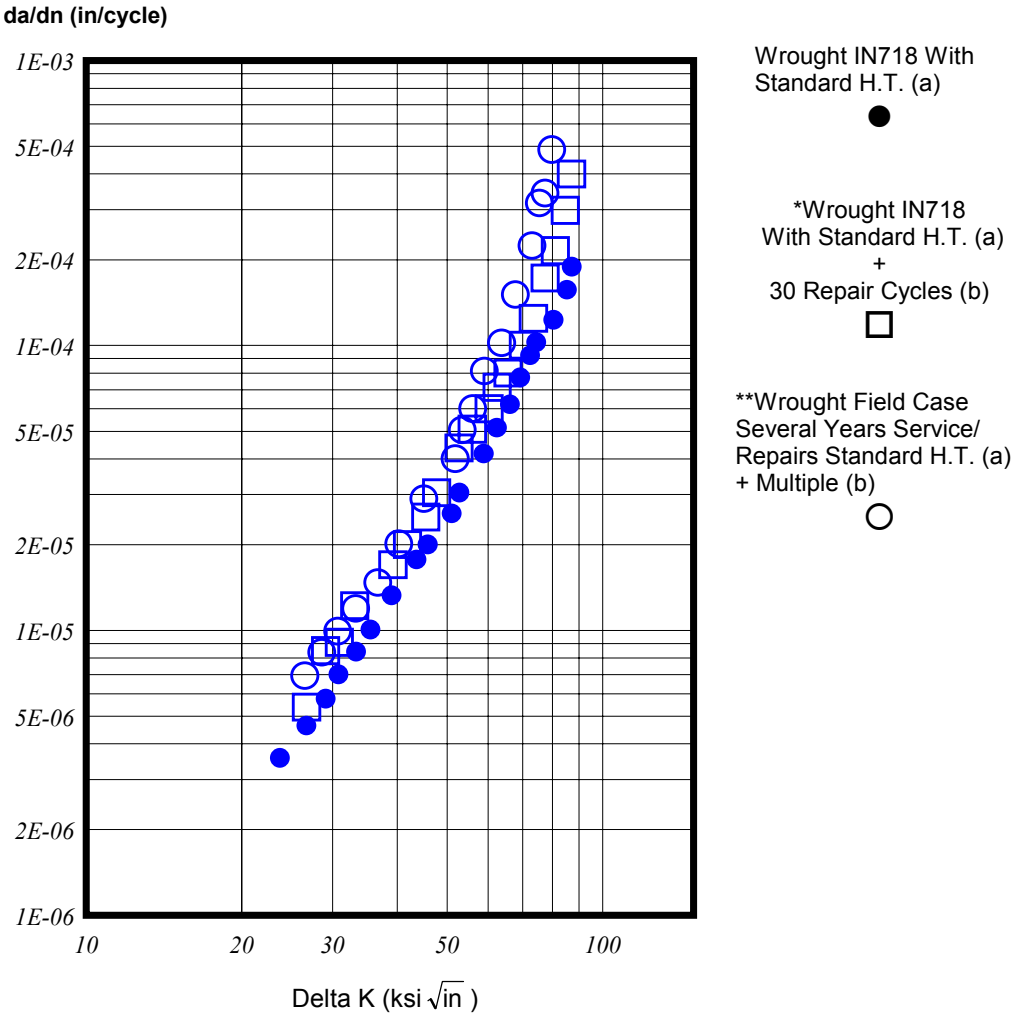

FIGURE 21. EFFECT OF MULTIPLE REPAIR (1700°F) CYCLES ON WROUGHT IN718 REGIONS II AND III CRACK GROWTH 800°F, R = 0.05, FREQUENCY = 0.33 Hz

These differences in the grain structure and size and amount of delta are apparent from microphotographs (figure 22).

Figure 23 shows the FCGR of cast+HIP IN718 in the unexposed, exposed, and in-service conditions. Data scatter was a problem with the cast material as the cracks propagate tortuously (e.g., accelerate/decelerate) through the coarse structure. FCGR data from the exposed new casing and the field casing follow a slightly steeper slope than the baseline data. This is similar to the wrought behavior except that the field case has a slower crack growth rate than the exposed material. The field case microstructure (figure 24) has very little delta precipitated into the matrix unlike the abundance of delta needles present in the new casting exposed to 30 simulated repairs.

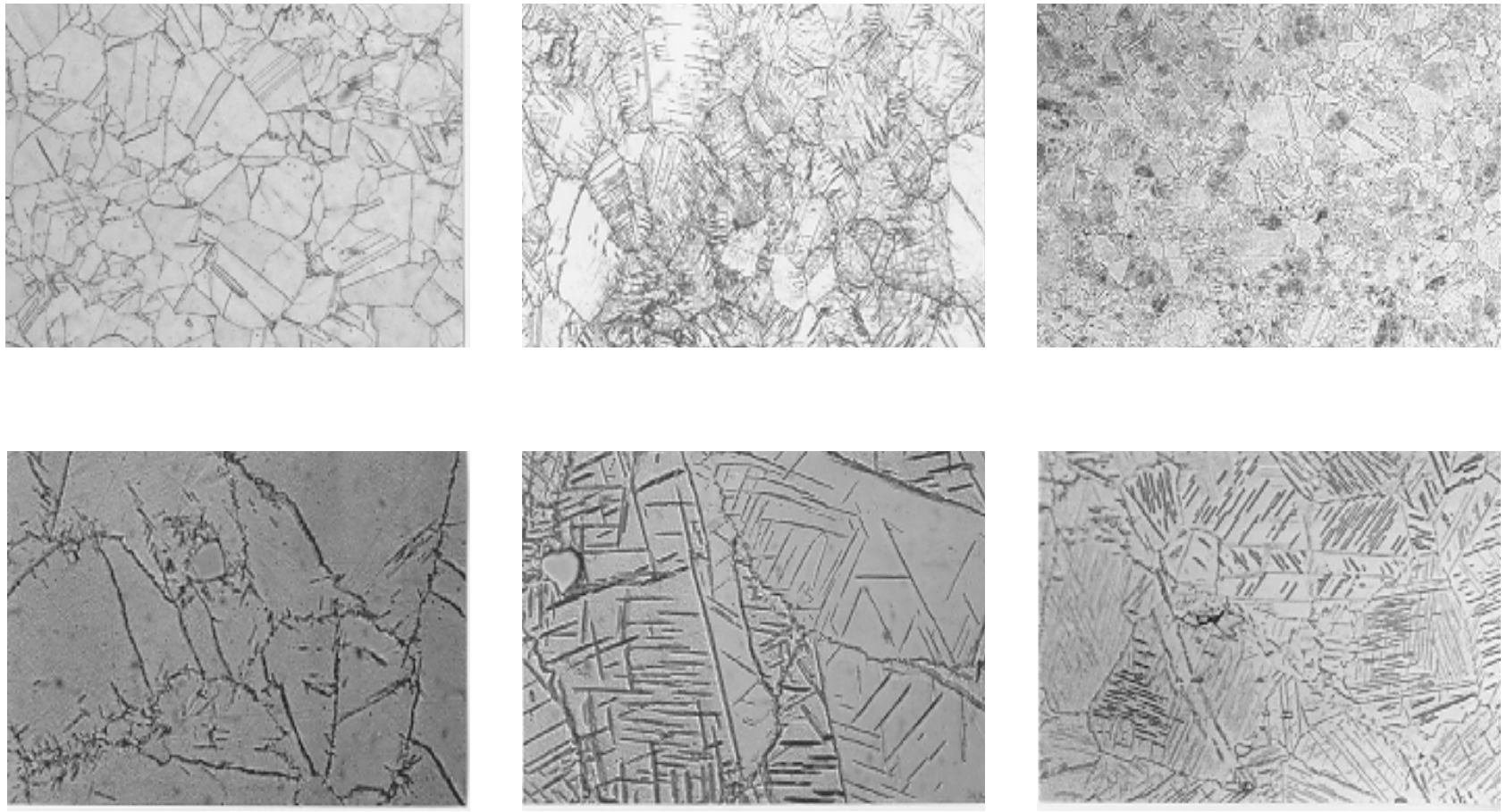

CF6-80 LPT Case (New)
Standard H.T.

CF6-80 LPT Case (New)
Standard H.T. +
30 Repair (1700°F) Cycles

CF6-6 CRF (Field)
Standard H.T. + Several Years
Service and Multiple Repairs

FIGURE 22. MICROSTRUCTURES FROM WROUGHT IN718 (NEW CF6-80 LPT CASE) EXPOSED TO STANDARD HEAT TREATMENT AND 30 SIMULATED REPAIR (1700°F) CYCLES AND CF6-6 COMPRESSOR REAR FRAME RETIRED AFTER SEVERAL YEARS SERVICE AND MULTIPLE REPAIR CYCLES

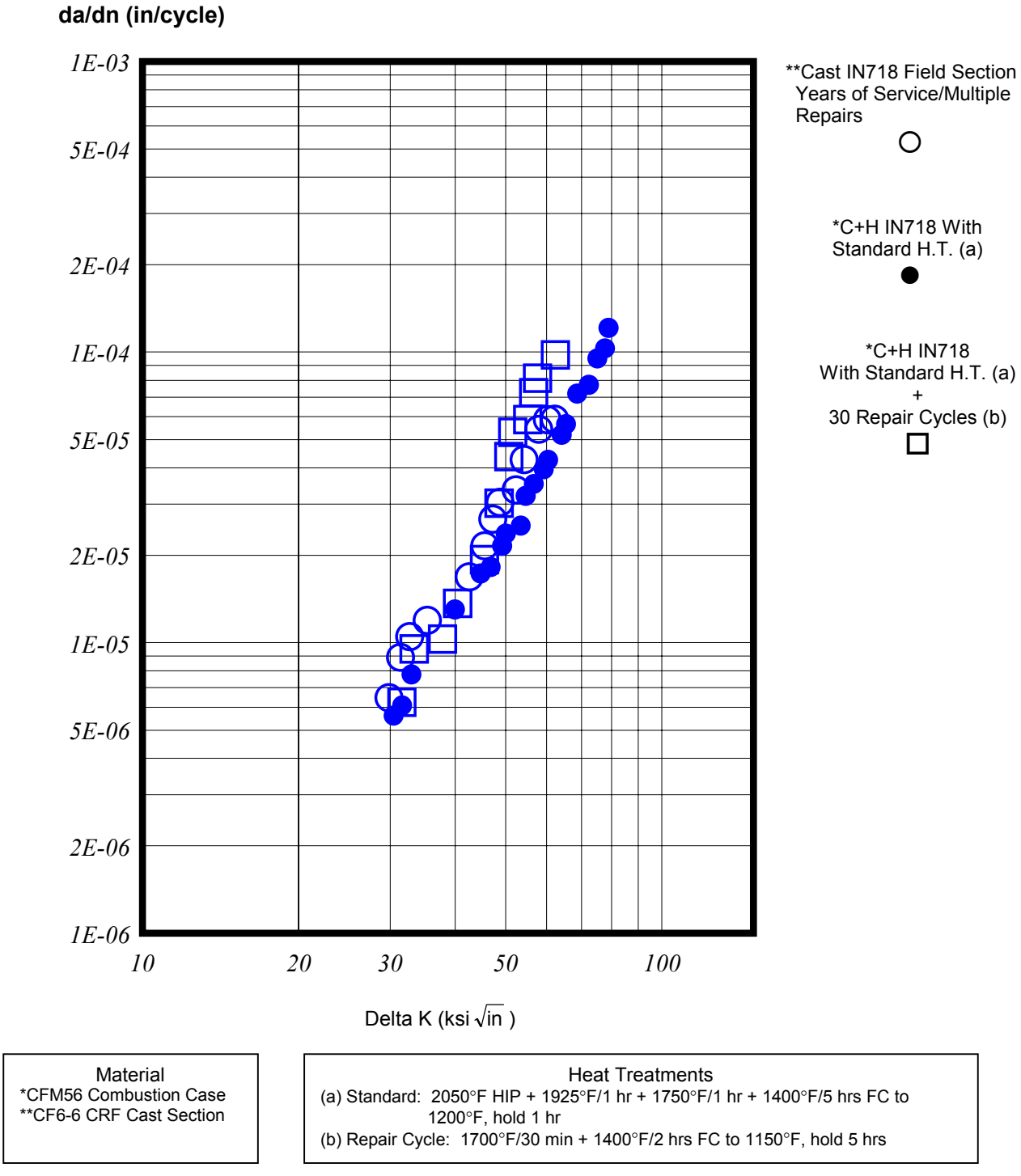

FIGURE 23. EFFECT OF MULTIPLE REPAIR (1700°F) CYCLES ON CAST IN718 REGIONS II AND III CRACK GROWTH 800°F, R = 0.05, FREQUENCY = 0.33 Hz

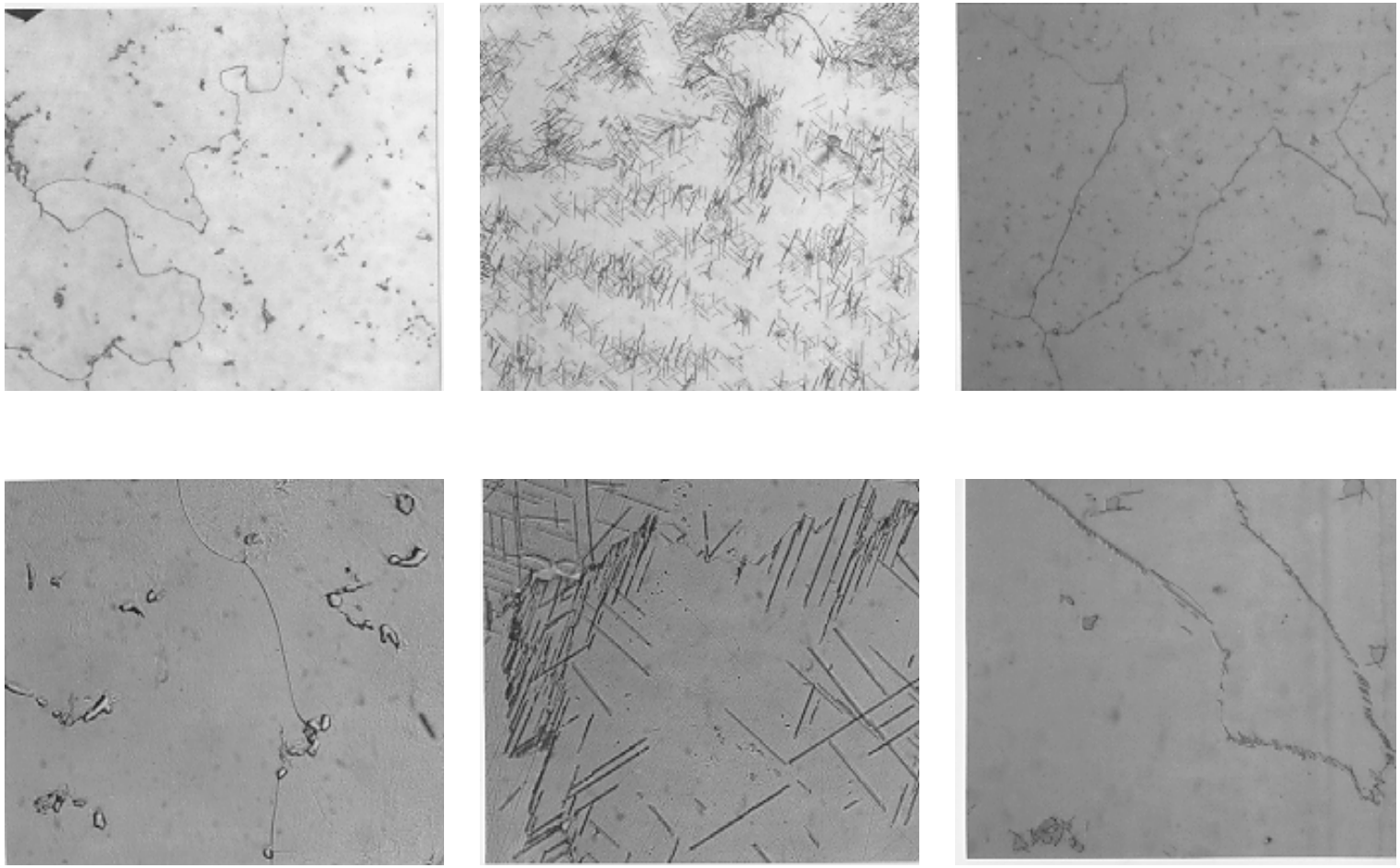

FIGURE 24. MICROSTRUCTURES FROM CAST+HIP IN718 (NEW CFM56 COMBUSTION CASE) EXPOSED TO STANDARD HEAT TREATMENT AND 30 SIMULATED REPAIR (1700°F) CYCLES AND CAST IN718 SECTION FROM CF6-6 COMPRESSOR REAR FRAME RETIRED AFTER SEVERAL YEARS SERVICE AND MULTIPLE REPAIR CYCLES

2.2.2 Subtask II: Crack Growth Rate in Weld Repairs Versus Parent Metal (Wrought and Cast IN718).

Multiple exposures were found to have little effect on the crack growth rate of TIG welds in either wrought or cast IN718 (figures 25 and 26). The fine dendritic structure of the weld shows precipitation of delta phase after the 30 simulated repairs (figures 27 and 28); however, it is not as extensive as shown in the exposed parent metal (figure 24).

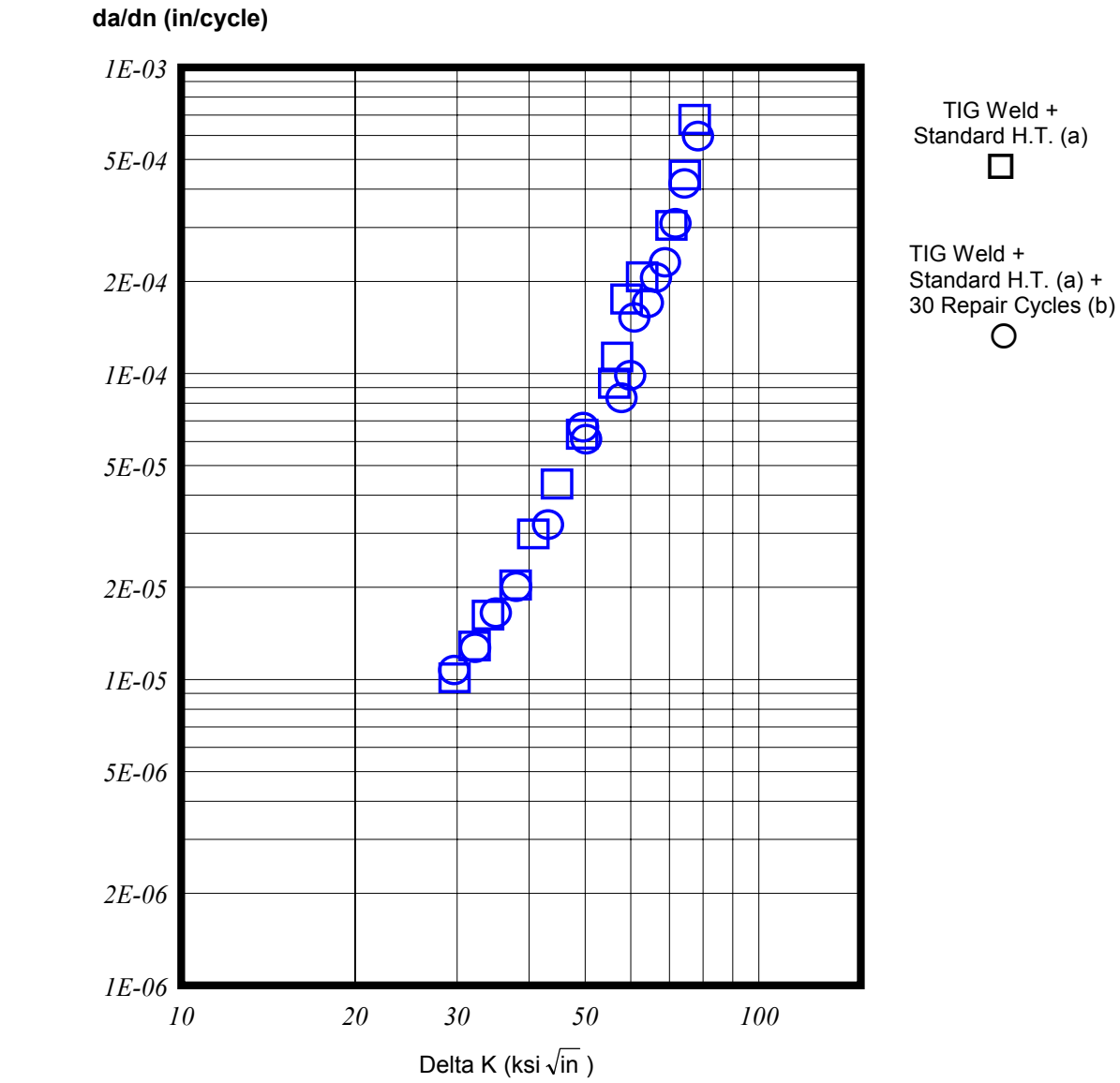

FIGURE 25. EFFECT OF MULTIPLE REPAIR (1700°F) CYCLES ON WROUGHT IN718 TUNGSTEN INERT GAS WELD REGIONS II AND III CRACK GROWTH 800°F, R = 0.05, FREQUENCY = 0.33 Hz

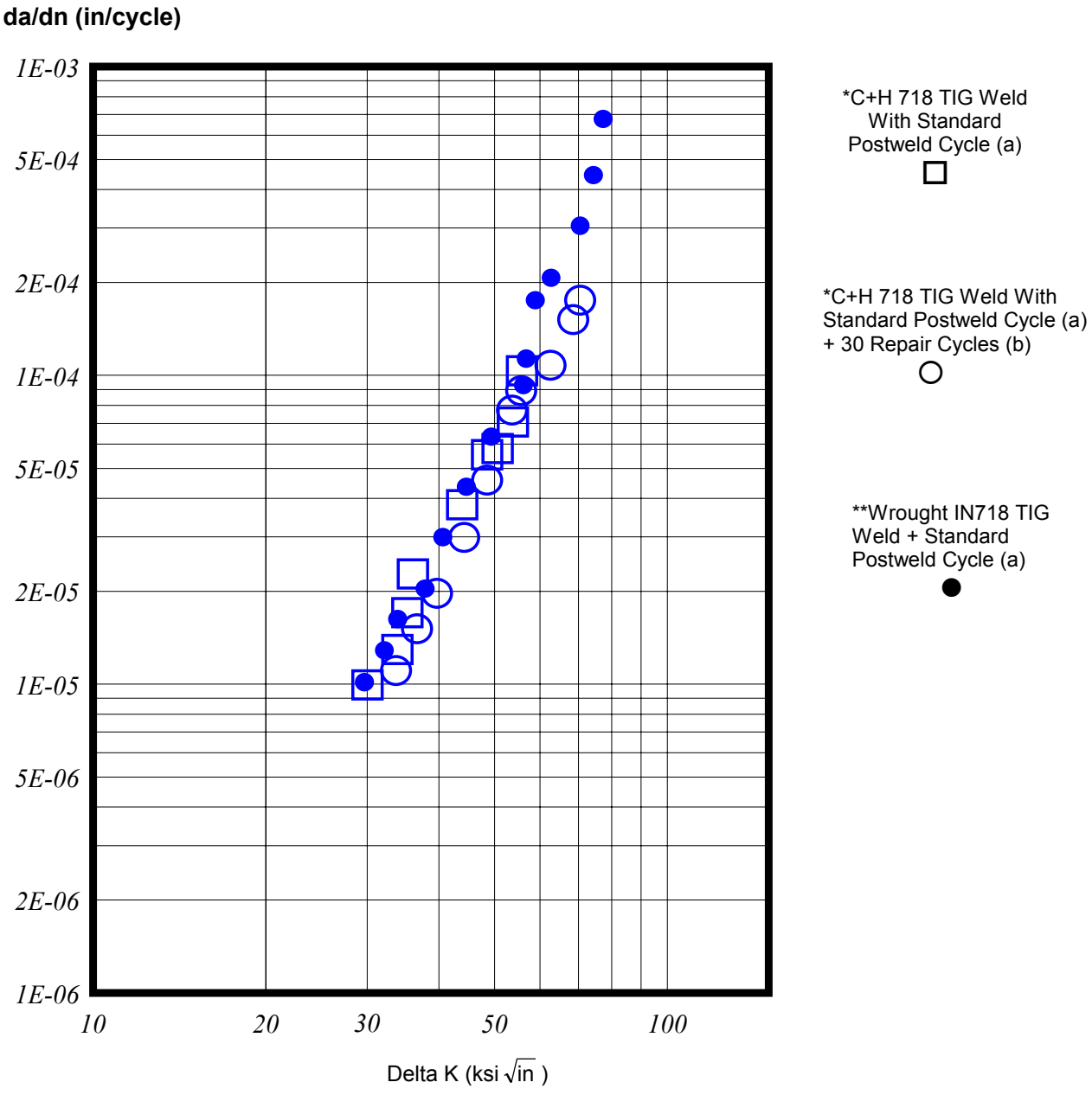

FIGURE 26. EFFECT OF MULTIPLE REPAIR (1700°F) CYCLES ON CAST IN718 TUNGSTEN INERT GAS WELD REGIONS II AND III CRACK GROWTH 800°F, R = 0.05, FREQUENCY = 0.33 Hz

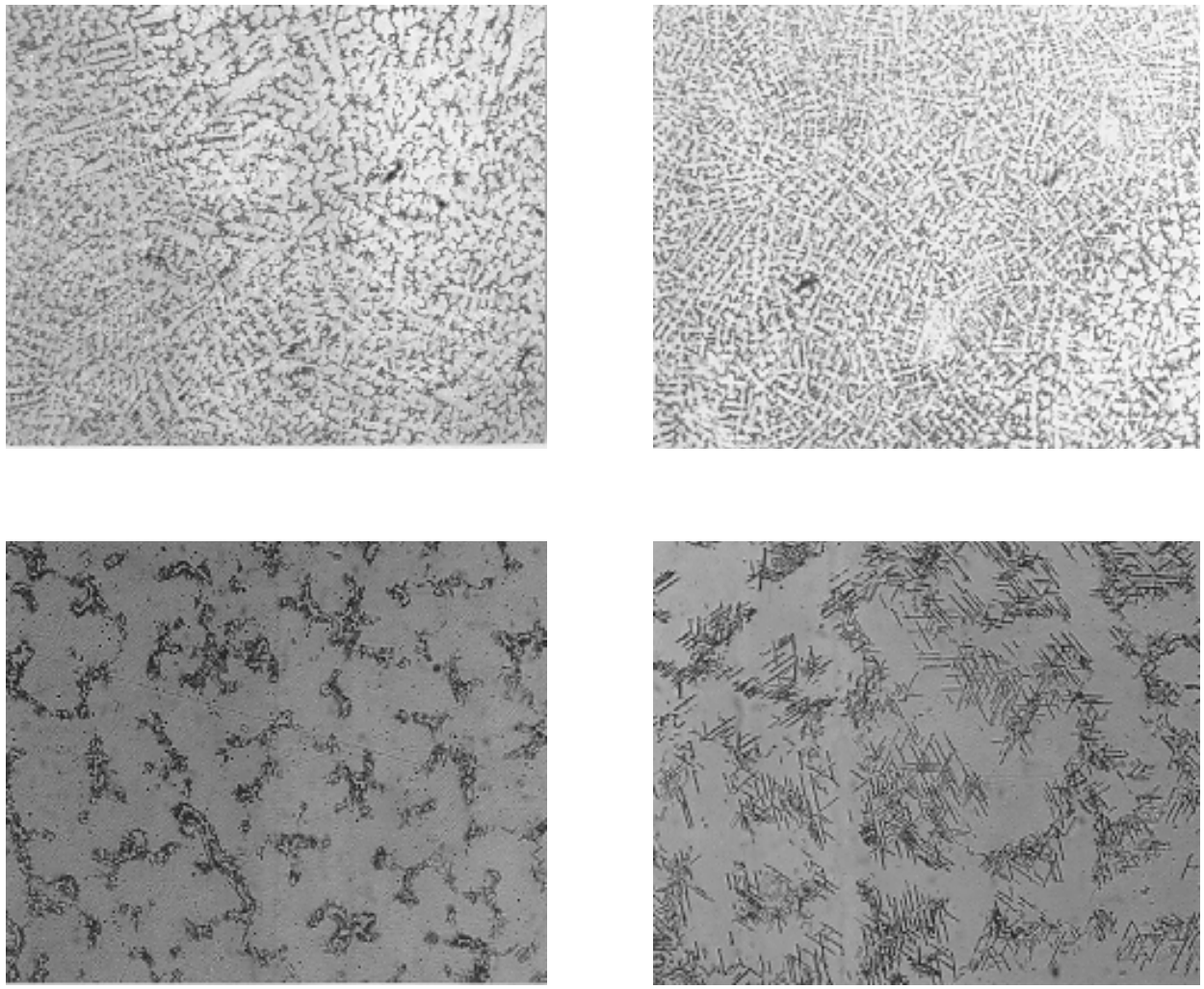

FIGURE 27. MICROSTRUCTURES FROM WROUGHT IN718 TUNGSTEN INERT GAS WELD HEAT AFFECTED ZONE EXPOSED TO STANDARD HEAT TREATMENT AND 30 SIMULATED REPAIR (1700°F) CYCLES

100X

500X

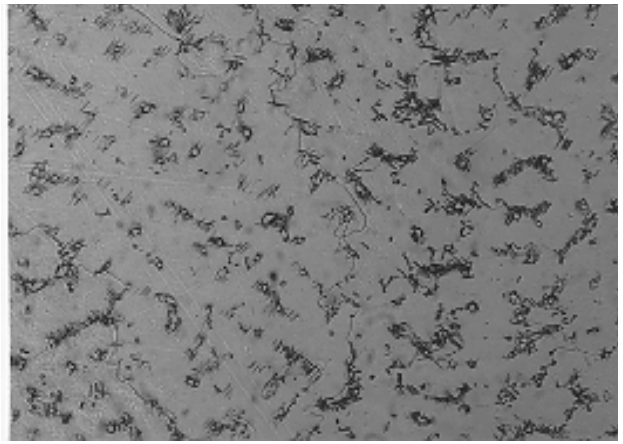

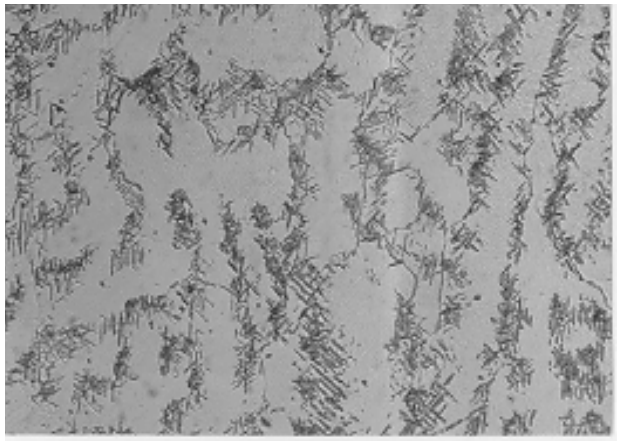

Cast+HIP IN718 Weld
Standard H.T.

Cast+HIP IN718 Weld
Standard H.T. + 30 Repair (1700°F) Cycles

FIGURE 28. MICROSTRUCTURES FROM CAST+HIP IN718 TUNGSTEN INERT GAS WELD EXPOSED TO STANDARD HEAT TREATMENT AND 30 SIMULATED REPAIR (1700°F) CYCLES

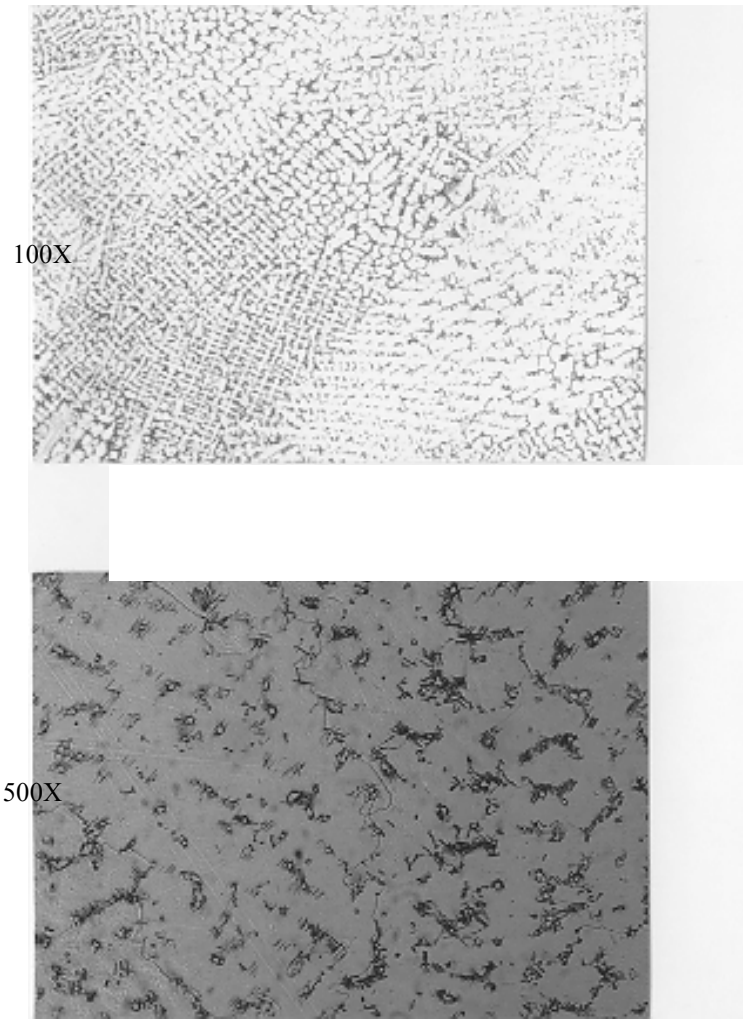

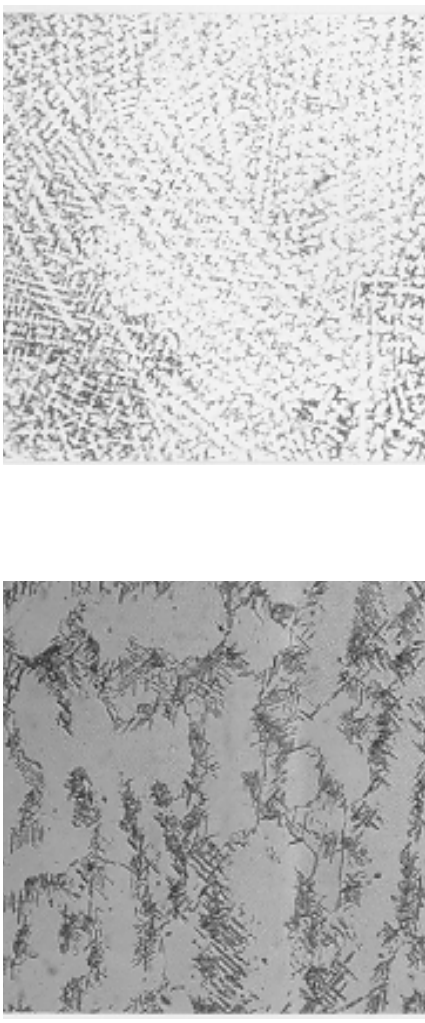

Cast+HIP IN718 Weld
Standard H.T.

Cast+HIP IN718 Weld
Standard H.T. + 30 Repair (1700°F) Cycles

28

FIGURE 28. MICROSTRUCTURES FROM CAST+HIP IN718 TUNGSTEN INERT GAS WELD EXPOSED TO STANDARD HEAT TREATMENT AND 30 SIMULATED REPAIR (1700°F) CYCLES

Crack growth rates in the weld heat affected zones (HAZ) were comparable to nonwelded baselines. However, the HAZ in both materials shows some crack growth rate acceleration after exposure to 30 thermal cycles. Results (figures 29 and 30) indicate a greater effect (i.e., faster acceleration) of the exposures in the cast HAZ than the wrought HAZ. However, the cast material tests again had a high degree of scatter which had to be edited over larger da/dn vs. ΔK ranges in order to achieve a reasonable comparison. Extensive delta phase precipitated throughout the HAZ after exposure (figures 31 and 32).

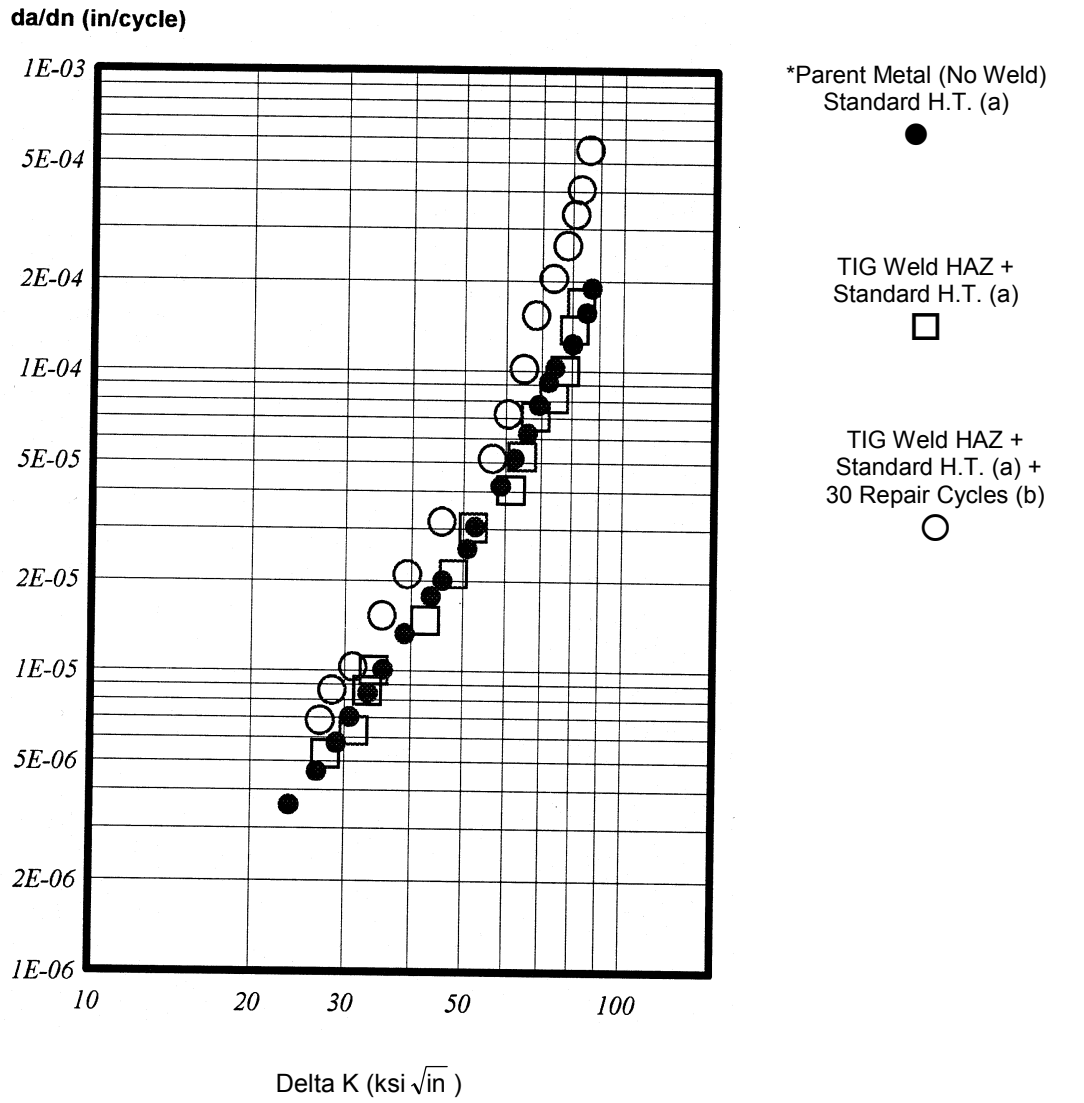

FIGURE 29. EFFECT OF MULTIPLE REPAIR (1700°F) CYCLES ON WROUGHT IN718 WELD HEAT AFFECTED ZONE REGIONS II AND III CRACK GROWTH 800°F, R = 0.05, FREQUENCY = 0.33 Hz

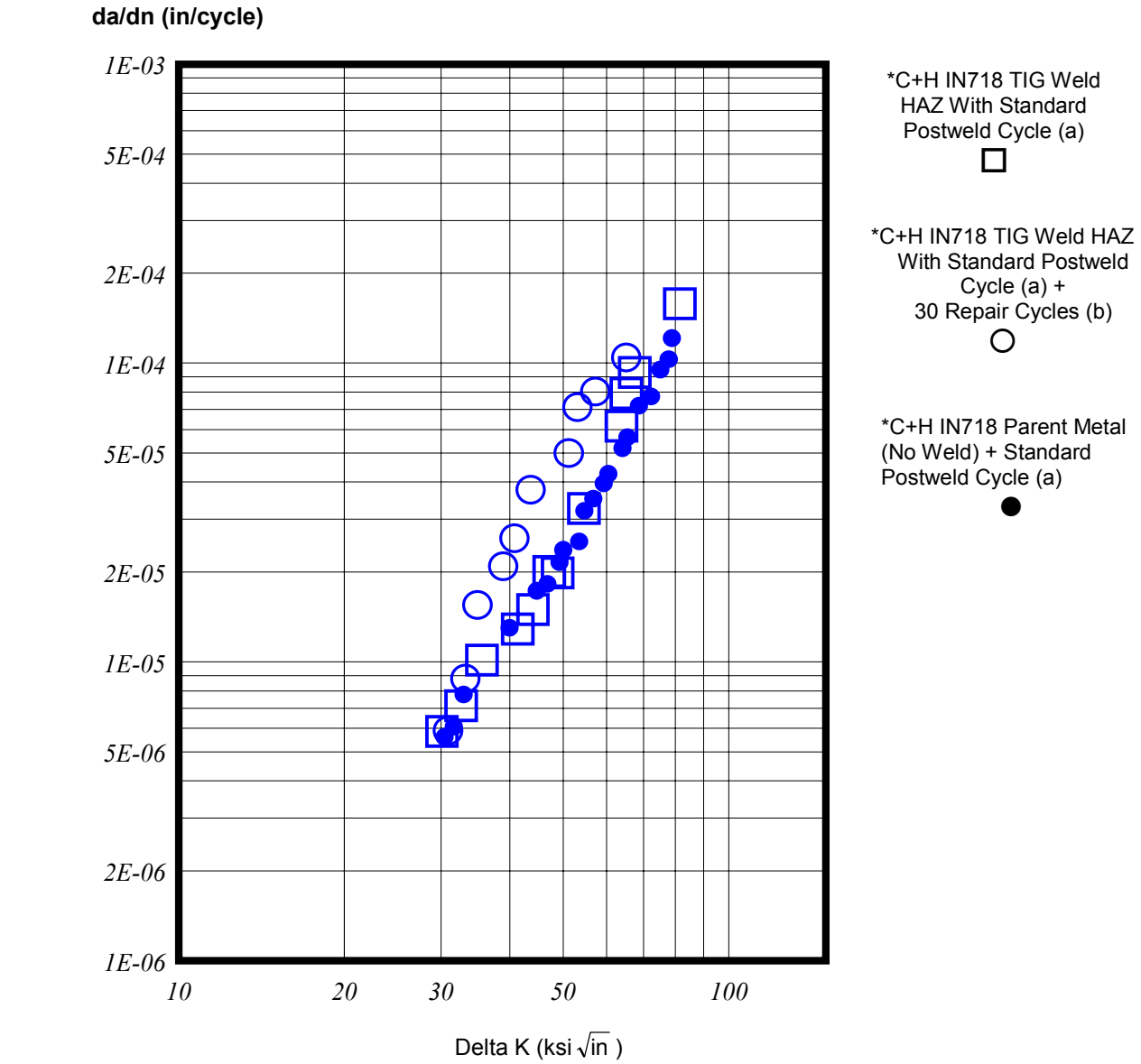

FIGURE 30. EFFECT OF MULTIPLE REPAIR (1700°F) CYCLES ON CAST IN718 TUNGSTEN INERT GAS WELD HEAT AFFECTED ZONE REGIONS II AND III CRACK GROWTH 800°F, R = 0.05, FREQUENCY = 0.33 Hz

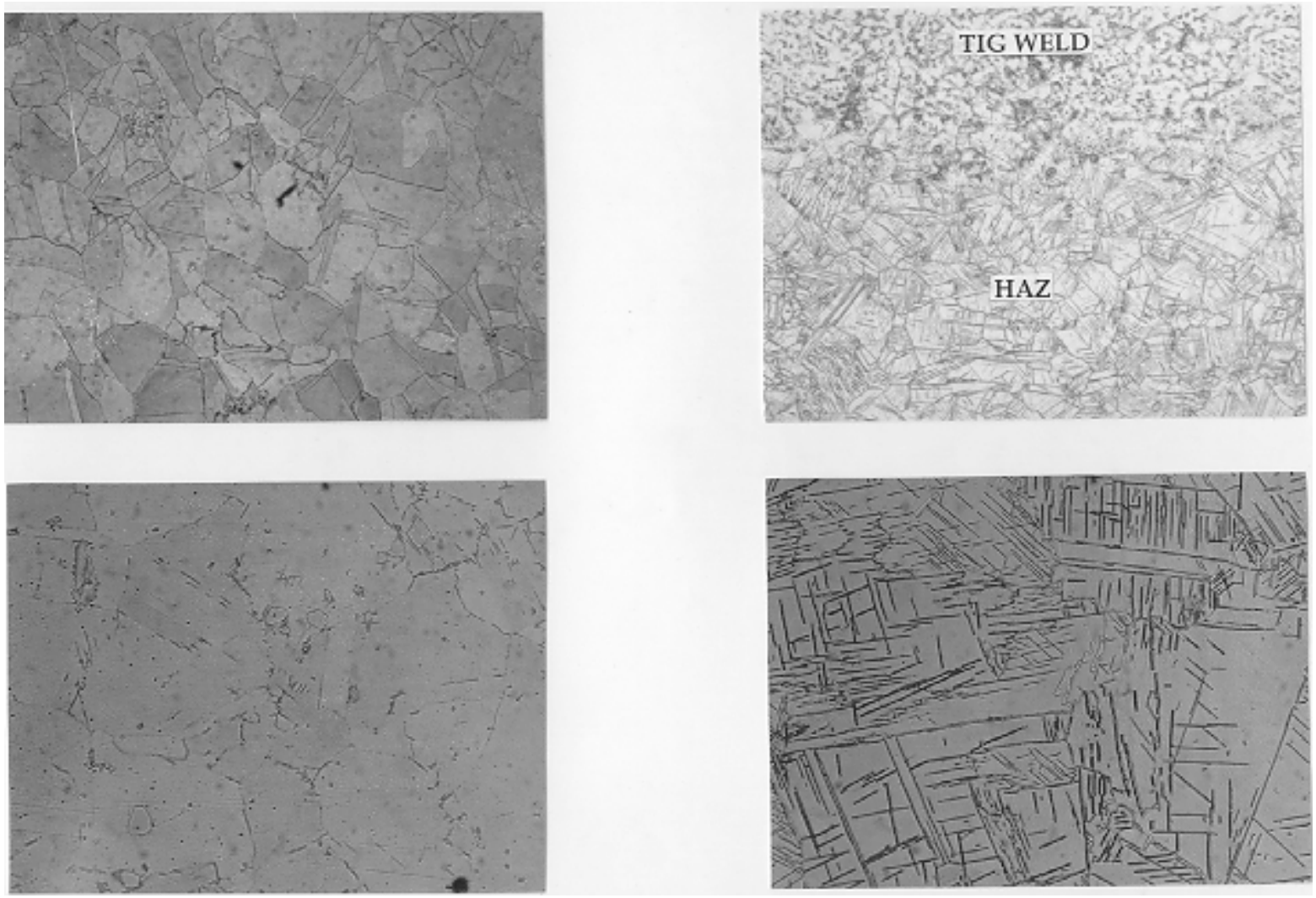

FIGURE 31. MICROSTRUCTURES FROM WROUGHT IN718 TUNGSTEN INERT GAS WELD HEAT AFFECTED ZONE EXPOSED TO STANDARD HEAT TREATMENT AND 30 SIMULATED REPAIR (1700°F) CYCLES

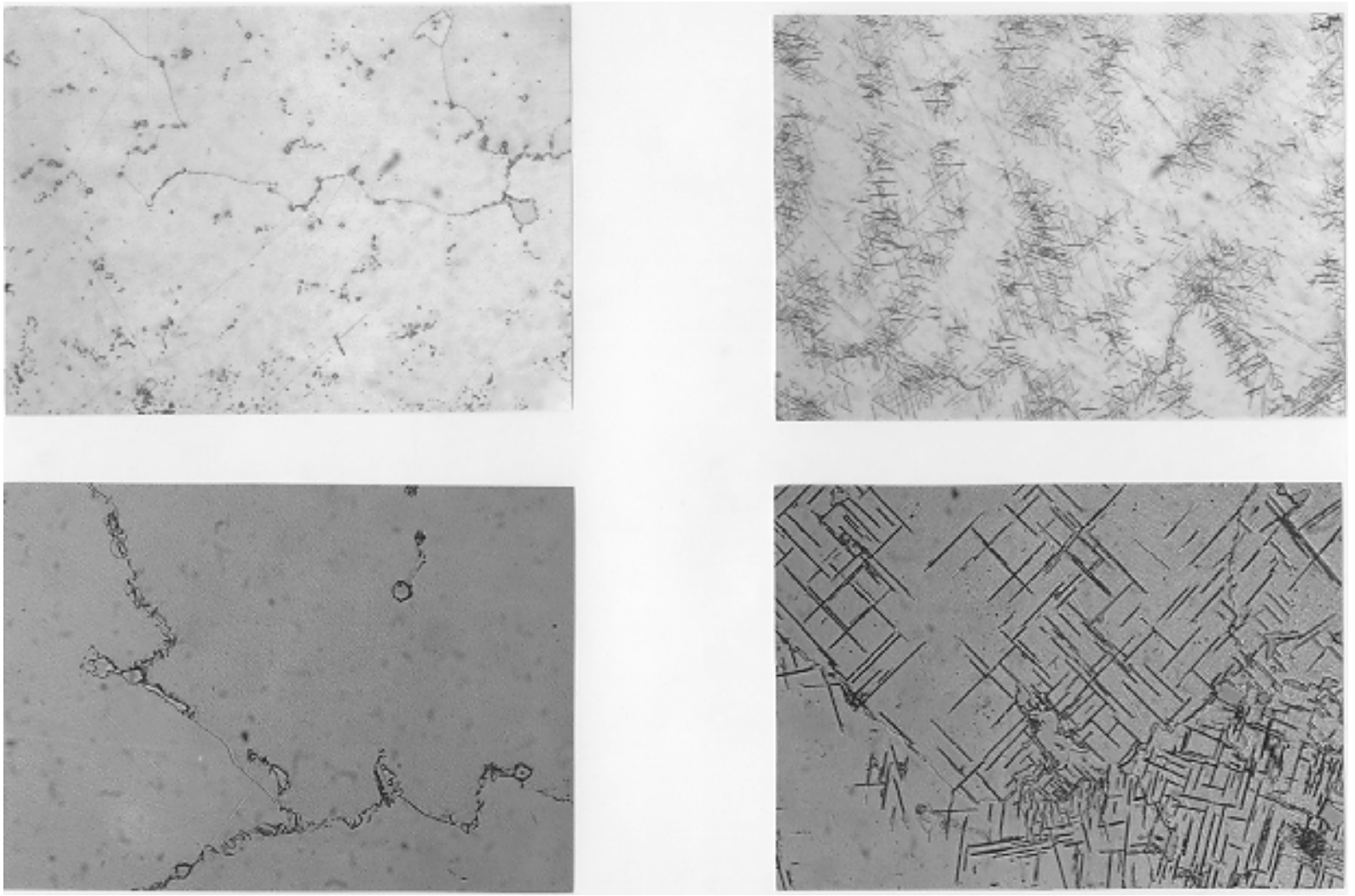

Cast+HIP IN718 Weld HAZ
Standard H.T.

Cast+HIP IN718 Weld HAZ
Standard H.T. + 30 Repair (1700°F) Cycles

FIGURE 32. MICROSTRUCTURES FROM CAST+HIP IN718 TUNGSTEN INERT GAS WELD HEAT AFFECTED ZONE EXPOSED TO STANDARD HEAT TREATMENT AND 30 SIMULATED REPAIR (1700°F) CYCLES

2.2.3 Subtask III: Material Testing to Investigate New Heat Treatment Developed for Weldability.

A 1-hour 1825°F preweld thermal cycle was being studied to improve the weldability of IN718 field casings exposed to several repair cycles. Casings are typically retired due to poor weldability as a result of extensive delta (Ni_3Cb) precipitating into the matrix during numerous stress relief (1700°F) cycles. The 1825°F treatment was expected to rejuvenate the weldability by partially solutioning the delta without an accompanying growth in grain size.

Wrought heat W997 (lowest Nb/B) having the best weldability and cast heat C996 (highest Nb/B) having the worst weldability were used for testing the effect of the 1825°F treatment on tensile, stress rupture, LCF, and crack growth rate properties. Both heats were exposed to 20 simulated repair cycles followed by a 1-hour 1825°F cycle plus age.

Delta phase (needles) in the wrought heat appear reduced (i.e., solutioned) and somewhat spherical after the 1825°F cycle (figure 33). The cast heat (figure 34), however, had a heavier precipitation of delta after the 1825°F treatment. The higher Nb content in the cast material probably requires higher temperatures for solutioning the delta. Grain size was not affected by the 1-hour 1825°F exposure.

Although delta content and morphology of the wrought and cast heats are affected differently by the 1825°F treatment, mechanical properties behave in a similar manner. Yield and tensile strengths of the wrought heat (figures 35 and 36) increase slightly but not to baseline levels. Rupture lives (figure 37) are still at about 30 hours for 1200°F/100 Kpsi but ductility remains high with an average elongation of 32 percent. Tensile and rupture properties of the cast heat show only slight effects of the 1825°F treatment (figures 38, 39, and 40). LCF strength and crack growth rates in both materials (figures 41, 42, 43, and 44) are not affected by the 1825°F treatment which probably relates to the grain size remaining constant through all treatments.

2.2.4 Subtask IV: Cast+HIP IN718 Crack Growth Properties at 300°F.

A sigmodial crack growth rate curve and Walker (mean stress) exponent were generated at 300°F for cast+HIP IN718 (figure 45). This expands the existing database which was required for the task I crack growth analysis of cast+HIP IN718 casings. Specimens machined from a CFM56 combustion case were tested for threshold determination and crack growth rates at four different positive R-ratios. The curve was fit through the Walkerized data which was then used for back-predicting specimen lives to a 4X scatterband.

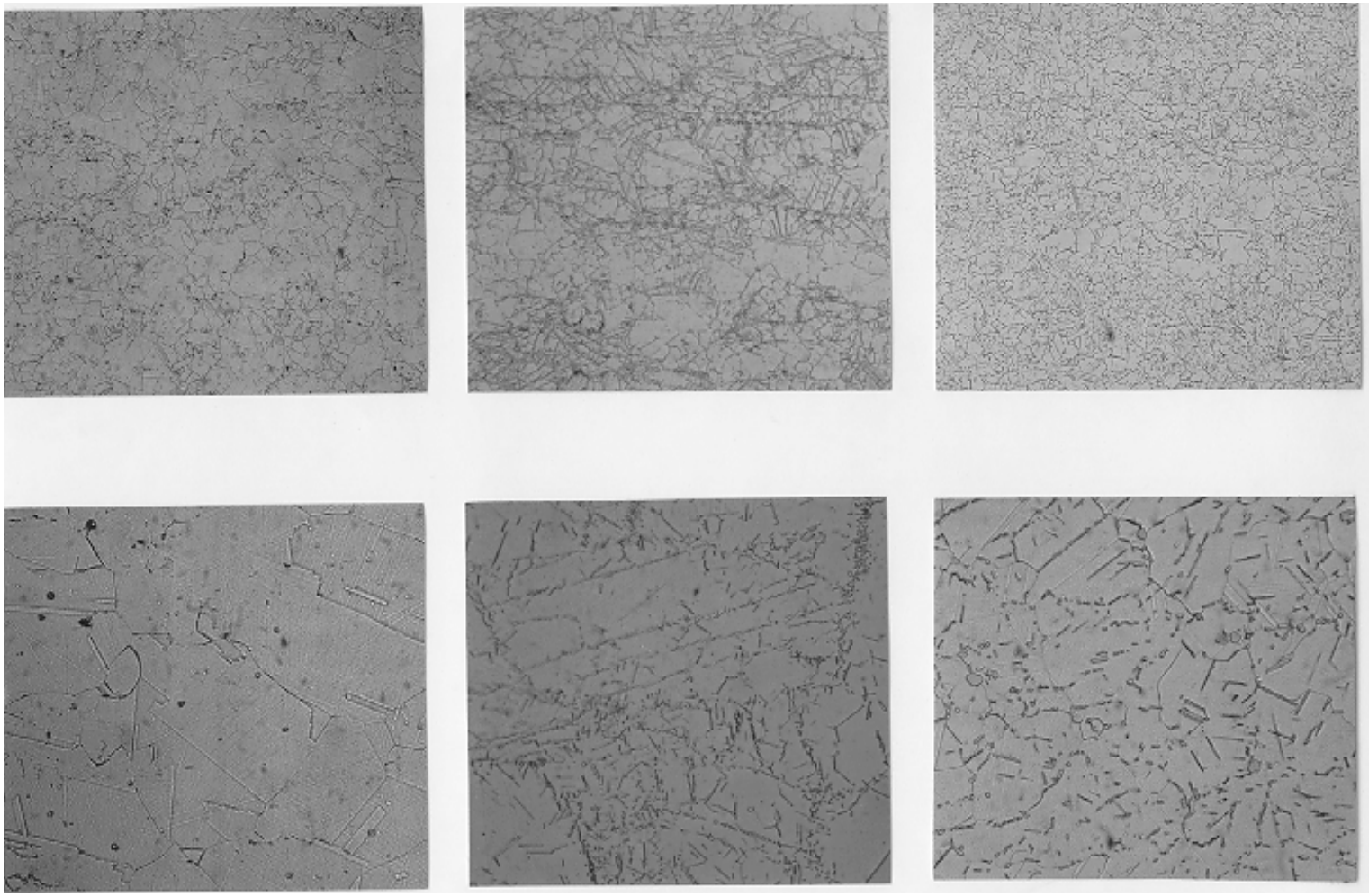

FIGURE 33. MICROSTRUCTURES OF IN718 PLATE WG997 (4.33%-4.55% Nb) AFTER EXPOSURE TO STANDARD HEAT TREATMENT, 20 SIMULATED REPAIR (1700°F) CYCLES, AND 20 REPAIR CYCLES PLUS 1825°F REJUVENATION CYCLE

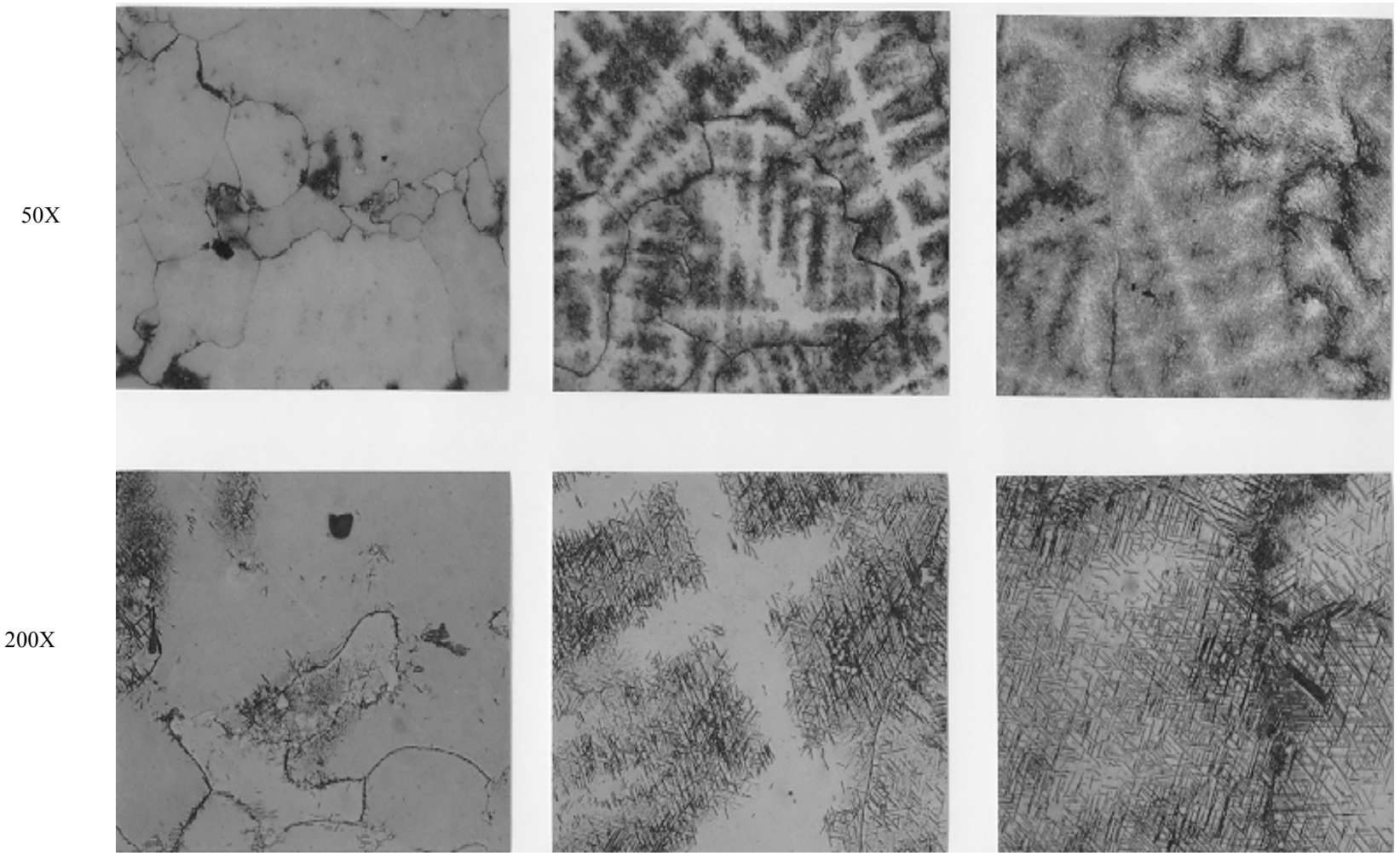

FIGURE 34. MICROSTRUCTURES OF CAST+HIP IN718 PLATE CG996 (5.41%-5.49% Nb) AFTER EXPOSURE TO STANDARD HEAT TREATMENT, 20 SIMULATED REPAIR (1700°F) CYCLES, AND 20 REPAIR CYCLES PLUS 1825°F REJUVENATION CYCLE

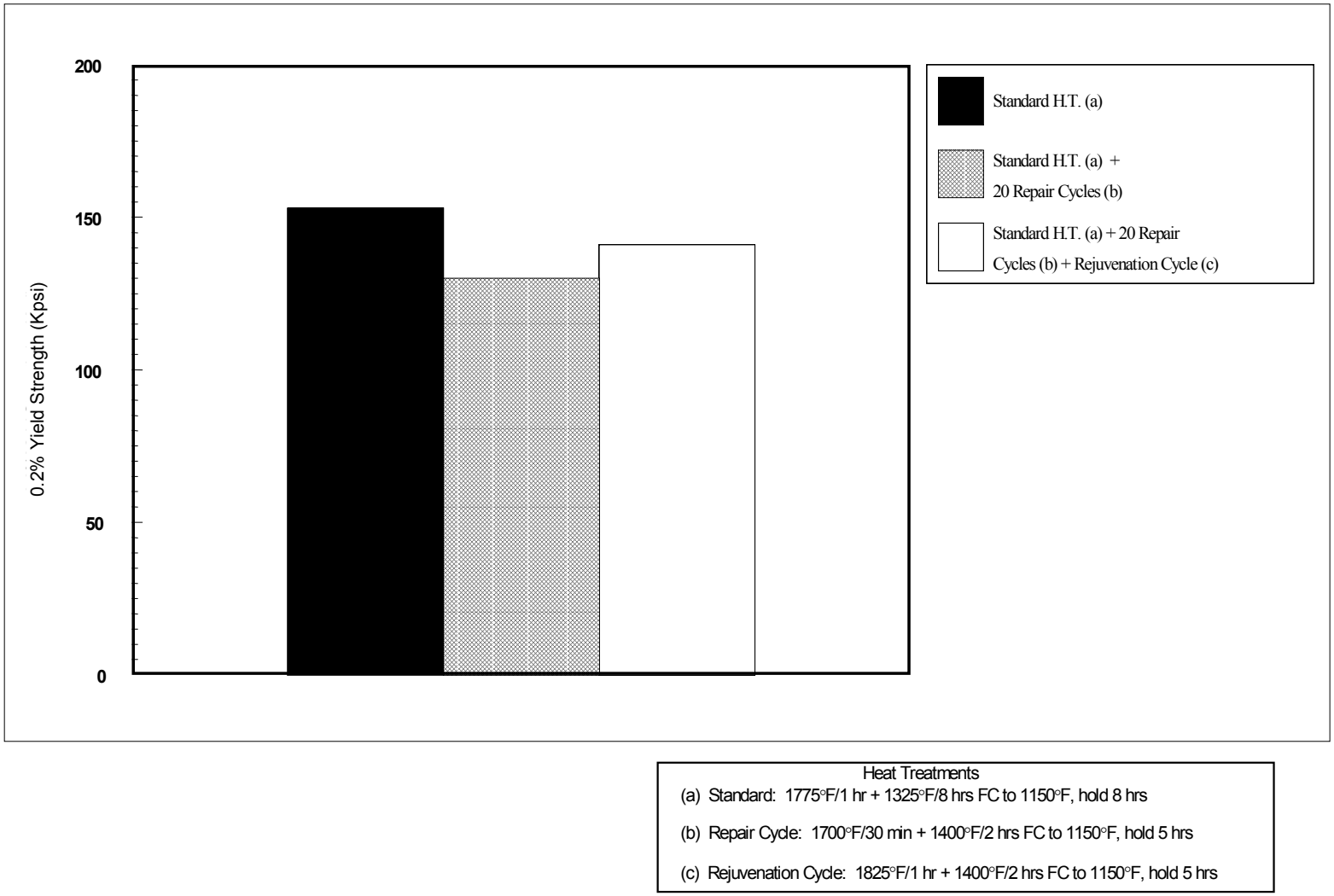

FIGURE 35. EFFECT OF 1825°F REJUVENATION HEAT TREATMENT CYCLE ON WROUGHT IN718 0.2% YIELD STRENGTH (ROOM TEMPERATURE)

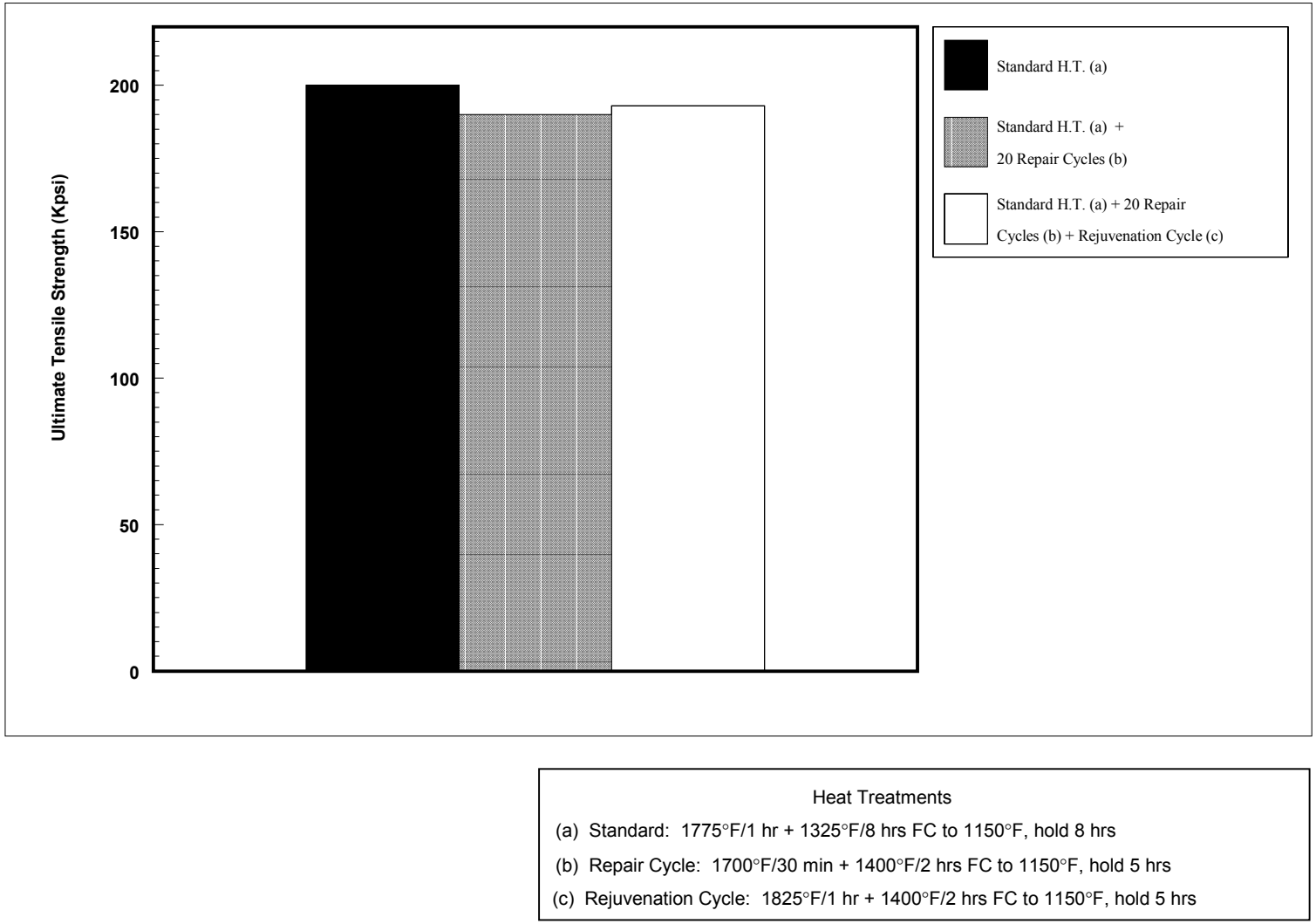

FIGURE 36. EFFECT OF 1825°F REJUVENATION HEAT TREATMENT CYCLE ON WROUGHT IN718 ULTIMATE TENSILE STRENGTH (ROOM TEMPERATURE)

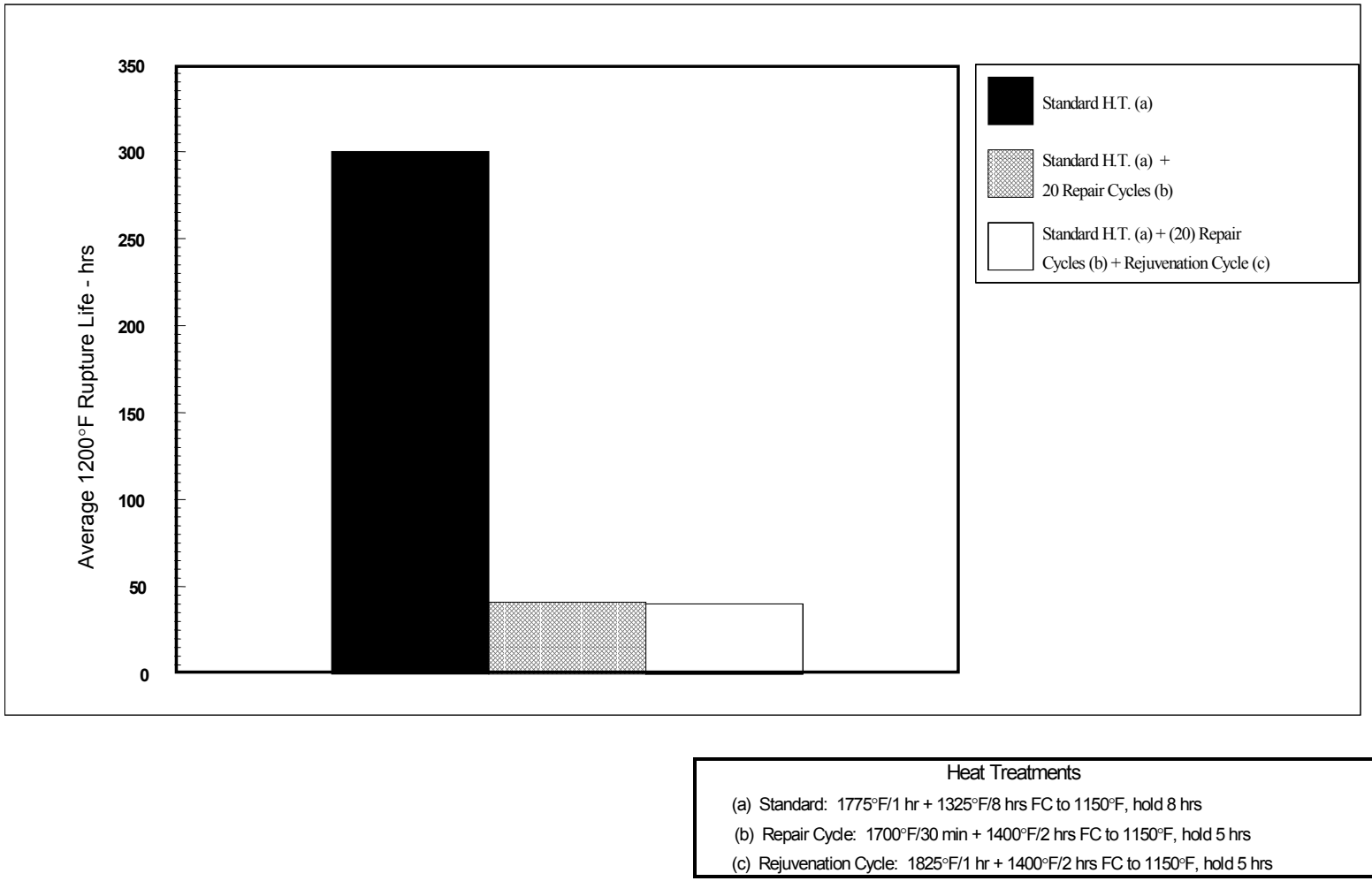

FIGURE 37. EFFECT OF 1825°F REJUVENATION HEAT TREATMENT CYCLE ON WROUGHT IN718 STRESS RUPTURE (1200°F AT 100 Kpsi)

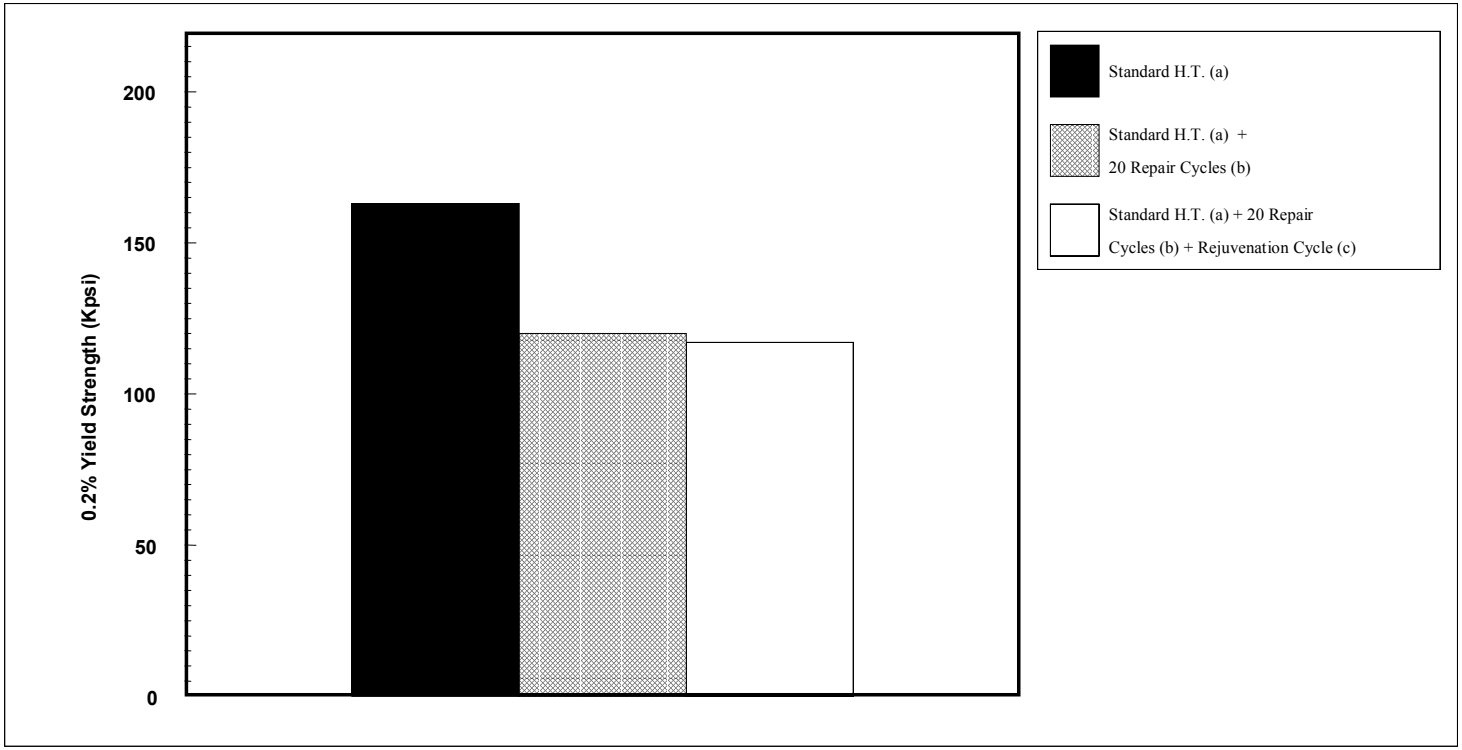

FIGURE 38. EFFECT OF 1825°F REJUVENATION HEAT TREATMENT CYCLE ON CAST+HIP IN718 0.2% YIELD STRENGTH (ROOM TEMPERATURE)

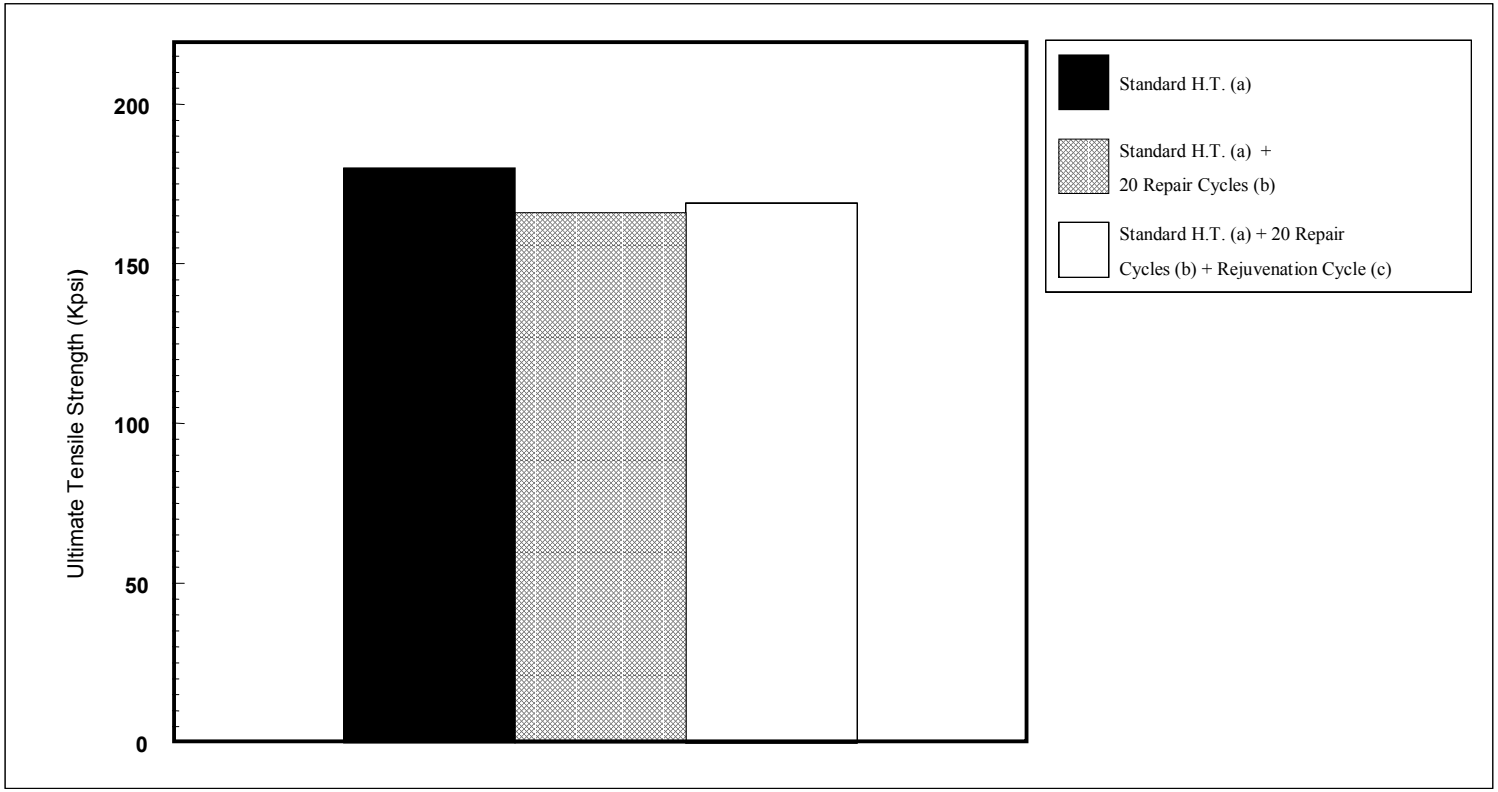

FIGURE 39. EFFECT OF 1825°F REJUVENATION HEAT TREATMENT CYCLE ON CAST+HIP IN718 ULTIMATE TENSILE STRENGTH (ROOM TEMPERATURE)

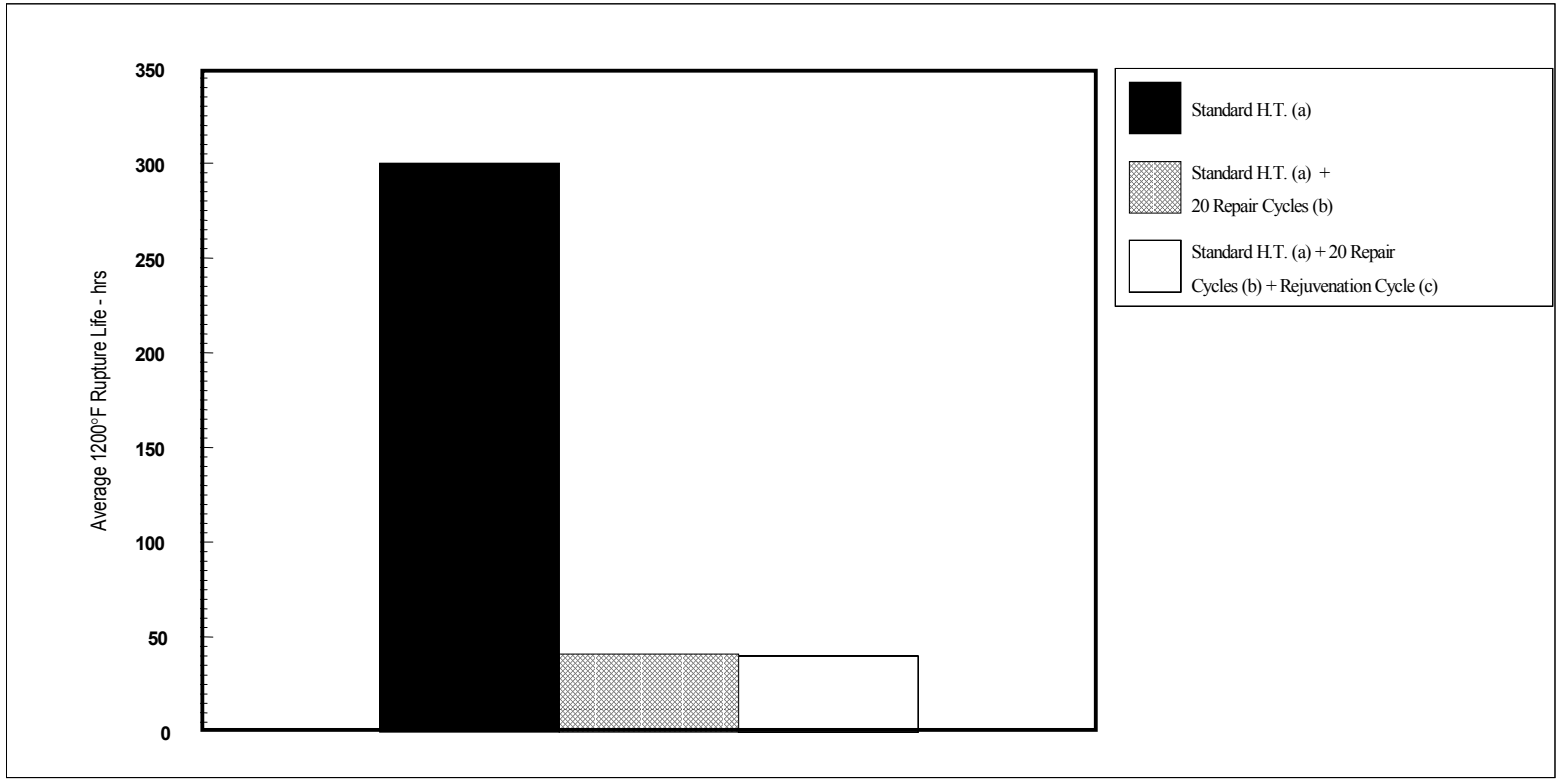

Material

Cast+HIP Plate (0.3" Thick)
5.41%-5.49% Nb, 0.006%B

Heat Treatments

(a) Standard: 2050°F HIP + 1925°F/1 hr + 1750°F/1 hr + 1400°F/5 hrs FC to 1200°F, hold 1 hr
(b) Repair Cycle: 1700°F/30 min + 1400°F/2 hrs FC to 1150°F, hold 5 hrs
(c) Rejuvenation Cycle: 1825°F/1 hr + 1400°F/2 hrs FC to 1150°F, hold 5 hrs

FIGURE 40. EFFECT OF 1825°F REJUVENATION HEAT TREATMENT CYCLE ON CAST+HIP IN718 STRESS RUPTURE LIFE (1200°F AT 95 Kpsi)

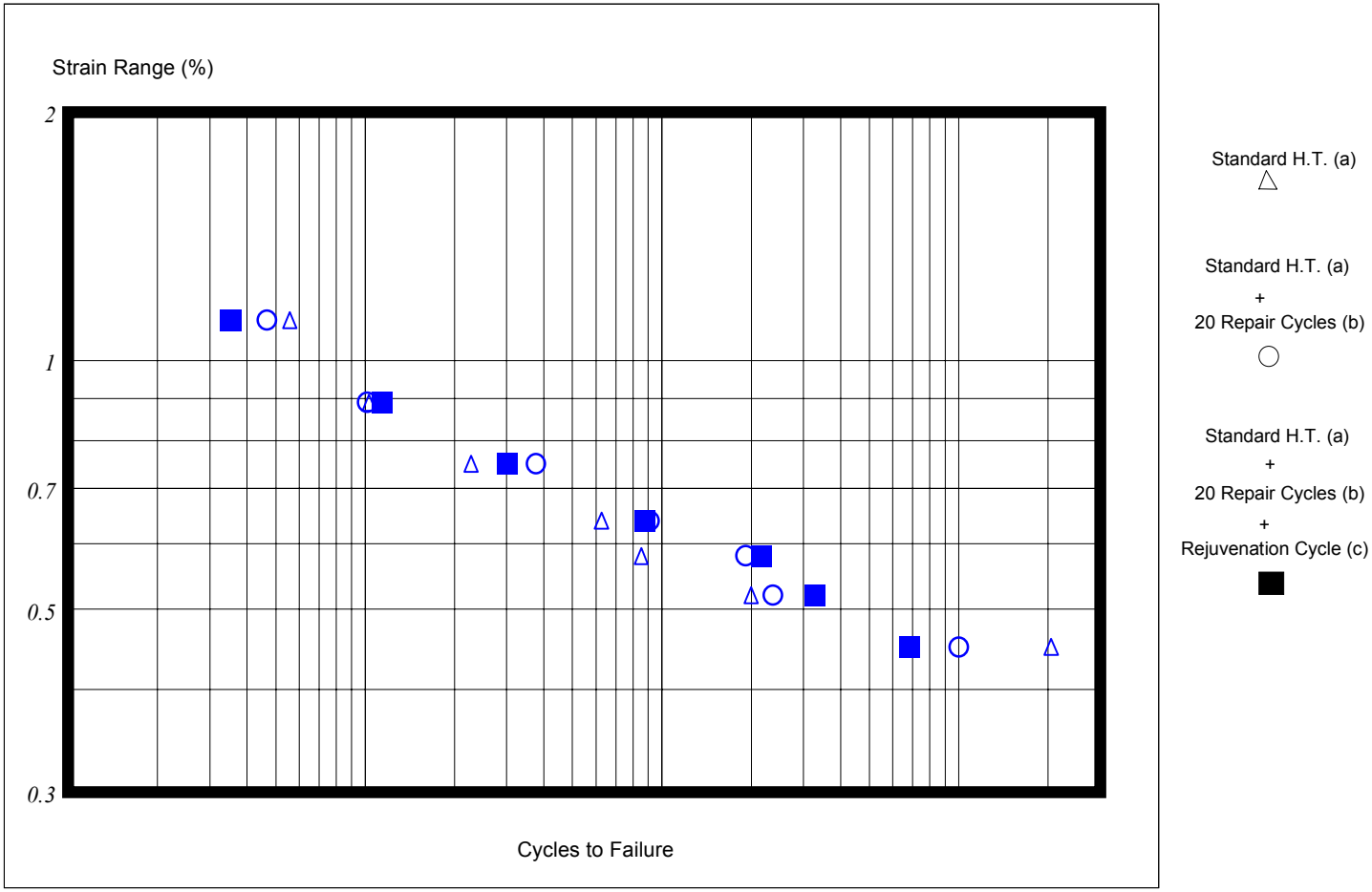

Material
Wrought Plate (0.3" Thick)
4.33%-4.55% Nb, 0.003%B
ASTM 7.5 Grain Size

Heat Treatments
(a) Standard: 1775°F/1 hr + 1325°F/8 hrs FC to 1150°F, hold 8 hrs
(b) Repair Cycle: 1700°F/30 min + 1400°F/2 hrs FC to 1150°F, hold 5 hrs
(c) Rejuvenation Cycle: 1825°F/1 hr + 1400°F/2 hrs FC to 1150°F, hold 5 hrs

FIGURE 41. EFFECT OF 1825°F REJUVENATION HEAT TREATMENT CYCLE ON WROUGHT IN718 LOW-CYCLE FATIGUE 800°F, R = 0.0, STRAIN CONTROL

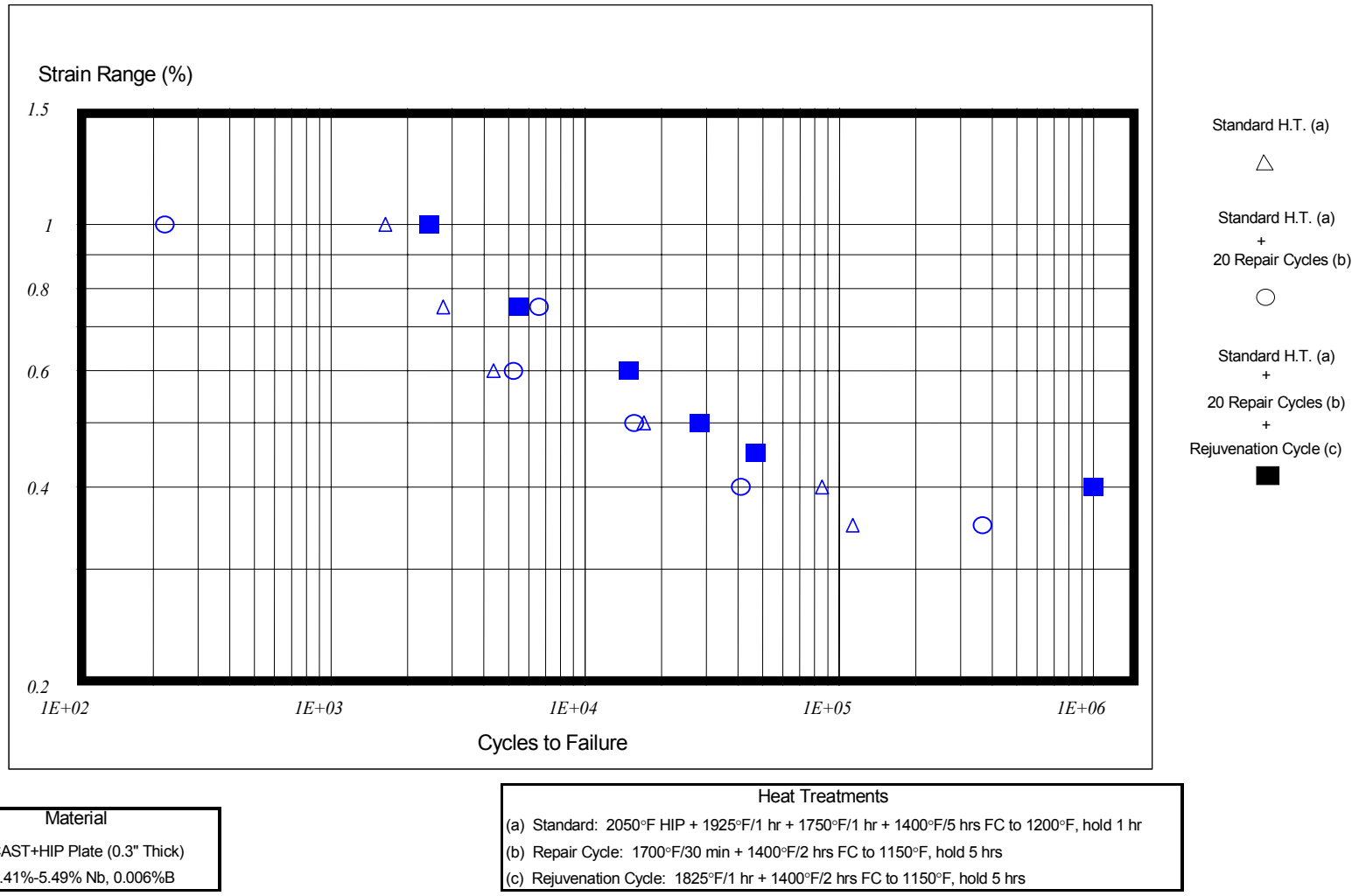

FIGURE 42. EFFECT OF 1825°F REJUVENATION HEAT TREATMENT CYCLE ON CAST+HIP IN718 LOW-CYCLE FATIGUE 800°F, R = 0.0, FREQUENCY = 0.33 Hz

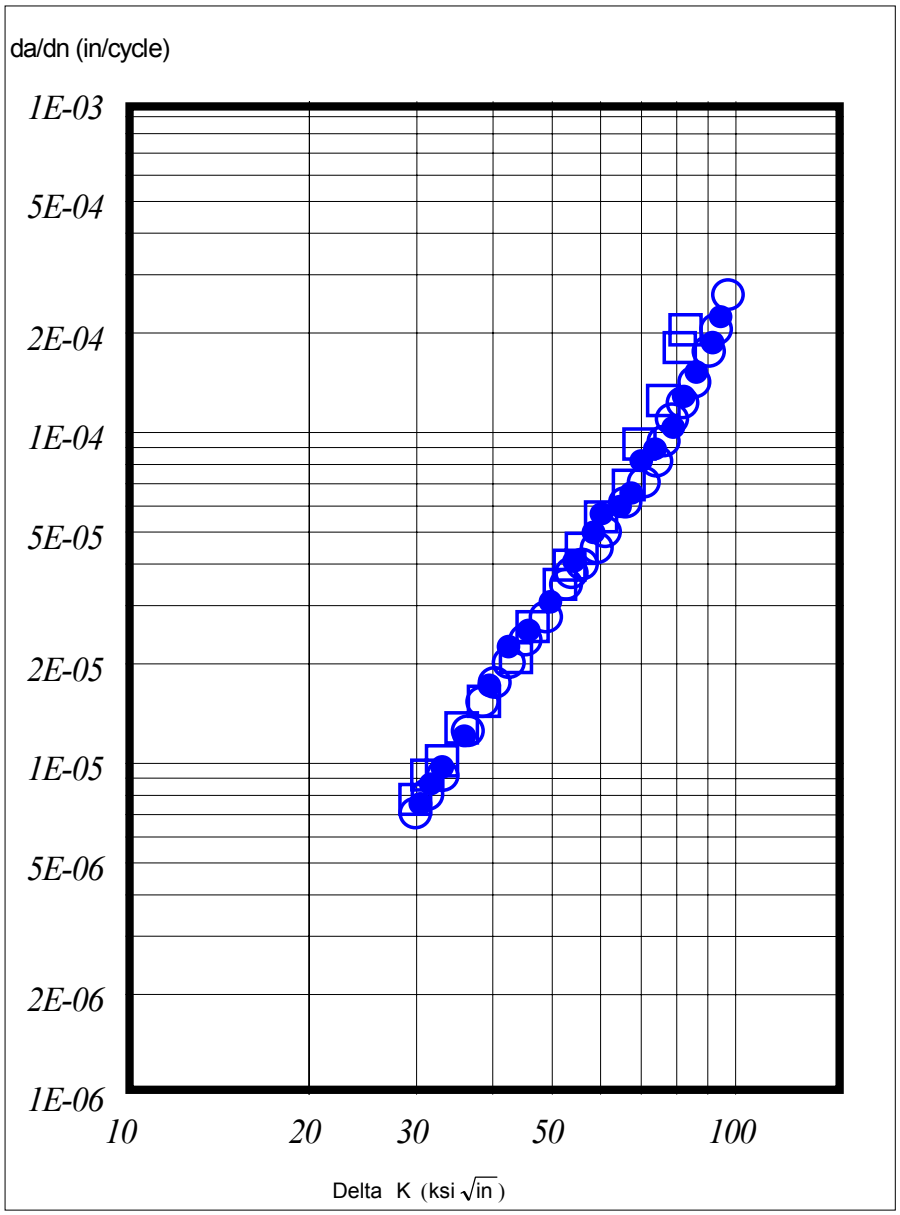

Material	Heat Treatments
Wrought Plate (0.3" Thick) 4.33%-4.55% Nb, 0.003%B ASTM 7.5 Grain Size	(a) Standard: 1775°F/1 hr + 1325°F/8 hrs FC to 1150°F, hold 8 hrs (b) Repair Cycle: 1700°F/30 min + 1400°F/2 hrs FC to 1150°F, hold 5 hrs (c) Rejuvenation Cycle: 1825°F/1 hr + 1400°F/2 hrs FC to 1150°F, hold 5 hrs

FIGURE 43. EFFECT OF 1825°F REJUVENATION HEAT TREATMENT CYCLE ON WROUGHT IN718 CRACK GROWTH RATE 800°F, R = 0.05, FREQUENCY = 0.33 Hz

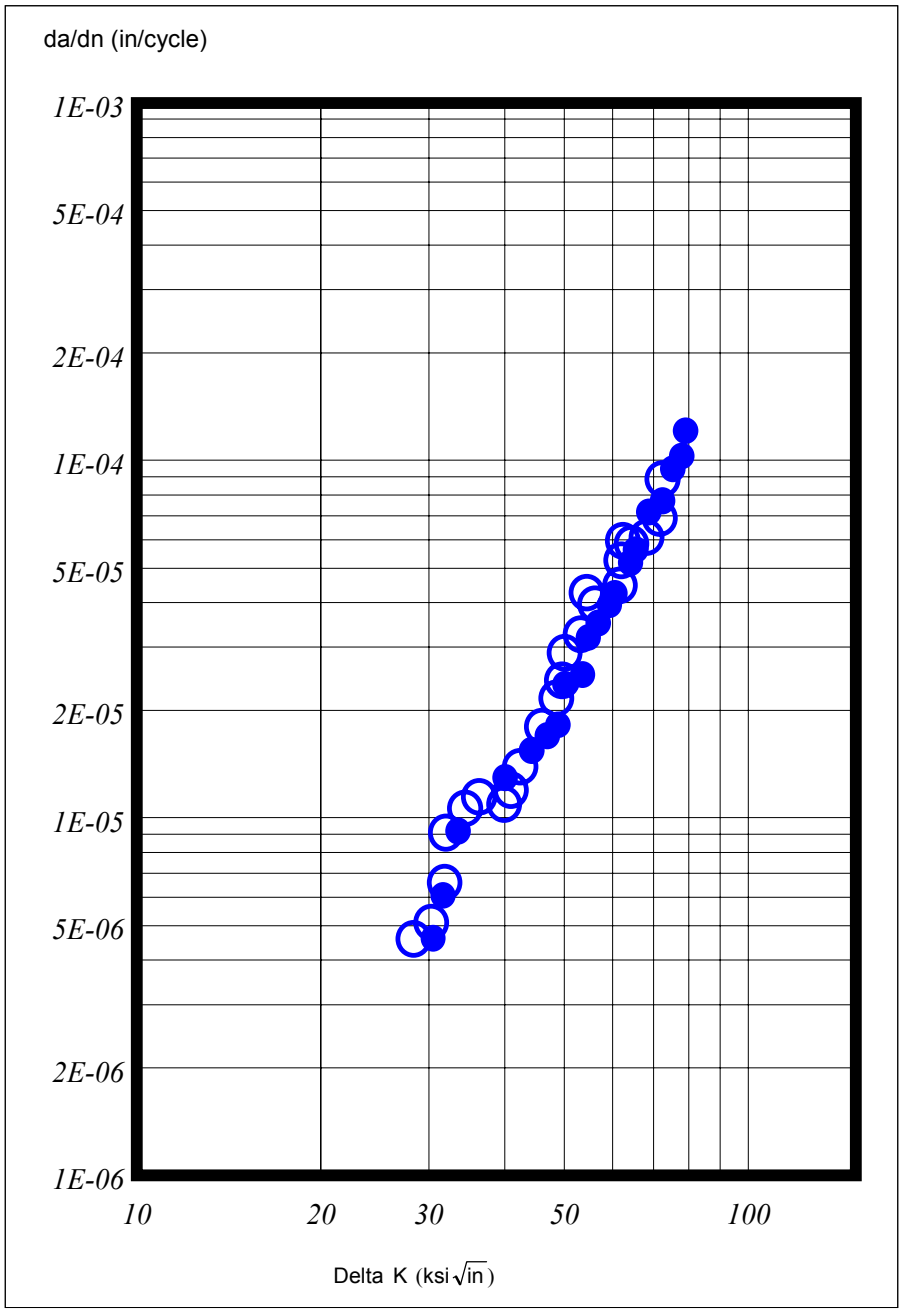

Material
Cast+HIP Plate (0.3" Thick)
5.41%-5.49% Nb, 0.006%B
*CFM56 Case (5.41% Nb)

Heat Treatments
(a) Standard: 2050°F HIP + 1925°F/1 hr + 1750°F/1hr + 1400°F/5 hrs FC to 1200°F, hold 1 hr
(b) Repair Cycle: 1700°F/30 min + 1400°F/2 hrs FC to 1150°F, hold 5 hrs
(c) Rejuvenation Cycle: 1825°F/1 hr + 1400°F/2 hrs FC to 1150°F, hold 5 hrs

FIGURE 44. EFFECT OF 1825°F REJUVENATION HEAT TREATMENT CYCLE ON CAST+HIP IN718 CRACK GROWTH RATE 800°F, R = 0.05, FREQUENCY = 0.33 Hz

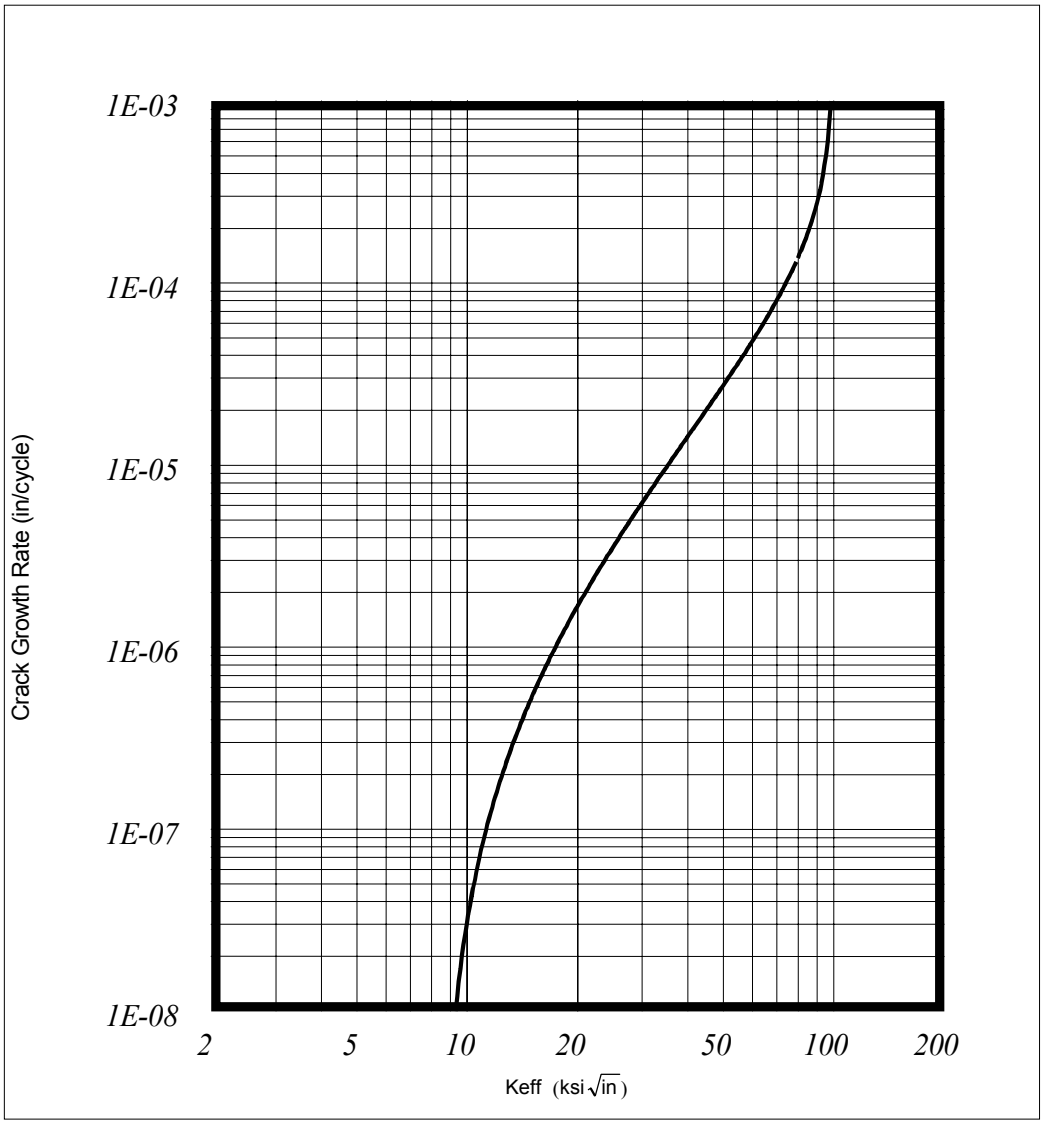

Material:	Cast+HIP IN718
Part Name:	CFM56 Combustion Case
Heat Treatment:	2050°F HIP + 1925°F/1 hr + 1750°F/1 hr + 1400°F/5 hrs FC to 1200°F, hold 1 hr

FIGURE 45. CAST+HIP IN718 CRACK GROWTH RATE CURVE 300°F, FREQUENCY = 0.33 Hz, m+ = 0.52505

2.2.5 Subtask IV: Material Property Testing in Support of EWI.

Tensile, stress rupture, and LCF testing in support of the weldability studies by EWI (Edison Welding Institute) shows the effect of multiple repair cycling on cast+HIP IN718 and wrought IN718 from three different heats of material (e.g., Nb/B variations). These elements are major factors in the weldability of IN718. Tensile and stress rupture data are presented in bar graph form as the average from three tests while LCF results are plotted as individual points.

Reductions in tensile (yield, ultimate) strength and stress rupture life occur in both materials following multiple thermal cycles (figures 46-51), however, rupture ductility remains high (figure 52). Higher Nb/B heats trended toward higher tensile strength and more extensive delta precipitation with multiple treatments (figures 53 and 54).

Multiple thermal treatments did not degrade the low-cycle fatigue strength of either material at any Nb/B level (figures 55-60). Some cast (low Nb/B heat) data fell below baseline, however, most of these were due to heavy microporosity at the fatigue origin. Although the cast material was hipped, several specimens contained porosity. Results from wrought heat W995 (medium Nb/B) indicate a higher fatigue strength for the multiple treatments over the baseline. However, for some unknown reason, the grain size was much coarser in the baseline specimens than it was in the exposed groups which could account for this unexpected result.

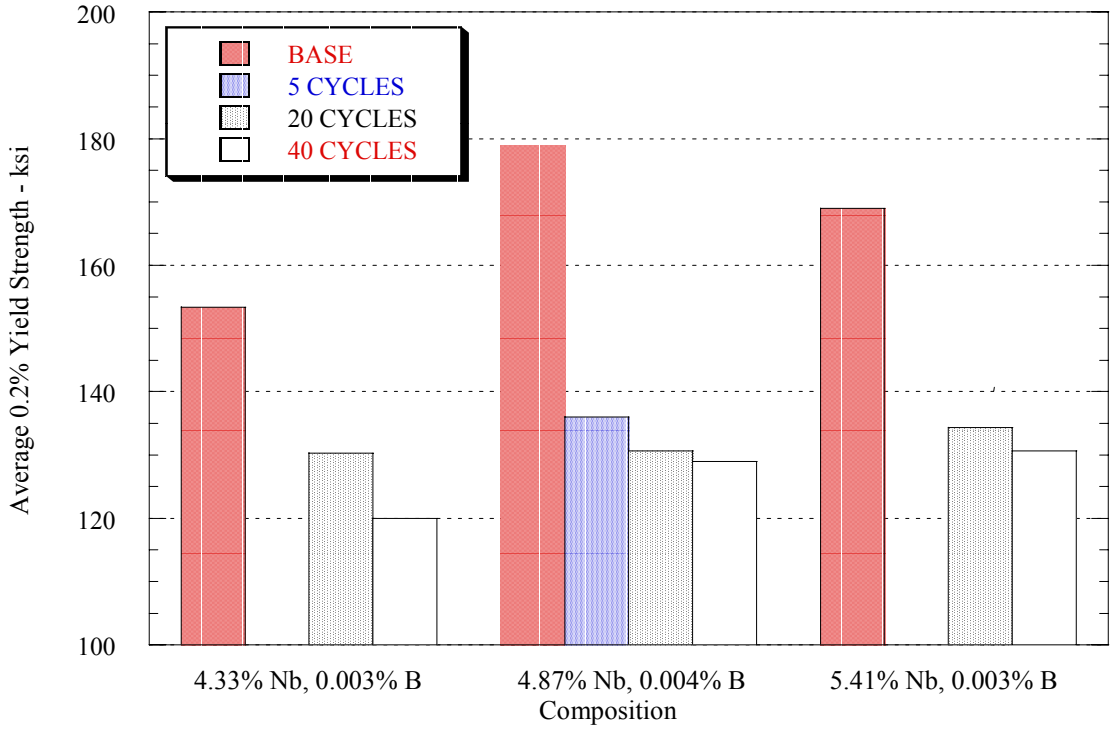

FIGURE 46. EFFECT OF MULTIPLE POSTREPAIR THERMAL CYCLES ON WROUGHT IN718 0.2% YIELD STRENGTH

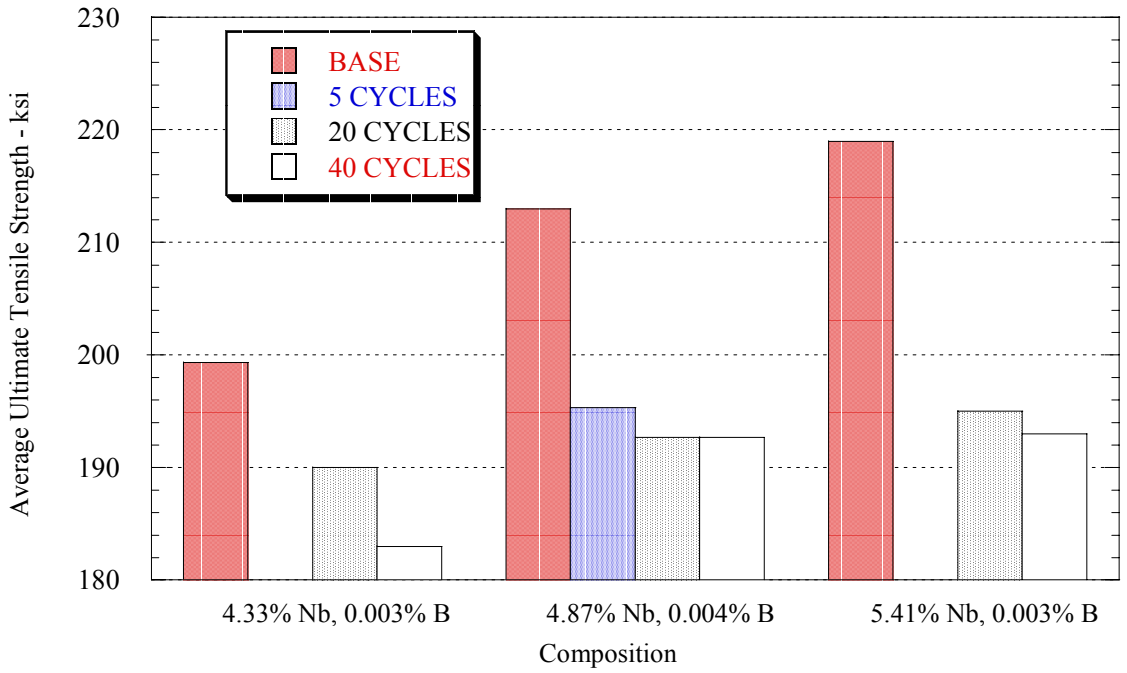

FIGURE 47. EFFECT OF MULTIPLE POSTREPAIR THERMAL CYCLES ON WROUGHT IN718 ULTIMATE TENSILE STRENGTH

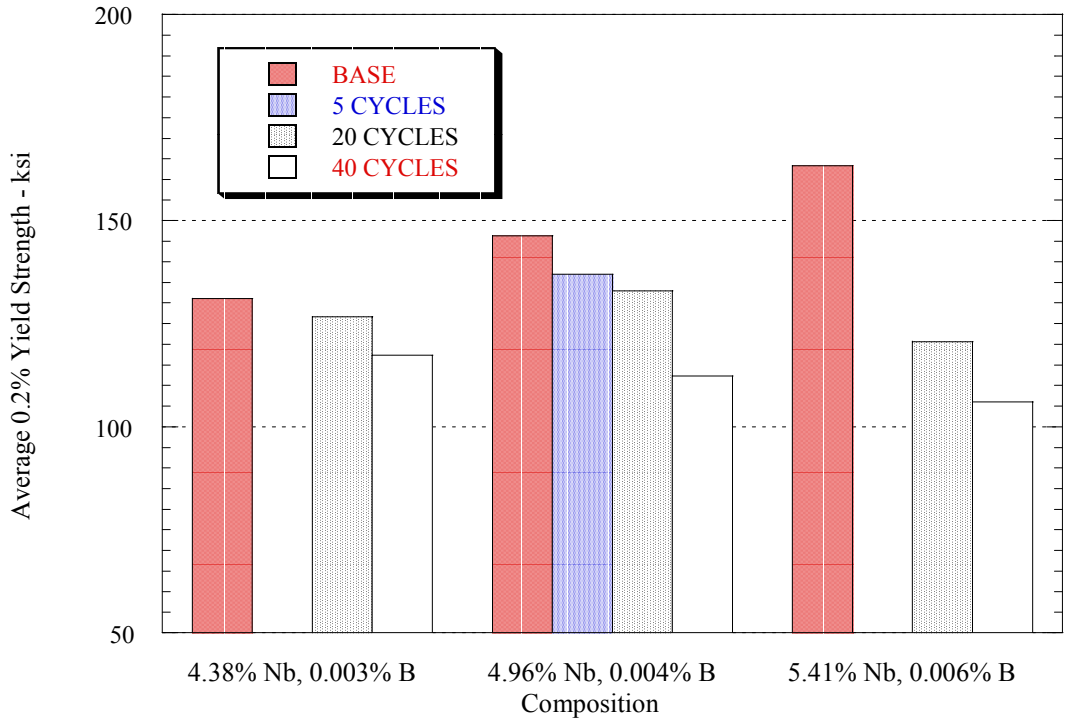

FIGURE 48. EFFECT OF MULTIPLE POSTREPAIR THERMAL CYCLES ON CAST+HIP IN718 0.2% YIELD STRENGTH

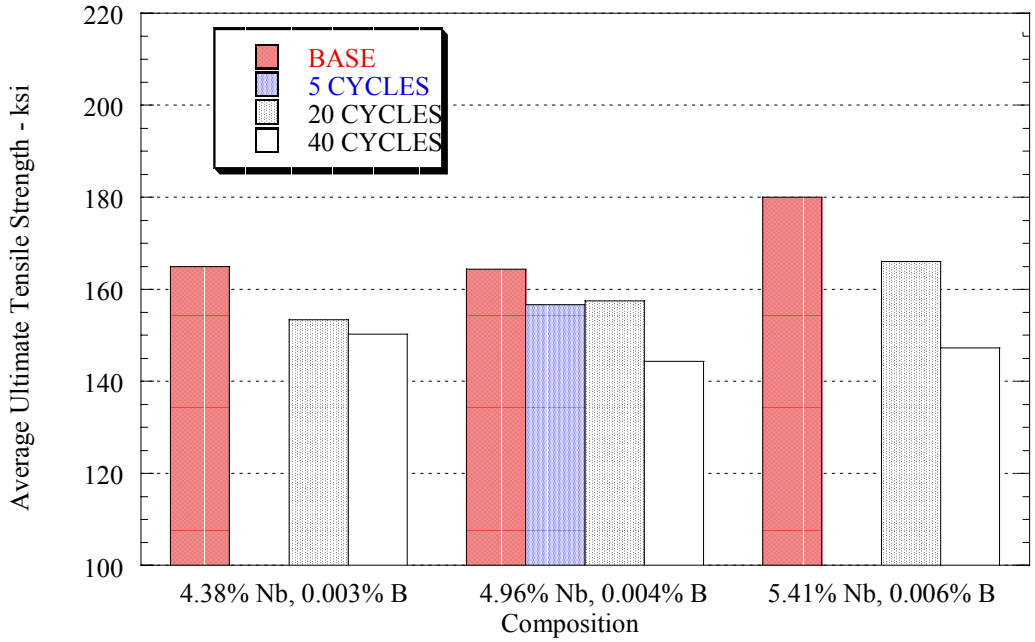

FIGURE 49. EFFECT OF MULTIPLE POSTREPAIR THERMAL CYCLES ON CAST+HIP IN718 ULTIMATE TENSILE STRENGTH

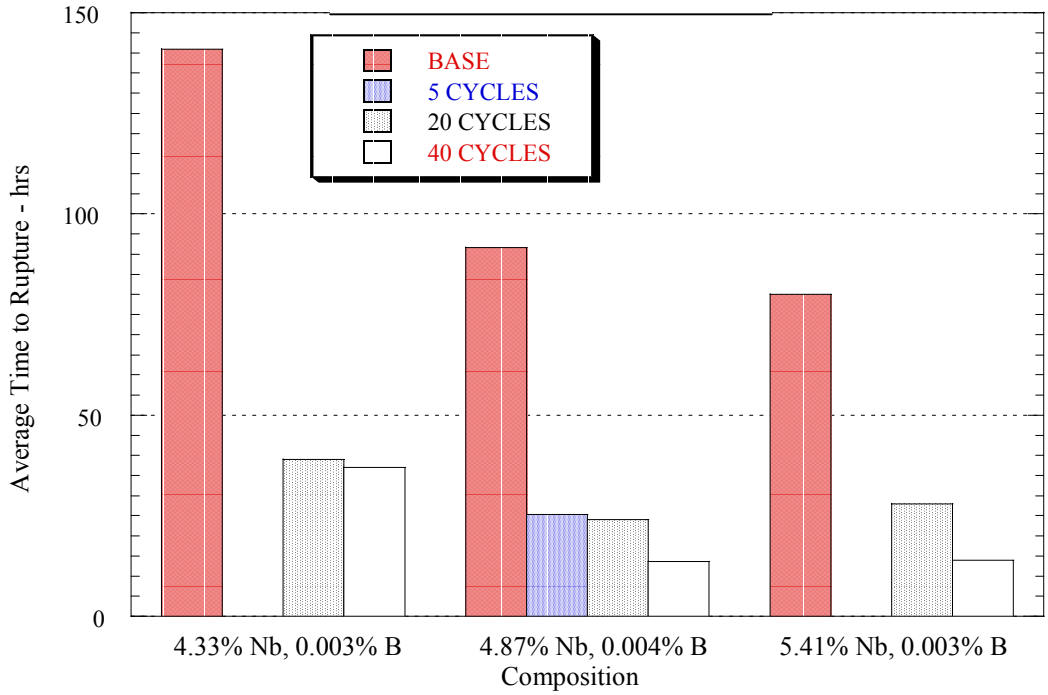

FIGURE 50. EFFECT OF MULTIPLE POSTREPAIR THERMAL CYCLES ON WROUGHT IN718 1200°F RUPTURE LIFE

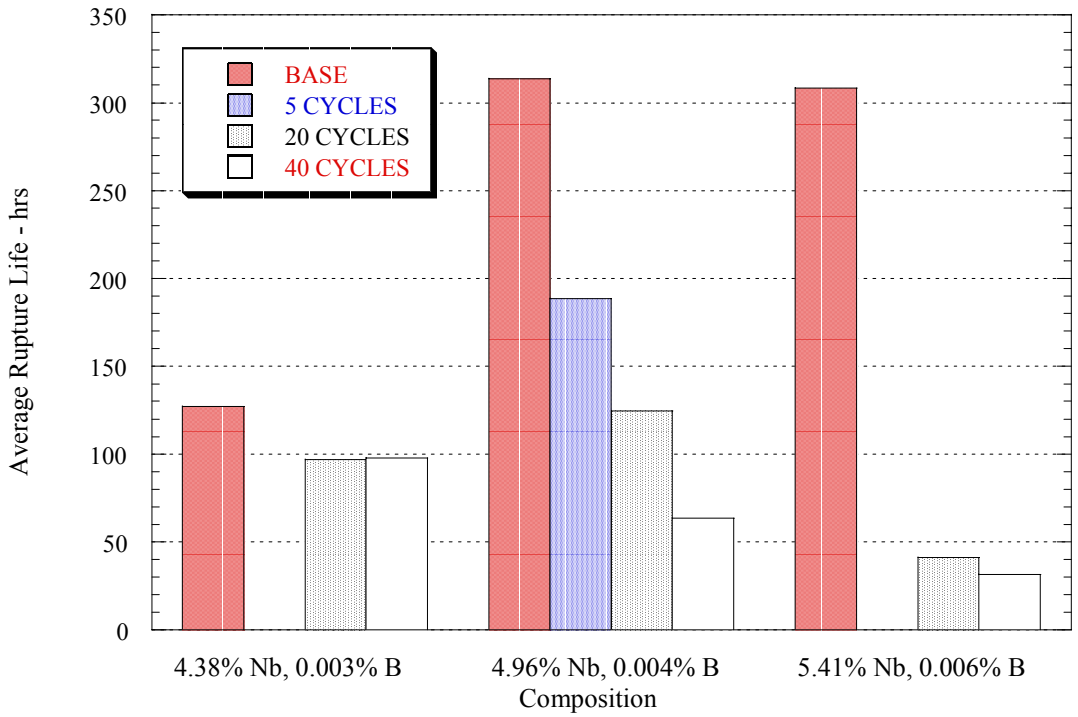

FIGURE 51. EFFECT OF MULTIPLE POSTREPAIR THERMAL CYCLES ON CAST+HIP IN718 1200°F RUPTURE LIFE

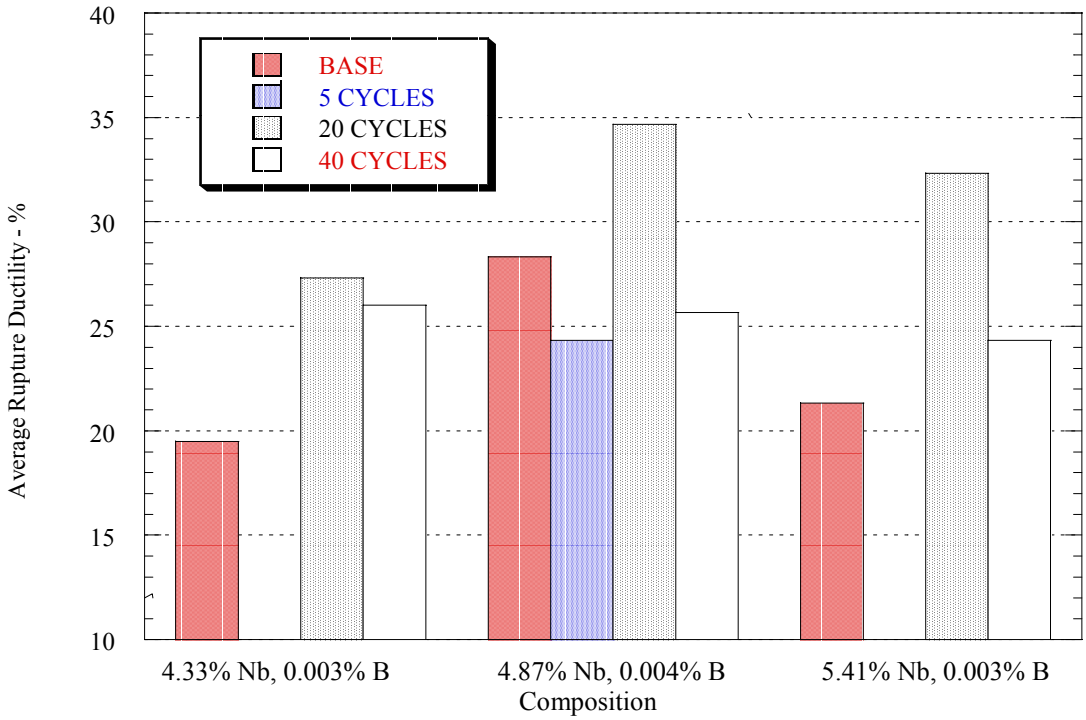

FIGURE 52. EFFECT OF MULTIPLE POSTREPAIR THERMAL CYCLES ON WROUGHT IN718 RUPTURE LIFE

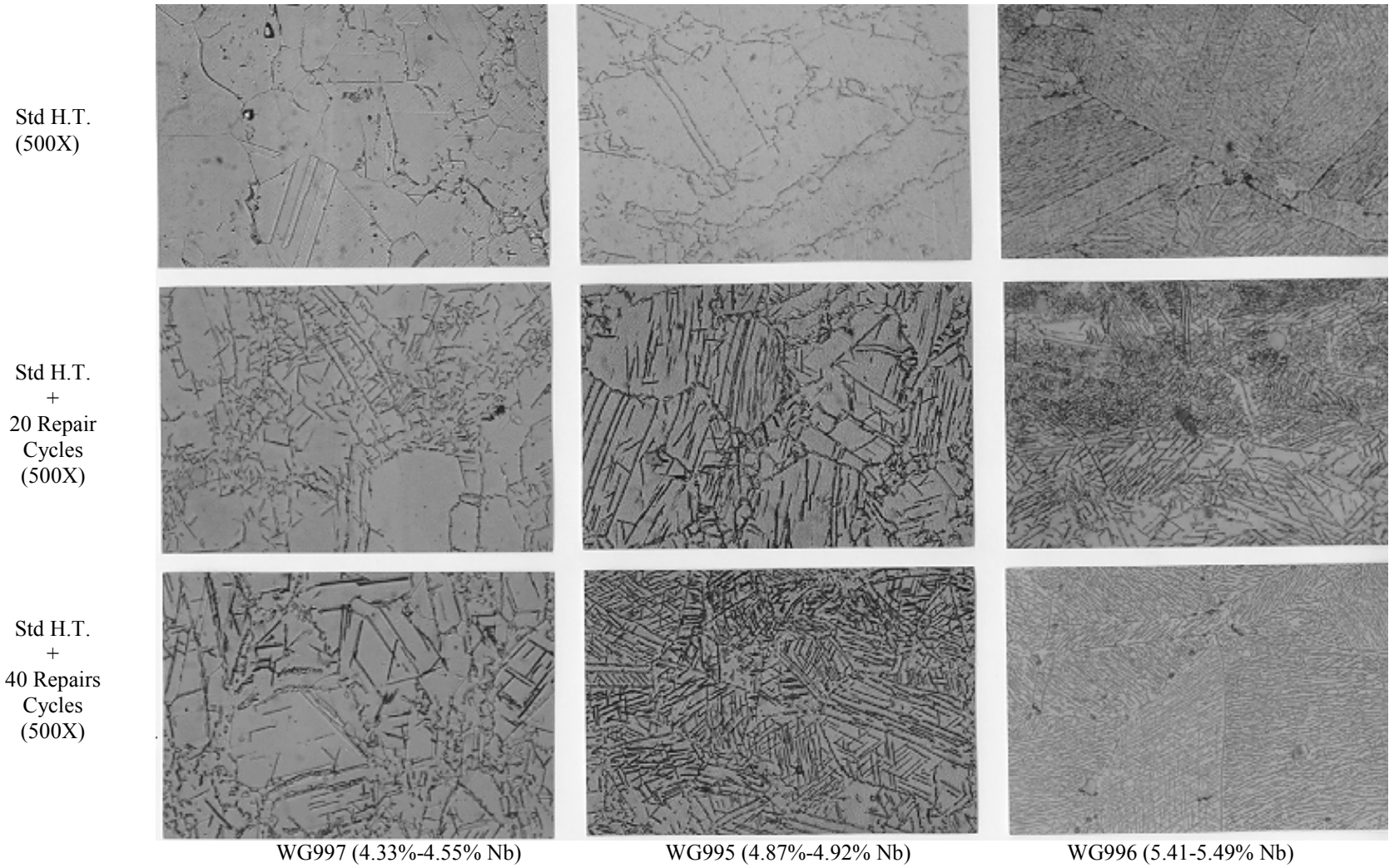

FIGURE 53. MICROSTRUCTURES OF IN718 PLATES WG997, WG995, AND WG996 WITH AND WITHOUT SIMULATED REPAIR (1700°F) CYCLES

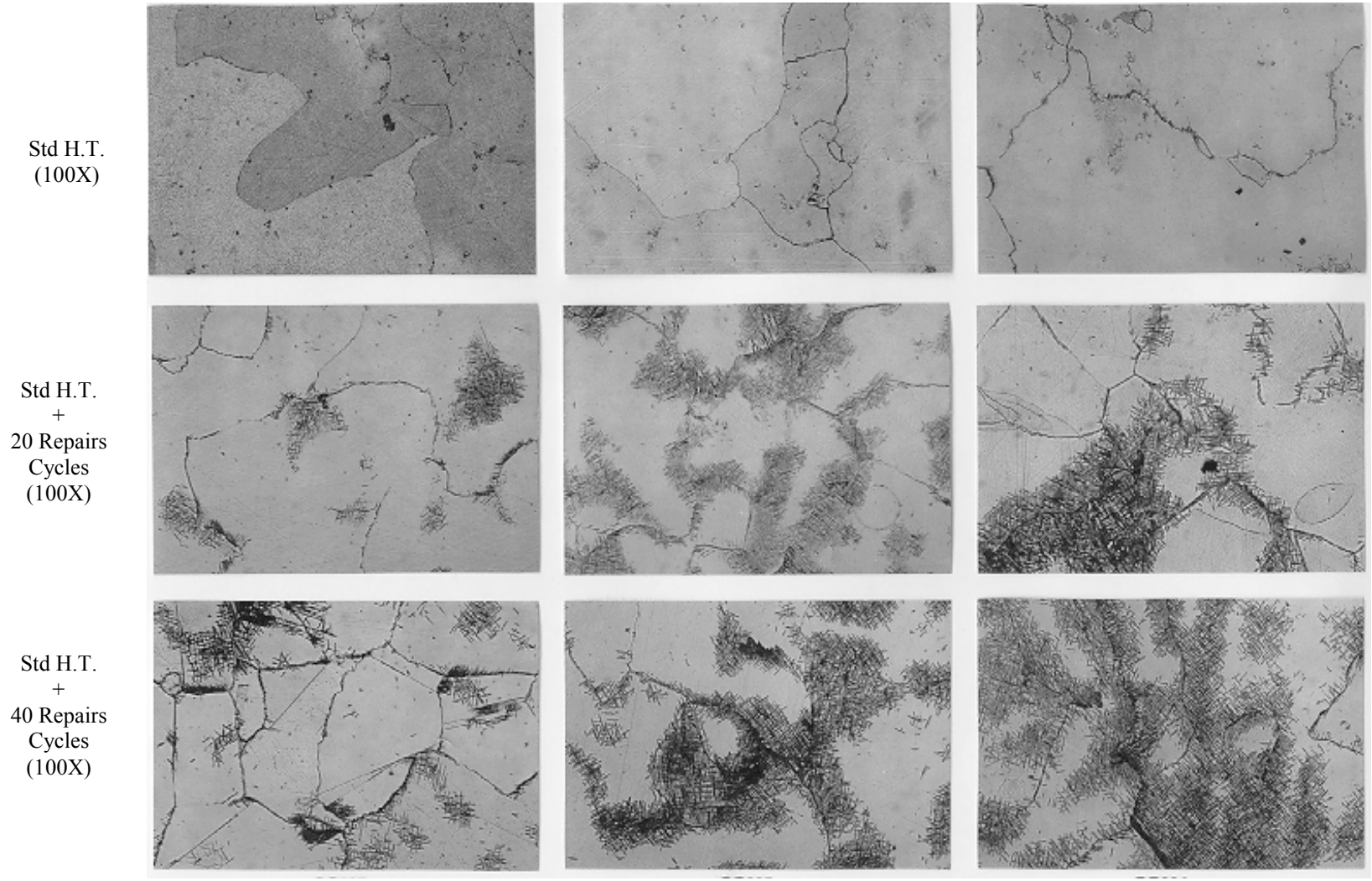

FIGURE 54. MICROSTRUCTURES OF CAST+HIP IN718 PLATES CG997, CG995, AND CG996 WITH AND WITHOUT SIMULATED REPAIR (1700°F) CYCLES

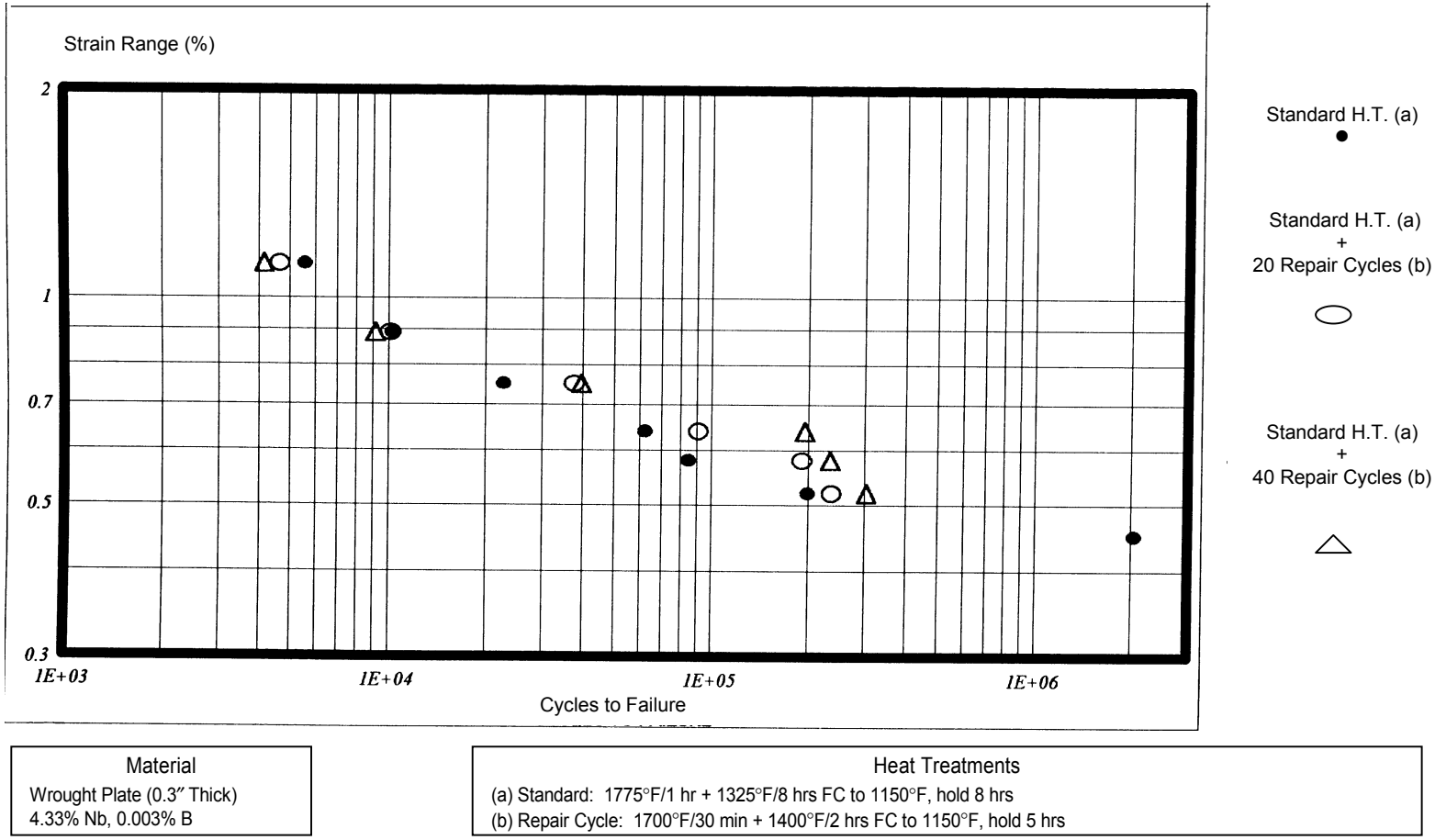

FIGURE 55. EFFECT OF MULTIPLE POSTREPAIR THERMAL CYCLES ON WROUGHT IN718 (LOW Nb HEAT) 800°F, R = 0.0, STRAIN CONTROL

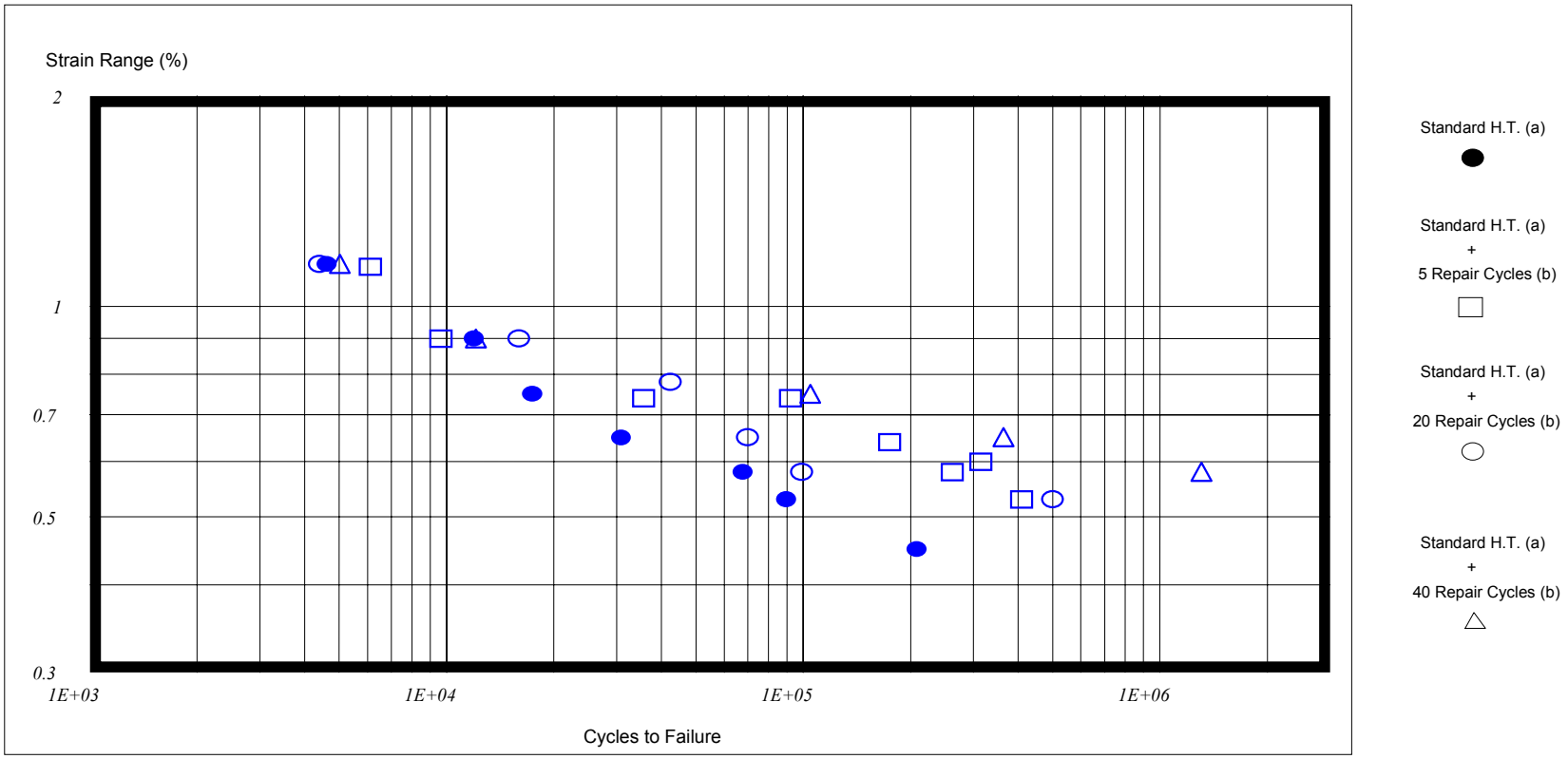

FIGURE 56. EFFECT OF MULTIPLE POSTREPAIR THERMAL CYCLES ON WROUGHT IN718 (MEDIUM Nb HEAT) 800°F, R = 0.0, STRAIN CONTROL

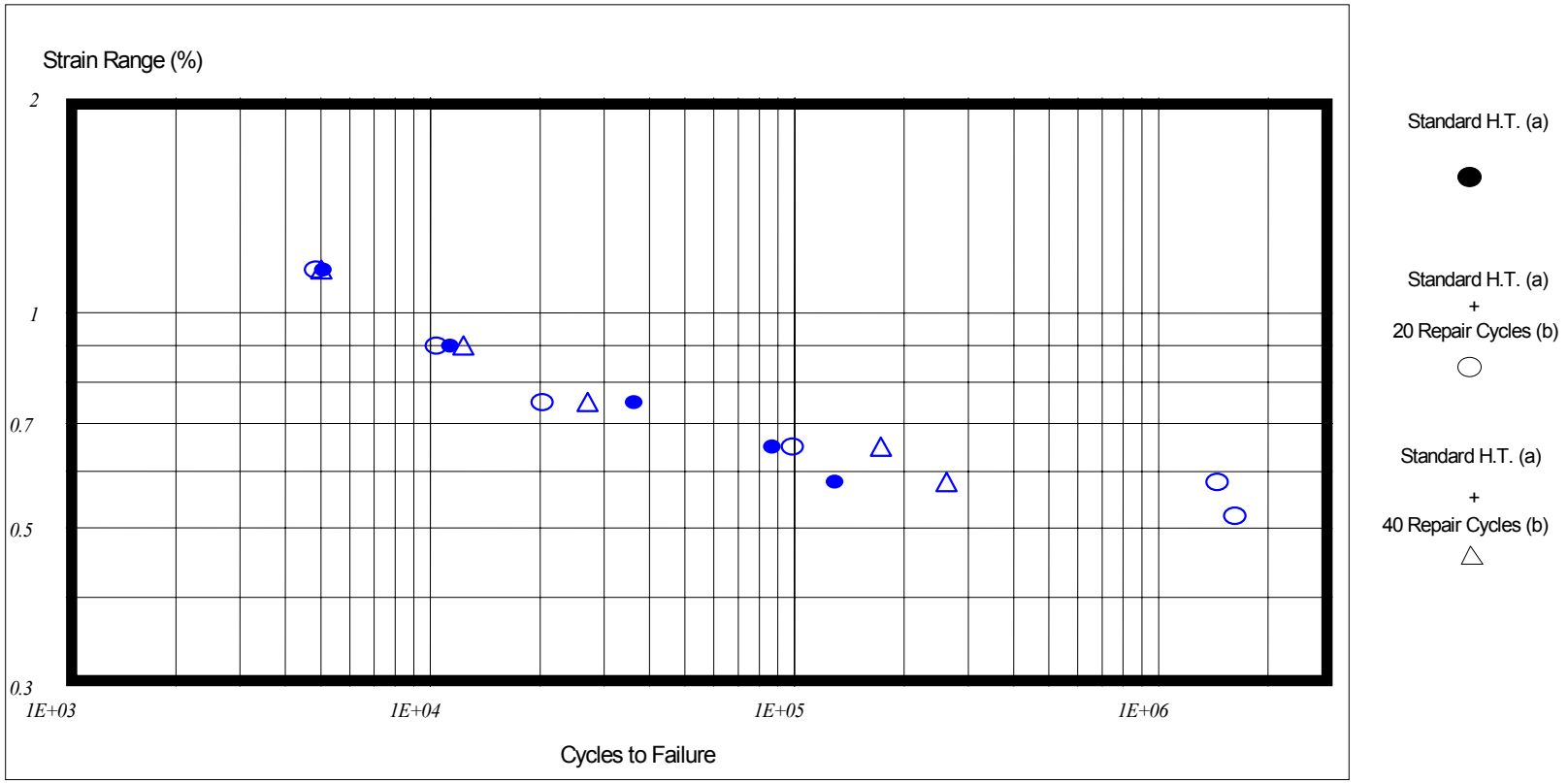

Material
Wrought Plate (0.3" Thick)
5.31% Nb, 0.006%B

Heat Treatments
(a) Standard: 1775°F/1 hr + 1325°F/8 hrs FC to 1150°F, hold 8 hrs
(b) Repair Cycle: 1700°F/30 min + 1400°F/2 hrs FC to 1150°F, hold 5 hrs

FIGURE 57. EFFECT OF MULTIPLE POSTREPAIR THERMAL CYCLES ON WROUGHT IN718 (HIGH Nb HEAT) 800°F, R = 0.0, STRAIN CONTROL

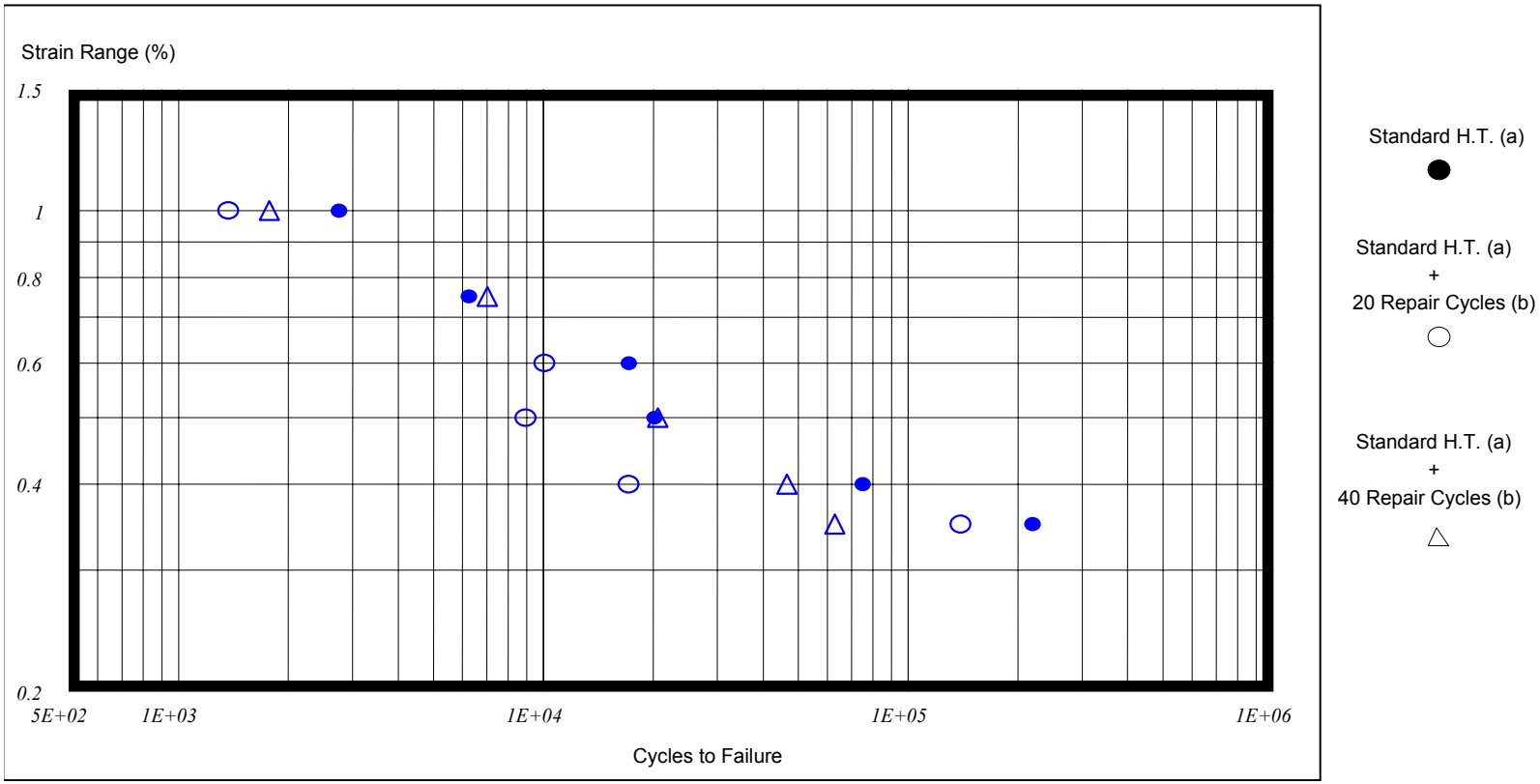

Material
Cast Plate (0.3" Thick)
4.38% Nb, 0.003%B

Heat Treatments

(a) Standard: 2050°F HIP + 1925°F/1 hr + 1750°F/1 hr + 1400°F/5 hrs FC to 1200°F, hold 1 hr
(b) Repair Cycle: 1700°F/30 min + 1400°F/2 hrs FC to 1150°F, hold 5 hrs

FIGURE 58. EFFECT OF MULTIPLE POSTREPAIR THERMAL CYCLES ON CAST+HIP IN718 (LOW Nb HEAT) 800°F, R = 0.0, STRAIN CONTROL

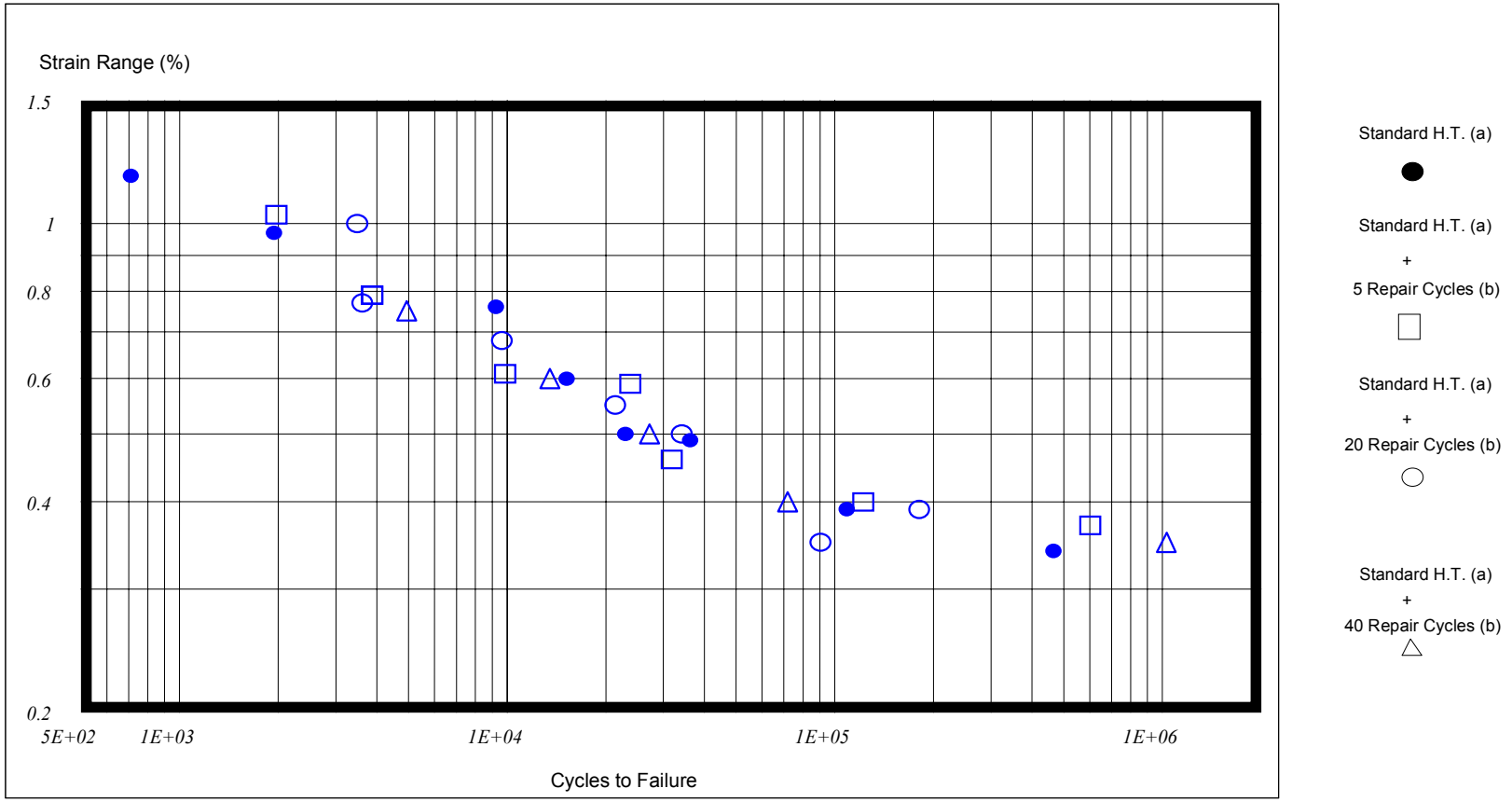

Material
Cast Plate (0.3" Thick)
4.94% Nb, 0.004%B

Heat Treatments
(a) Standard: 2050°F HIP + 1925°F/1 hr + 1750°F/1 hr + 1400°F/5 hrs FC to 1200°F, hold 1 hr
(b) Repair Cycle: 1700°F/30 min + 1400°F/2 hrs FC to 1150°F, hold 5 hrs

FIGURE 59. EFFECT OF MULTIPLE POSTREPAIR THERMAL CYCLES ON CAST+HIP IN 718 (MEDIUM Nb HEAT) 800°F, R = 0.0, STRAIN CONTROL

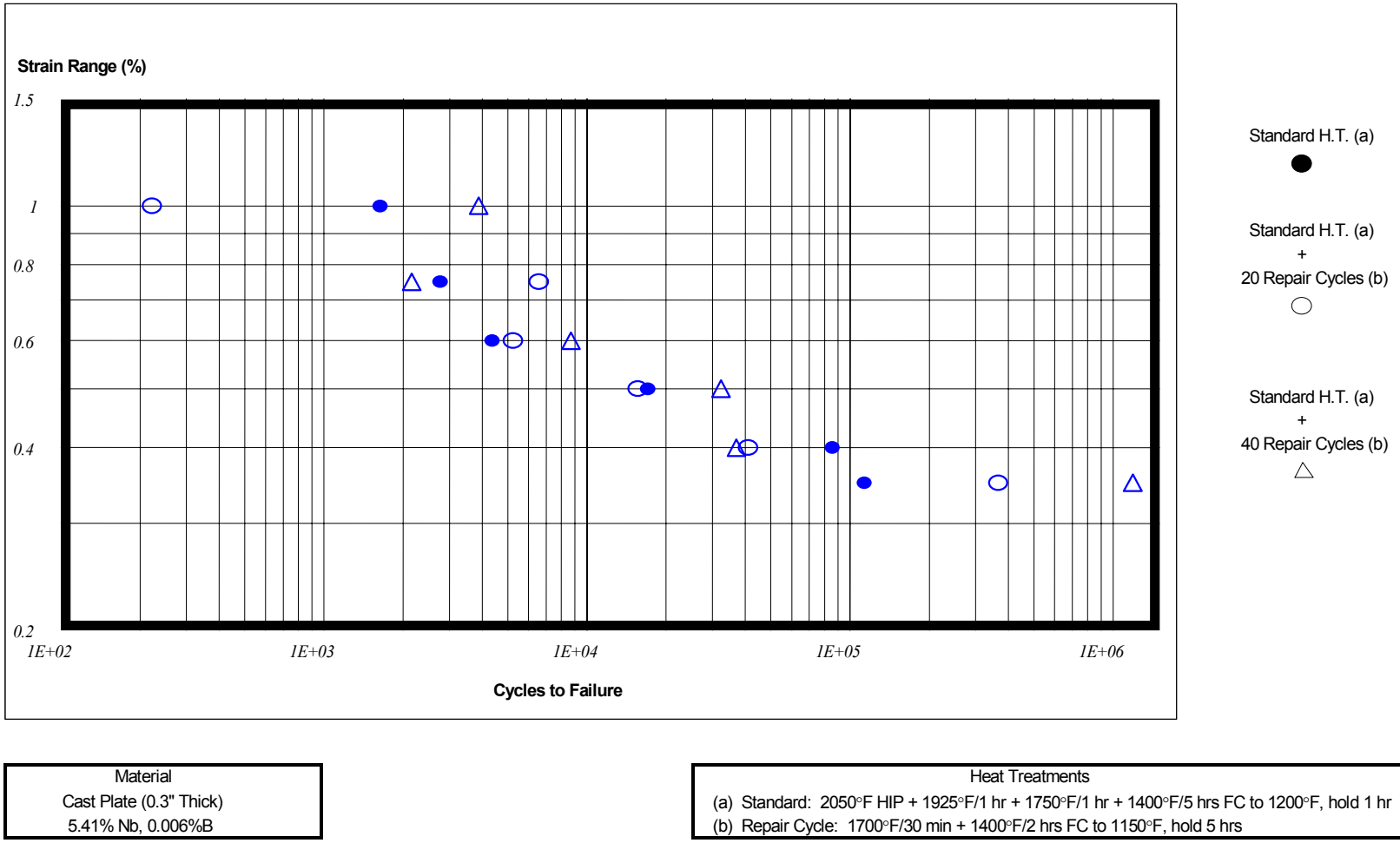

Material
Cast Plate (0.3" Thick)
5.41% Nb, 0.006%B

Heat Treatments
(a) Standard: 2050°F HIP + 1925°F/1 hr + 1750°F/1 hr + 1400°F/5 hrs FC to 1200°F, hold 1 hr
(b) Repair Cycle: 1700°F/30 min + 1400°F/2 hrs FC to 1150°F, hold 5 hrs

FIGURE 60. EFFECT OF MULTIPLE POSTREPAIR THERMAL CYCLES ON CAST+HIP IN718 (HIGH Nb HEAT) 800°F, R = 0.0, STRAIN CONTROL

2.3 TASK III: WELDABILITY IMPROVEMENTS.

Inconel 718 has been used extensively in static components of conventional turbine engines because of its good mechanical and corrosion properties at elevated temperature and its fabricability. The compressor rear frames and combustion cases of the CF6-6, CF6-50, and CFM56-3 engines are constructed from both wrought and cast forms of IN718. Service exposure often results in cracking in these static components that must be corrected by repair welding. Engines that have been in service for many years have typically undergone multiple inspection/ repair events.

A typical repair scenario, as shown in figure 61, consists of a prerepair solution heat treatment, manual repair welding, postweld heat treatment, and inspection. The prerepair solution heat treatment is normally used with Ni-base superalloys in order to improve weldability. The philosophy is that the lower strength of the surrounding base metal reduces the stresses in and around the weld, thus reducing the likelihood of cracking during repair welding. The postweld heat treatment, which usually includes both a solution heat treatment and an aging treatment, is required to optimize the strength in the weld metal and heat-affected zone (HAZ) relative to that of the base metal. The combination of pre- and postweld heat treatments occurring multiple times over the service lifetime of the engine is known to alter the microstructure of both cast and wrought forms of IN718, and it has been reported that repair weldability degrades as a function of repair/heat treatment cycles. Some preliminary weldability testing had demonstrated this effect in cast IN718 and provided additional impetus for the program, figure 62.

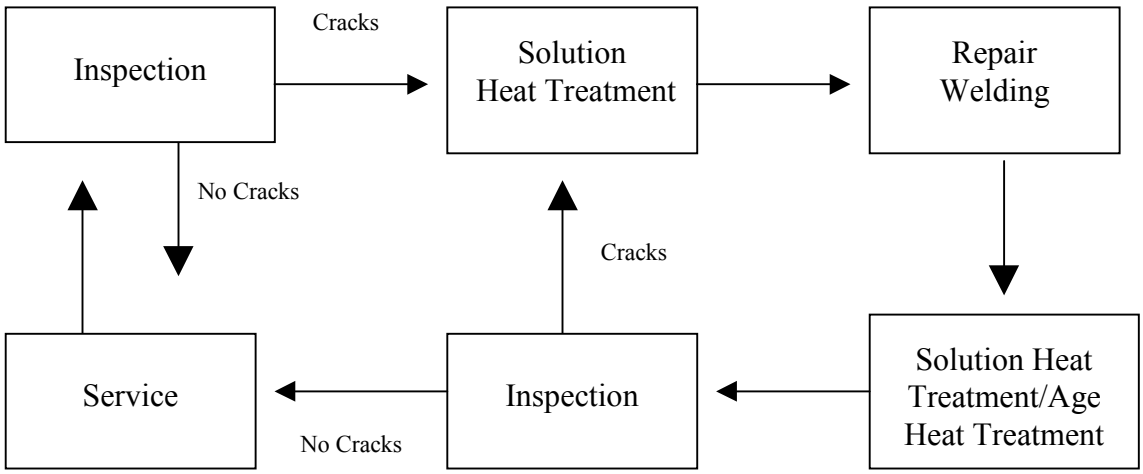

FIGURE 61. REPRESENTATIVE INSPECTION AND REPAIR CYCLE FOR COMPRESSOR REAR FRAMES

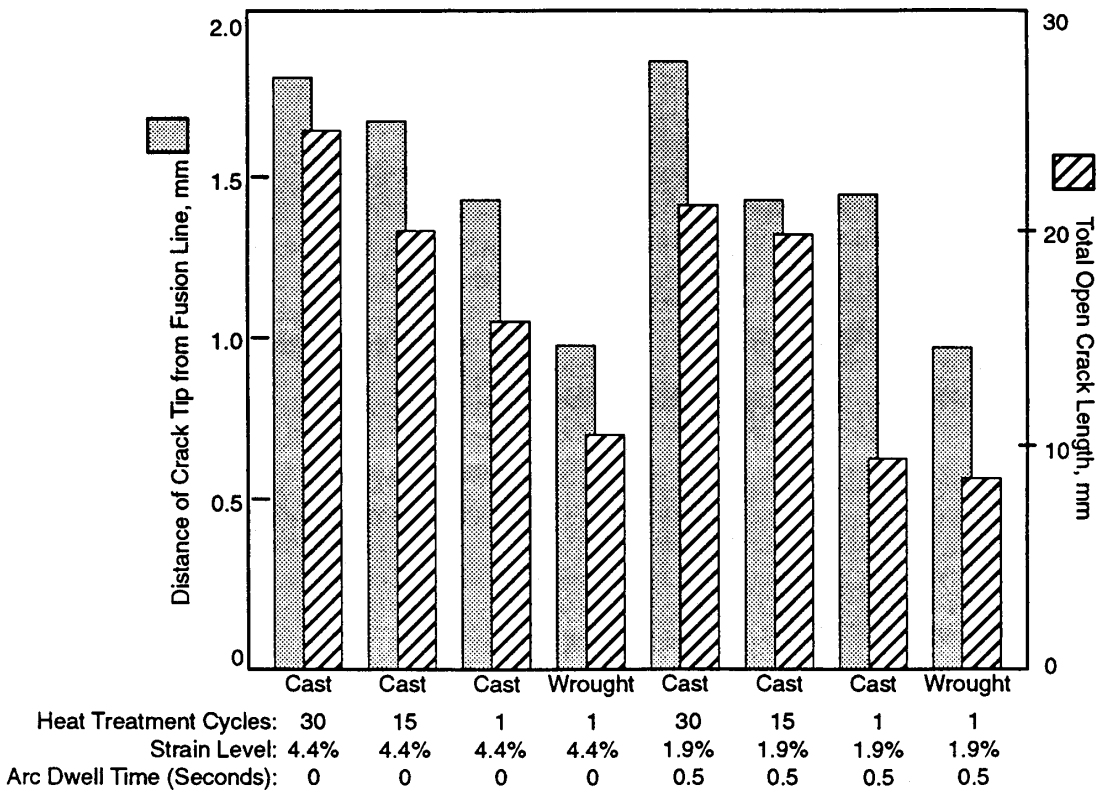

FIGURE 62. RESULTS OF PRELIMINARY WELDABILITY TESTING IN IN718

The following summarizes an investigation conducted by the Edison Welding Institute (EWI) to systematically determine the effect of composition, product form (cast versus wrought), and number of heat treatment cycles on the weldability of IN718. The three principal areas in this investigation follow.

2.3.1 Subtask I: Field Evaluation and Analysis.

This included visits to two repair facilities and discussions with engineers, metallurgists, and welders regarding the repair weldability of compressor rear frames. Some retired hardware was also obtained and evaluated in order to determine the nature of microstructural alteration during multiple repair and heat treatment.

2.3.2 Subtask II: Effect of Composition, Product Form, and Heat Treatment Cycles on Weldability.

Special compositions were prepared in both cast and wrought forms and subjected to up to 40 heat treatment cycles. These materials were then subjected to a variety of weldability tests and metallurgical analysis to determine the effect of multiple repair/heat treatment on cracking susceptibility.

2.3.3 Subtask III: Evaluate Preweld Heat Treatments to Improve Weldability.

Various rejuvenation heat treatments were performed to determine their effect on restoring the microstructure and improving weldability.

2.4 SUBTASK I: FIELD EVALUATION AND ANALYSIS.

2.4.1 Analysis of Retired Hardware.

Three scrapped CF6 compressor rear frames (CRFs) were obtained through GEAE for evaluation. Two of these were CF6-6 models and one was a CF6-50. Detailed service or inspection records for these components were unavailable and, thus, it was not known how many repair and heat treatment cycles these CRFs had experienced. Fluorescent penetrant inspection (FPI) of the CRFs was performed by GEAE personnel, and component damage indications were utilized to locate and identify defects. In addition to these defects, metallographic samples were extracted from assembly and repair weldments to identify defect types present in the weld regions.

Metallographic examination of the cast and wrought components in all of the CRFs revealed that significant delta phase (Ni_3Nb) had formed in the microstructure over its lifetime. Representative cast and wrought microstructures are shown in figures 63a and 63b. Note that the dark-etching, needle-like delta phase is relatively uniformly distributed in the wrought material, while in the cast components it forms preferentially along the cast grain boundaries.

Considerable characterization was also carried out to determine the nature of defects (cracks, pores, etc.) in these CRFs. Based on the detailed metallographic examination of these components, the following defect types were identified:

- Fatigue cracks associated with stress concentration
- Fatigue cracks associated with weld or casting porosity
- Fatigue cracks associated with a liquation crack
- Liquation cracking in the weld metal
- Liquation cracking in the HAZ adjacent to the weld
- Casting defects (shrinkage pores)

Most of the cracking that was observed (approximately 70 percent) was associated with either original fabrication welds or repair welds in the CRFs. Most of the fatigue cracks were observed in high-stress areas, particularly in the inner hub and strut regions. Examples of some of these defect types are shown in figures 64a, 64b, 64c, and 64d. Based on these results, it was determined that a significant amount of liquation-related cracking was present in both wrought and cast components in the CRFs. This observation supported the original hypothesis that liquation cracking was, at least in part, responsible for the degradation in weldability of these components as a function of repair and heat treatment cycles.

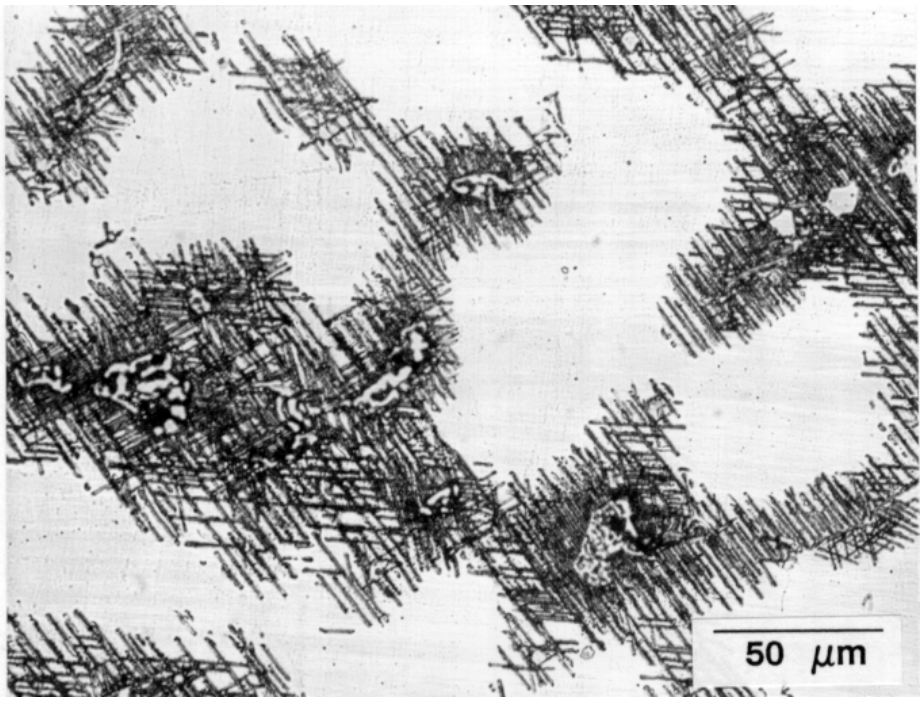

FIGURE 63a. CAST IN718 MICROSTRUCTURE FROM RETIRED CF6-6

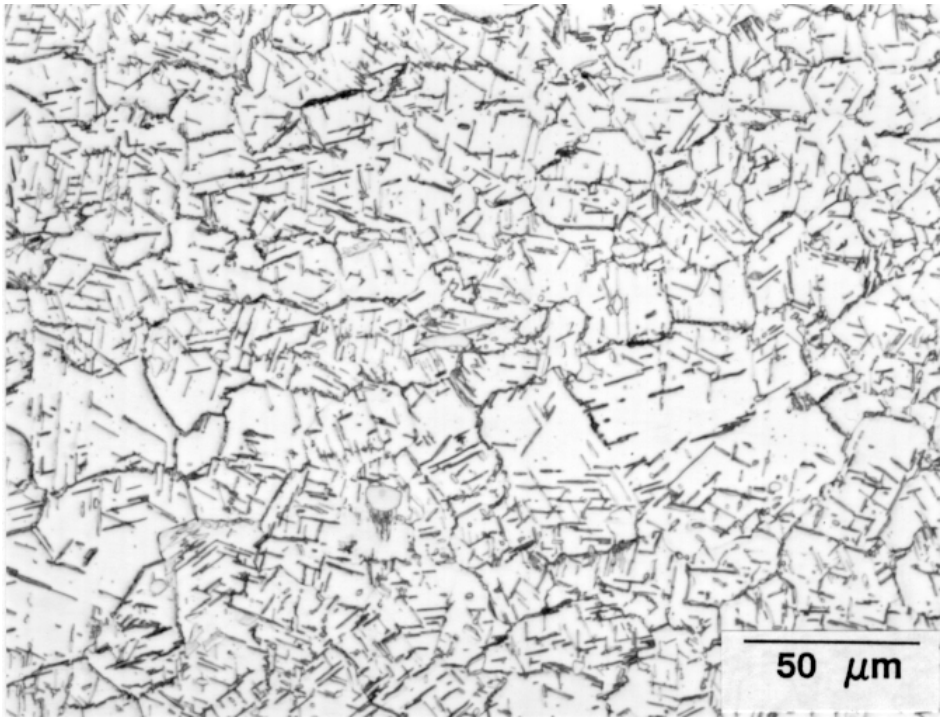

FIGURE 63b. WROUGHT IN718 MICROSTRUCTURE FROM RETIRED CF6-6

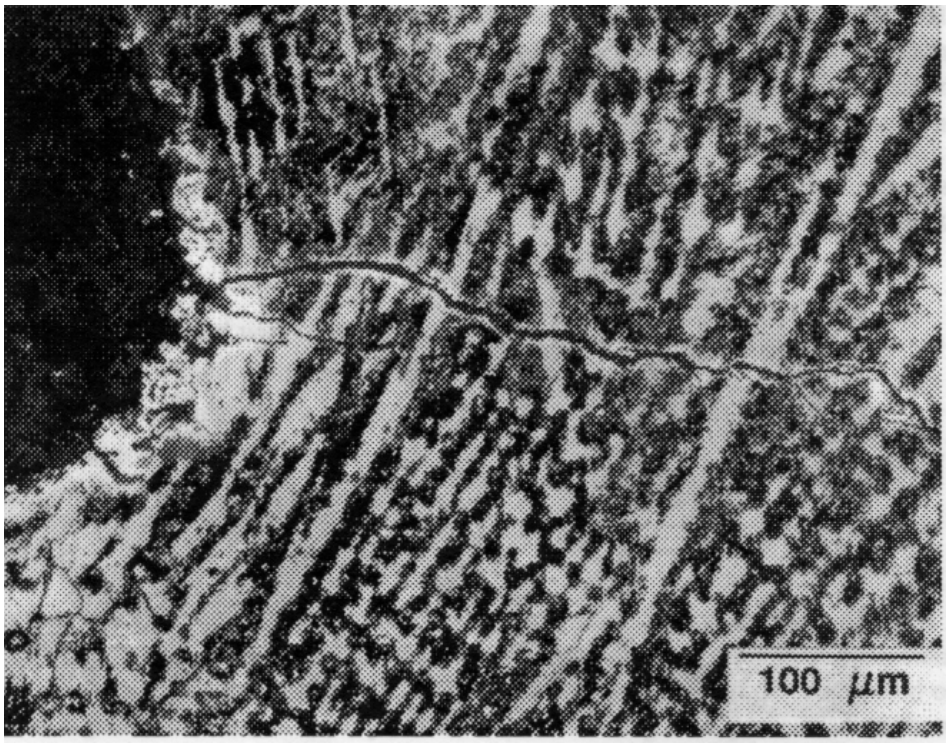

FIGURE 64a. DEFECT TYPES OBSERVED IN RETIRED COMPRESSOR REAR FRAMES: FATIGUE CRACK AT STRESS CONCENTRATION

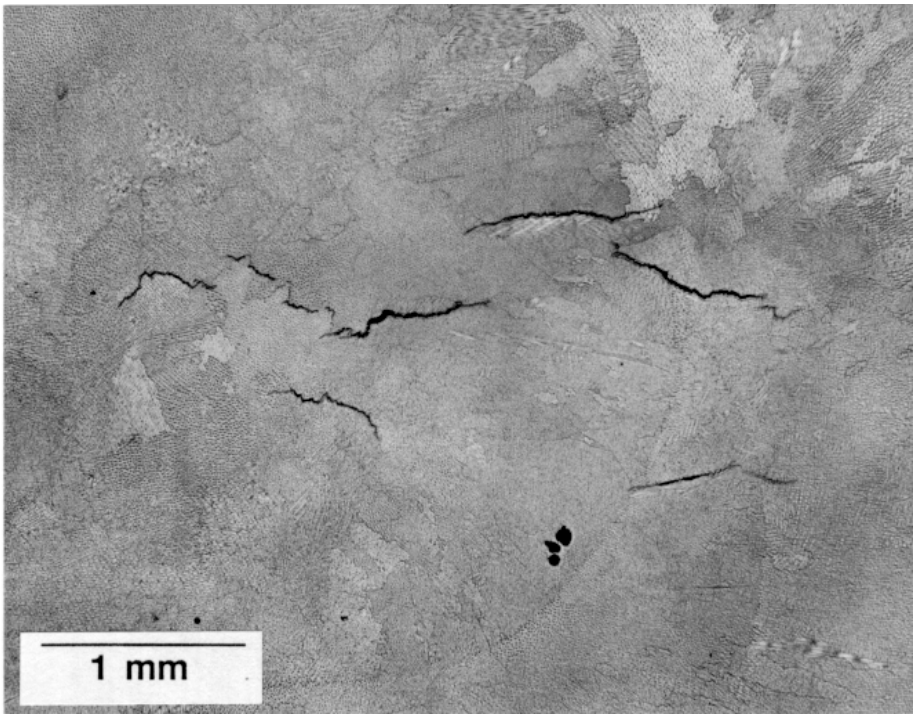

FIGURE 64b. DEFECT TYPES OBSERVED IN RETIRED COMPRESSOR REAR FRAMES: LIQUATION CRACKING IN CAST MICROSTRUCTURE

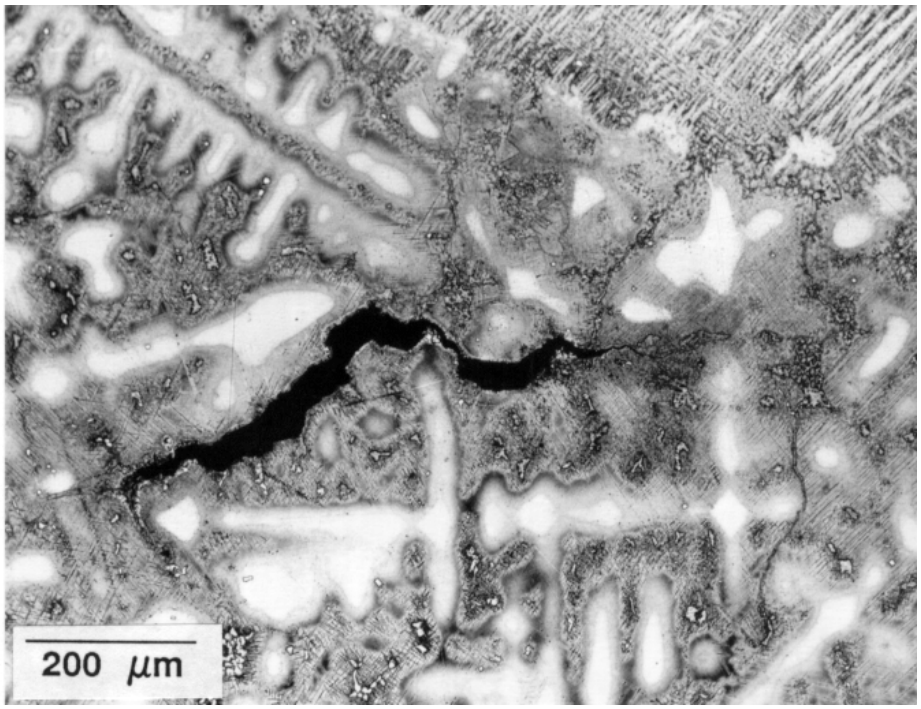

FIGURE 64c. DEFECT TYPES OBSERVED IN RETIRED COMPRESSOR REAR FRAMES: WELD METAL LIQUATION CRACKING

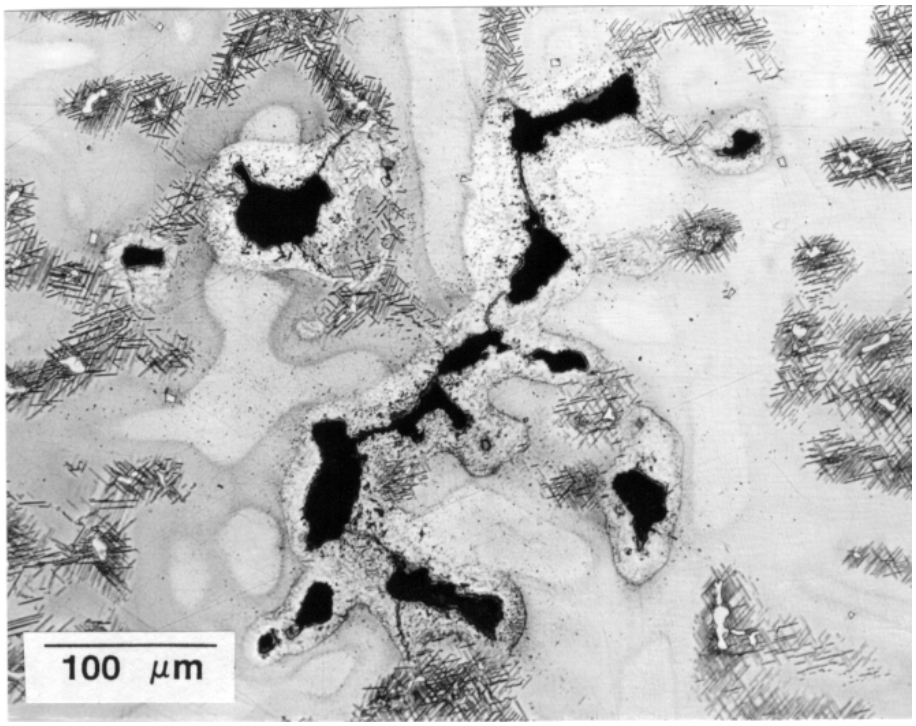

FIGURE 64d. DEFECT TYPES OBSERVED IN RETIRED COMPRESSOR REAR FRAMES: CASTING DEFECT

2.4.2 Repair and Heat Treatment Simulation.

Because the history of the CRFs obtained for analysis was unknown, the origin and nature of the weld-related defects reported in the previous section could not be definitively linked to a repair welding event. In an effort to produce some fresh defects representative of an actual repair scenario, a number of simulated repair welds were made at various locations on one of the CF6-6 CRF and on the CF6-50 CRF. These frames were then subjected to a standard postweld heat treatment (PWHT) cycle at the GE repair facility in Cincinnati, Ohio. Inspection following PWHT failed to reveal any cracking in or around these repairs.

Since many of these repairs were made in low-stress concentration areas of the CRF, it was felt that sufficient stresses were not developed during heat treatment to open up any cracking that may have been generated during welding. Subsequent metallographic examination of these repair welds revealed evidence of significant liquation in both the cast and wrought HAZ microstructures adjacent to the repair welds, but there was no evidence of cracking. It is likely that the stresses during welding were not sufficient to cause cracking despite the presence of this crack-susceptible microstructure.

2.4.3 Repair Facility Visits.

Both the GEAE Repair Engineering Facility in Cincinnati and the United Airlines Repair Facility at San Francisco International Airport were visited in order to obtain information on the inspection, repair, and heat treatment of CF6-6 and CF6-50 CRFs. These visits included discussions with supervisors, engineers, and welders. Following are the principal conclusions resulting from these visits.

- There is essentially no permanent documentation available on a given CRF over its repair lifetime. There was no way to determine, for example, the number of repair/heat treatment cycles to which a component had been exposed.

- There is a definite relationship between the number of repair events and the degradation in weldability. The CRFs seem to "hit the wall" after 2-3 repair events. Cracking then becomes progressively worse with each subsequent repair.

- A successful repair may require numerous repair welding/heat treatment cycles. Some CRFs may spend several months in the repair facility before they are released or retired. CF6-6 models were the most troublesome.

- Most cracking was associated with the strut and hub area of the CRF. Access to these areas of the CRF was difficult and many of the welders had developed special torches and gas shields to accommodate this problem.

- A couple of the welders claimed they could actually see cracks form as they made a repair. These cracks were adjacent to the weld in the HAZ.

- There was some variation in the repair process between facilities. For example, United Airlines had abandoned the preweld solution treatment.

- The general consensus at the repair facility was that repair weldability was a function of metallurgical degradation arising from multiple heat treatments. They were very receptive to the development of a rejuvenation heat treatment that would restore weldability.

2.4.4 Summary of Preliminary Evaluation and Repair Facility Visits.

The purpose of this phase of the project was to determine the nature of the problem in order to properly focus the weldability tasks to follow. Based on the evaluation of actual hardware, it was clear that significant alteration of the original cast and wrought microstructure occurs as a function of multiple repairs and associated heat treatments. Microstructural alteration was primarily manifested by the dramatic precipitation and growth of delta phase. All the retired hardware examined contained a high-volume fraction of this phase. It was unclear, based on this preliminary characterization, how the presence of delta phase may contribute to the weldability problem.

The inability to obtain a CRF with a documented repair weldability history, or one that had been retired specifically because of poor repair weldability, did not allow a clear relationship between metallurgical condition and weldability to be determined in this task. Although there was significant circumstantial evidence to suggest that multiple heat treatments and concomitant delta phase buildup in the microstructure increased liquation cracking susceptibility during repair welding, the *smoking gun* that would convincingly link them was not found. Based on the evidence at hand, it was decided to move forward with a weldability testing program that would clearly delineate the effect of multiple heat treatments on liquation cracking susceptibility in both cast and wrought IN718 over a range of composition.

2.5 SUBTASK II: EFFECT OF COMPOSITION, PRODUCT FORM, AND HEAT TREATMENT CYCLES ON WELDABILITY.

2.5.1 Materials and Heat Treatment.

Wrought IN718 material removed from a retired CF6-6 that had experienced numerous repair and heat treatment cycles was evaluated. For a baseline reference, a wrought heat of virgin-processed IN718 of similar composition to the service-exposed material was also tested. This reference material is a wrought IN718 with high niobium and boron content; it is further described below with the program materials. Samples for weldability testing were prepared in a variety of conditions, including wrought base metal and weld metal in both the as-received retired condition and after postweld heat treatment (PWHT). Microstructures of the *retired* base and weld metals are shown in figure 63.

Table 3 lists the compositions of the materials used. Table 4 summarizes the material conditions and designations of the CRF material. PWHT was conducted using a solution temperature of either 927°C or 1038°C (designated as 1700 or 1900 in table 4) followed by a two-step aging treatment of 718°C (1325°F) for 8 hours plus 621°C (1150°F) for 8 to 10 hours.

TABLE 3. COMPRESSOR REAR FRAME COMPOSITIONS

Condition	Ni	Fe	Cr	Nb	B	S	P	Al	Ti	C	Mo	Mn	Si
Reference	51.7	17.9	20.0	5.41	0.006	0.001	0.001	0.49	1.01	0.014	2.92	0.01	<0.10
BM BM1700 BM1900	53.0	18.2	18.1	5.37	0.003	0.002	0.015	0.47	1.34	0.055	3.00	0.17	<0.10
WM	51.8	19.4	18.4	5.04	0.003	0.001	0.014	0.51	1.03	0.046	2.97	0.29	0.22
WM1700 WM1900	53.7	18.1	18.1	5.35	0.003	0.001	0.015	0.50	1.01	0.041	2.95	<0.10	0.11

TABLE 4. CONDITION OF COMPRESSOR REAR FRAME MATERIAL BASE AND WELD METALS

Designation	Description of Condition
Reference	Wrought, virgin-processed (fully aged); (Described in table 3 as wrought, high Nb, B)
BM	Wrought, as-received (retired), solution annealed condition
BM1700	BM, 927°C for 15 minutes + age cycle
BM1900	BM, 1038°C for 15 minutes + age cycle
WM1700	Weld metal, as-received (retired), solution annealed condition
BM1900	WM, 912°C for 15 minutes + age cycle
WM1900	WM, 1038°C for 15 minutes + age cycle

TABLE 5. COMPOSITION OF PROGRAM MATERIALS

Wrought	Nb	B	Cast	Nb	B
Low	4.4	0.003	Low	4.5	0.004
Medium	4.9	0.004	Medium	5.1	0.005
High	5.5	0.005	High	5.4	0.006
Bulk Composition: 20.0 Cr, 18.0 Fe, 2.9 Mo, 1.0 Ti, 0.5 Al, 0.014 C, balance Ni					

In addition to the material from the retired CF6-6, three heats of IN718 with controlled levels of niobium and boron, hereafter referred to as the program materials, were vacuum melted in nominally 300-lb ingots. The niobium and boron contents of the samples were varied within the specification range. The other alloying elements of the cast and wrought forms were standardized. Thus the differences observed were depended only on the niobium and boron variation in the samples. The thickness of the wrought material was 0.4 in.; the thickness of the cast material was 0.3 in.

All heats were subjected to 5, 20, and 40 heat treatment cycles. The heat treatment cycle consisted of a solutionizing heat treatment, 1700°F for 30 minutes followed by a standard aging treatment of 1400°F for 2 hours plus 1150°F for 5 hours. This particular heat treatment for IN718 is used to minimize grain size and optimize mechanical properties, particularly fatigue. This heat treatment is standard at GEAE for IN718; a schematic of it is provided in figure 65. *All heat treatments were conducted in a vacuum.*

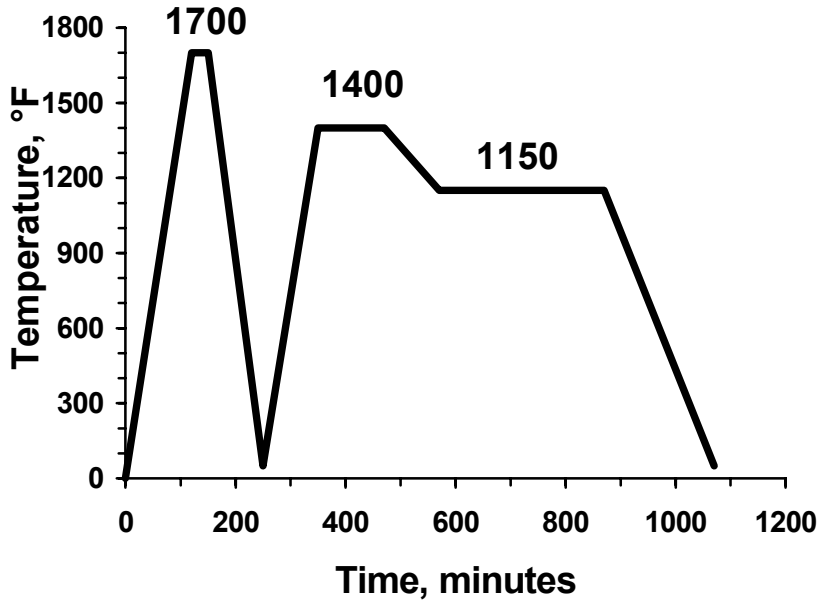

FIGURE 65. SCHEMATIC OF THE GEAE HEAT TREATMENT FOR IN718 USED FOR THIS INVESTIGATION

Microstructures for the medium composition wrought program material for both the as-received and 40-cycle PWHT conditions are shown in figures 66a and 66b. Cast microstructures of the medium composition program material in both the as-received and 40-cycle PWHT condition are shown in figures 67a and 67b. The rod-shaped precipitates, particularly noted in the 40-cycle cast program material, are delta phase (Ni_3Nb) and occur both at grain boundaries and intragranularly. An increase in the amount of delta phase precipitate between the as-received and 40-cycle PWHT condition is noted for the cast program material. The wrought material had a high percentage of delta phase in the as-received condition.

2.5.2 Weldability Testing.

Weldability of the CF6-6 and program materials was quantified through three methods. Circular weld tests were performed on the program material to evaluate the susceptibility of IN718 to strain-age cracking. Hot-ductility testing, performed on a Gleeble® HAZ 1000, determined the ductility of the CF6-6 and program materials at elevated temperatures, both upon heating as well as on cooling from a given peak temperature. Varestraint testing of the program materials measured the region over which the material was susceptible to cracking. These testing methods are described in subsequent sections.

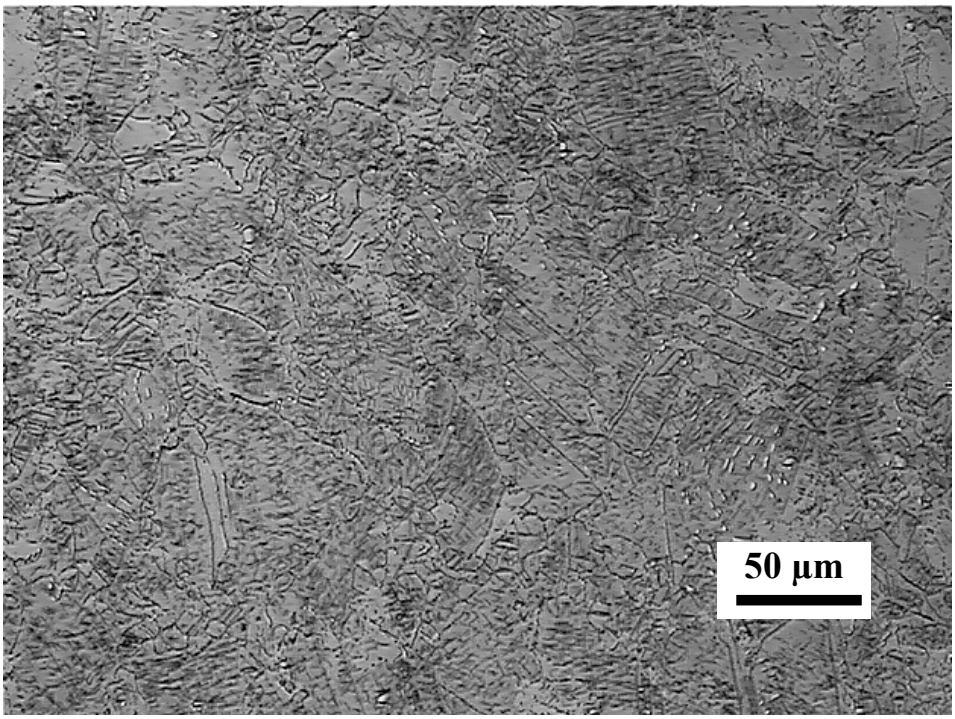

FIGURE 66a. MICROSTRUCTURE OF MEDIUM COMPOSITION WROUGHT PROGRAM MATERIAL IN THE AS-RECEIVED CONDITION

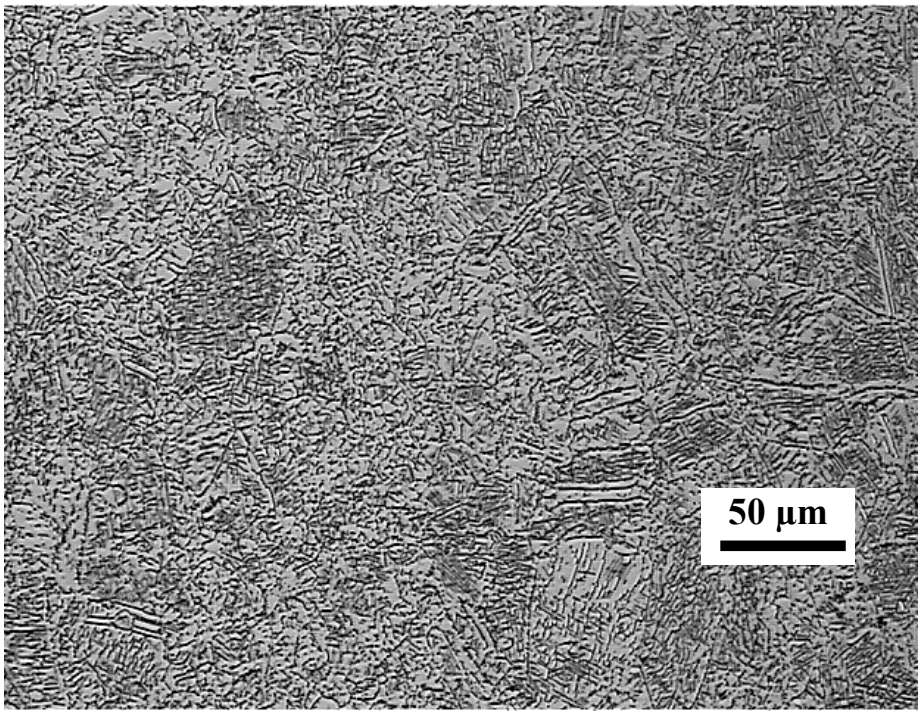

FIGURE 66b. MICROSTRUCTURE OF MEDIUM COMPOSITION WROUGHT PROGRAM MATERIAL AFTER 40 HEAT TREATMENT CYCLES

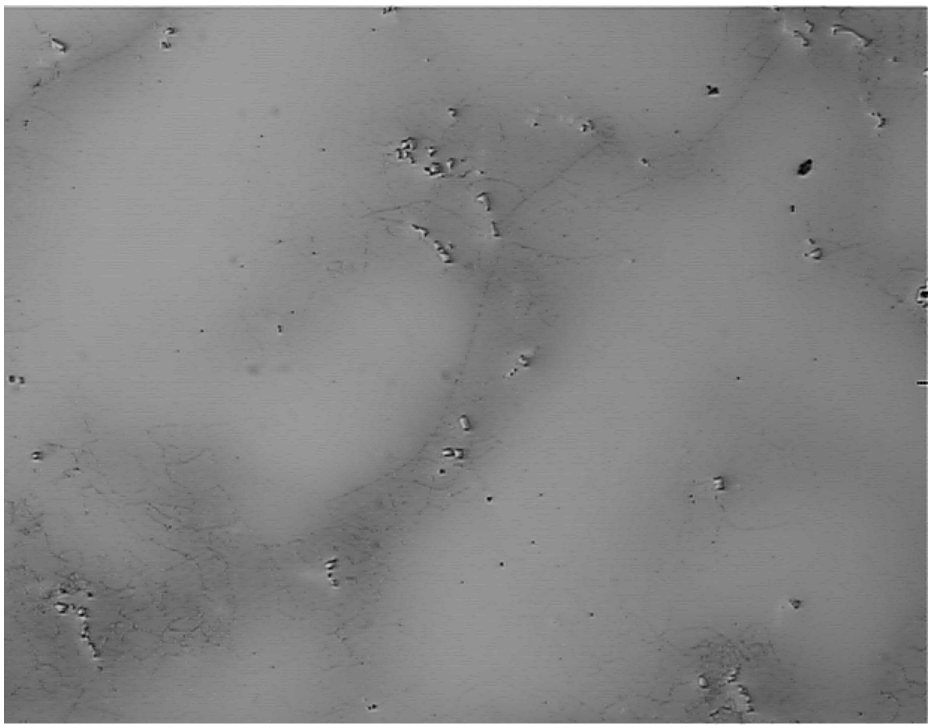

FIGURE 67a. MICROSTRUCTURE OF MEDIUM COMPOSITION CAST PROGRAM MATERIAL IN THE AS-RECEIVED CONDITION

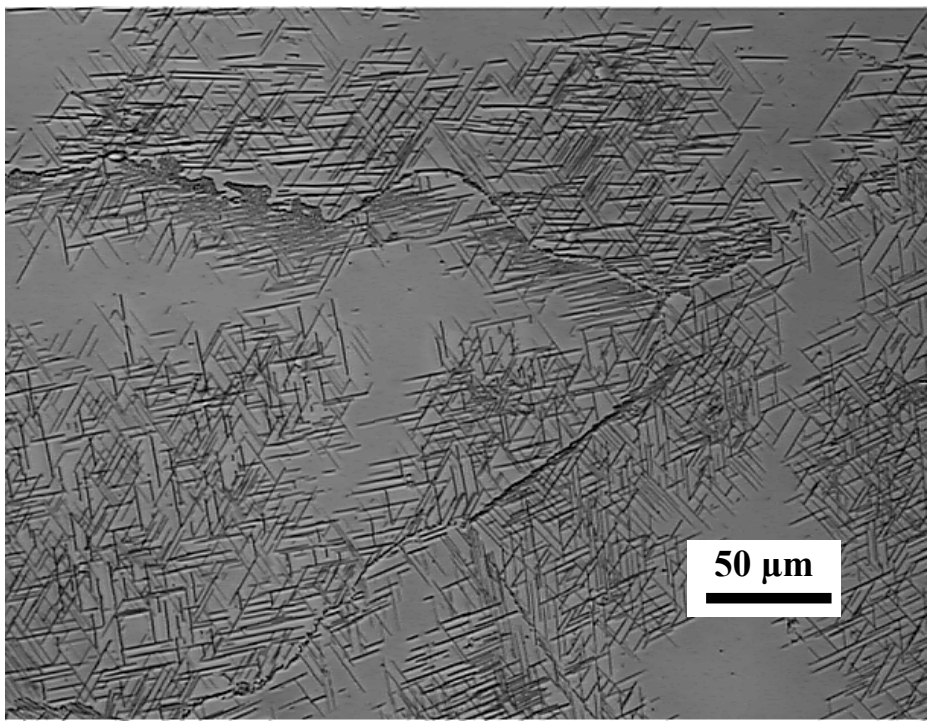

FIGURE 67b. MICROSTRUCTURE OF MEDIUM COMPOSITION CAST PROGRAM MATERIAL AFTER 40 HEAT TREATMENT CYCLES

2.5.3 Hot-Ductility Testing Method.

The weldability of all materials was evaluated using the Gleeble® hot-ductility test. This test simulates the thermal cycle that the material in the heat-affected zone undergoes during welding. Small tensile samples are fractured rapidly at specific temperatures during either the on-heating or the on-cooling portion of a duplicated weld thermal cycle. The ductility of the material during the thermal cycle is measured in terms of transverse reduction in area and plotted versus temperature to represent the hot-ductility *signature* of the material.

Figure 68 provides a schematic of the relation between the welding thermal cycle and the hot-ductility signature. When testing on-heating, the material will first exhibit a sharp reduction in ductility until reaching the nil-ductility temperature (NDT). With continued increase in temperature, the sample will eventually exhibit effectively no strength at the nil strength temperature (NST). Samples are then tested on cooling from the NST at progressively lower temperatures until ductility is recovered at the ductility recovery temperature (DRT). The temperature range between the peak temperature of the thermal cycle (T_P) and the DRT exhibits zero ductility and is, therefore, subject to liquation cracking during weld cooling. As such, the parameter (T_P-DRT) is one measure of the weldability of the material.

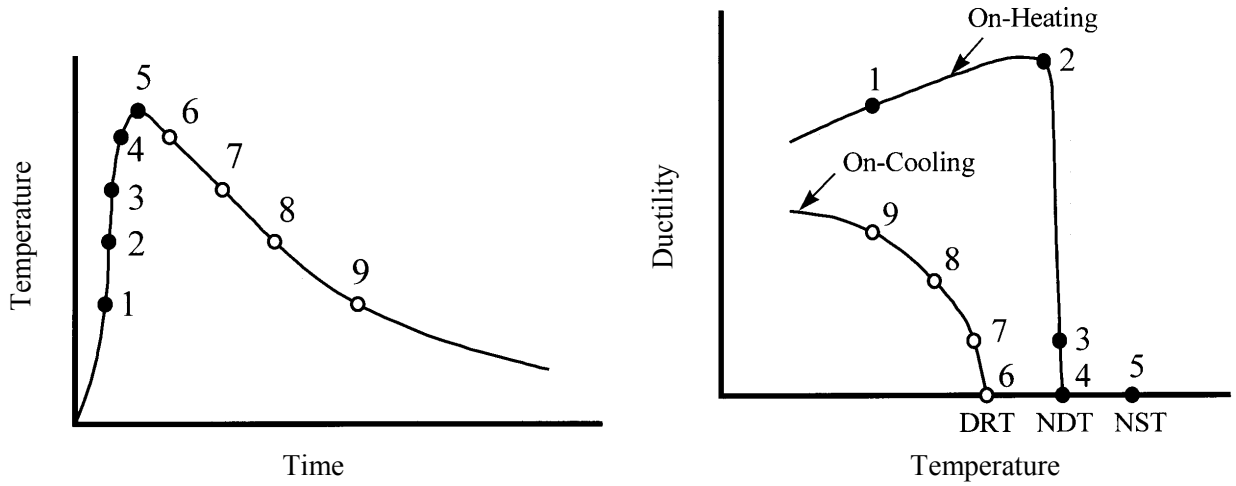

FIGURE 68. SCHEMATIC OF A WELDING THERMAL CYCLE (LEFT) AND THE CORRESPONDING HOT-DUCTILITY CURVE (RIGHT)

Testing was accomplished using cylindrical test specimens nominally 6.4 mm in diameter, 100 mm in length, and threaded on both ends. The sample free span between the Gleeble ® grips was on the order of 20 mm. Chromel-alumel thermocouples were attached to the middle of the specimen for temperature measurement and control. The heating rate was 111°C/s. The cooling rate was 20°C/s between 1260-1200°C and 43°C/s below 1200°C. This cooling rate schedule closely simulates actual weld cooling conditions. Samples were pulled to failure at a rate of 25.4 mm/s.

It was not possible to attain the NST as the peak temperature during the hot-ductility testing program for the CRF and program materials. Sample integrity was affected by the amount of

melting at the NST; subsequently, it was not possible to perform the on-cooling tests. A peak temperature of 1260°C was used for hot-ductility testing. Representative hot-ductility curves are shown in figures 69a and 69b for the medium composition wrought and cast program materials after 40 heat treatment cycles.

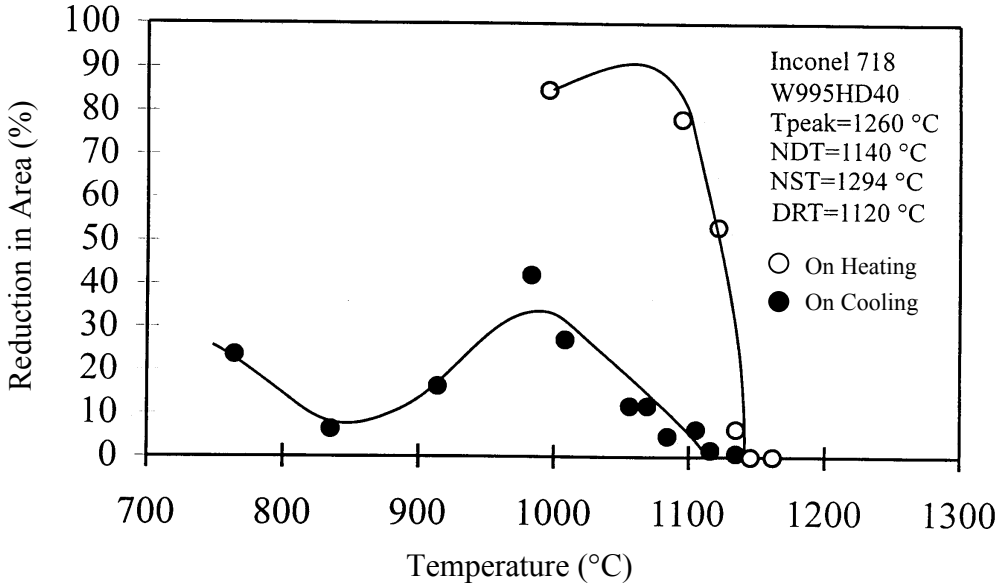

FIGURE 69a. HOT-DUCTILITY DATA FOR MEDIUM COMPOSITION WROUGHT PROGRAM MATERIAL AFTER 40 HEAT TREATMENT CYCLES

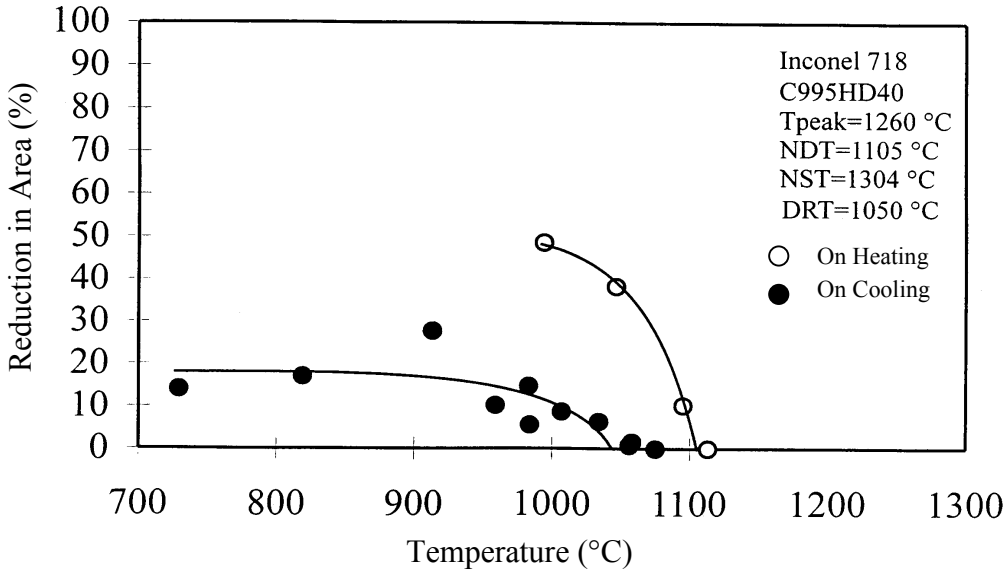

FIGURE 69b. HOT-DUCTILITY DATA FOR MEDIUM COMPOSITION CAST PROGRAM MATERIAL AFTER 40 HEAT TREATMENT CYCLES

2.5.4 Varestraint Testing Method.

The varestraint test measures the region over which the HAZ is subject to liquation cracking. Transverse, longitudinal, and spot welds can be evaluated in this test method. The current program utilized spot varestraint testing. The test sample was 1 in. in width and approximately 8 in. long; it could accommodate three individual weld spots for testing.

In varestraint testing, the spot-welded sample is bent over a radiused die block to a specific strain level at a particular bending rate. In this investigation, the cast program material had a thickness of 0.3 in. and was bent to a strain of 4 percent; the wrought program material had a thickness of 0.4 in. and was bent to a strain of 3 percent. These strain values represent *saturated strain* in the program materials. Saturated strain is defined as the limiting strain above which the resulting crack length does not increase. The bending rate used was 10 in. per second (ips). The time between when the arc is extinguished and when the sample is bent is referred to as the *cooling time* (CT).

The length of the longest HAZ liquation crack is measured radially outward from the weld pool edge. This measurement is carried out on opposite sides of the weld pool, and the results are averaged. For no cooling time, this maximum crack tip distance yields a measurement of the crack-susceptible region (CSR). The CSR value for a material is a measure of its weldability; larger CSR values represent a material's lower resistance to HAZ liquation cracking.

Varestraint tests are conducted at various cooling times to determine the CT at which no HAZ cracking occurs. This value of CT is also a measure of the weldability of the material. Higher CT values allow more time for strain from the welding process to accumulate; as such, the HAZ is more susceptible to liquation cracking. The crack tip distance is plotted against the cooling time in figures 70a and 70b for the medium composition cast and wrought program material after 40 heat treatment cycles. The Universal Varestraint Testing machine at EWI employs the gas-tungsten arc welding (GTAW) process. A welding current of 90 amps was used for cast program material; 100 amps was used for the wrought material. A 0.1-second upslope, 30-second arc hold time, and 0.125-in. arc gap were common to the tests on all materials.

2.5.5 Circular Patch Testing Results.

Circular patch tests were performed on the as-received compressor rear frame material to evaluate the strain-age cracking susceptibility of aged IN718. Four- by four-in. cast plates, that were removed from the as-received CF-50 compressor rear frame, were anchor welded to 1/2-in.-thick 304 stainless steel plates. An autogenous circular GTA weld was then produced at the center of each sample. The welding parameters for maximum heat input and controllable weld-bead shape were used. Three circular weld samples were prepared with diameters of 1.0, 1.5, and 2.0 in. PWHT was performed by GEAE using the heat treatment from figure 65. The test welds were thoroughly examined at 40x magnification using a binocular microscope; no cracking was observed in any sample. No further testing was performed to assess strain-age cracking susceptibility.

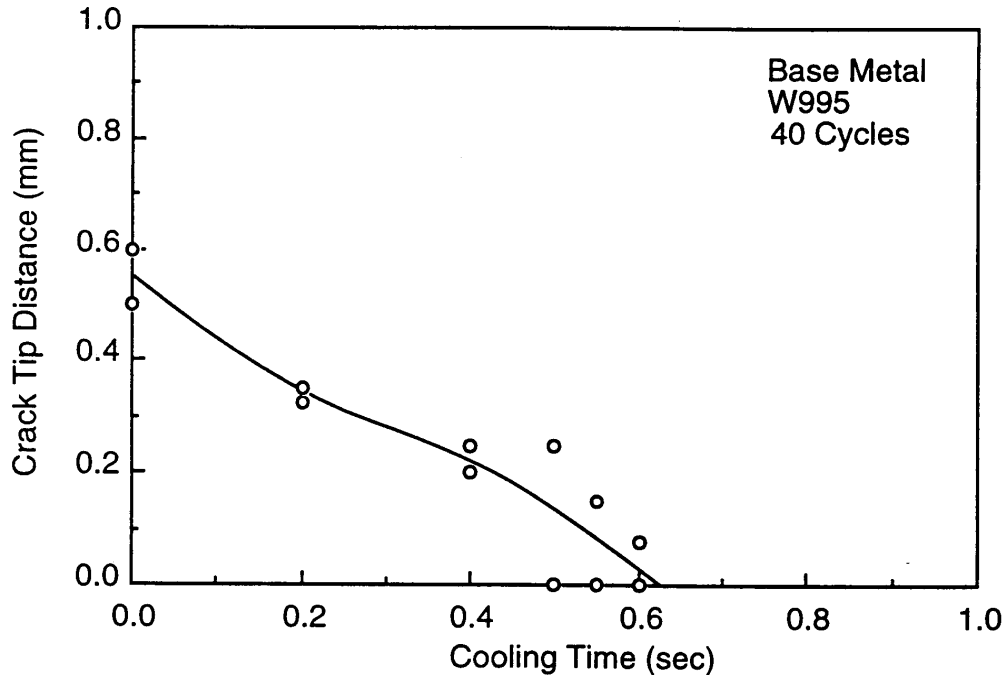

FIGURE 70a. SPOT VARESTRAINT DATA FOR MEDIUM COMPOSITION WROUGHT PROGRAM MATERIAL AFTER 40 HEAT TREATMENT CYCLES

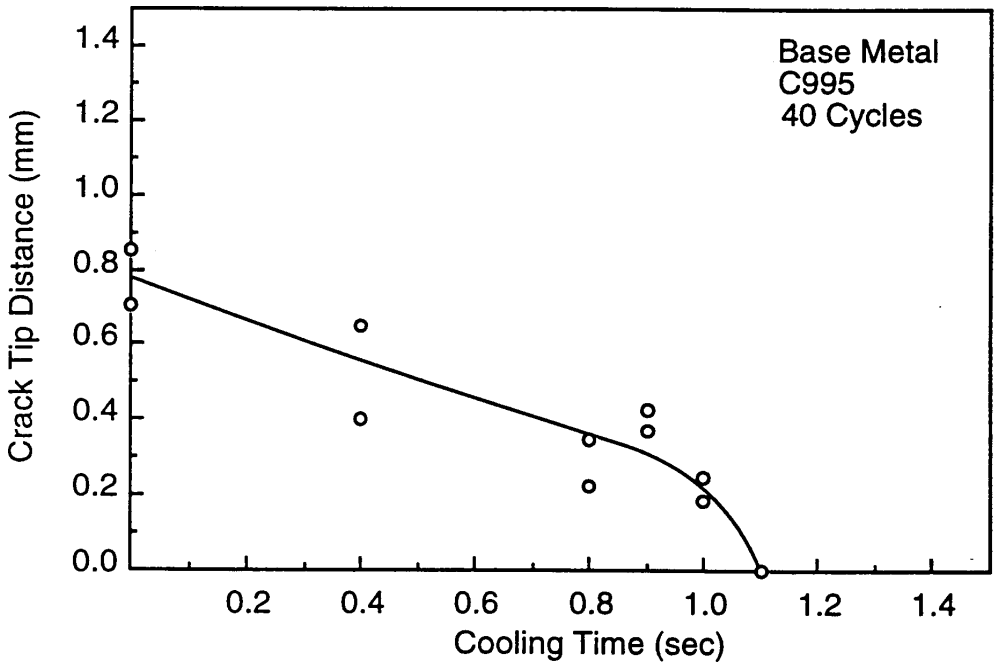

FIGURE 70b. SPOT VARESTRAINT DATA FOR MEDIUM COMPOSITION CAST PROGRAM MATERIAL AFTER 40 HEAT TREATMENT CYCLES

2.5.6 Hot-Ductility Testing Results.

Hot-ductility results for the CF6-6 material is given in table 6. The results for the program materials are listed in table 7. This information includes the NDT, NST, DRT, T_P, and (T_P-DRT).

TABLE 6. COMPRESSOR REAR FRAME HOT-DUCTILITY DATA

Condition	NDT (°C)	NST (°C)	DRT (°C)	T_P (°C)	T_P-DRT (°C)
Reference	1150	1283	1090	1260	170
Low (Nb, B) Version of Reference	1200	1311	1150	1260	110
BM	1145	1301	1070	1260	190
BM1700	1130	1294	1080	1260	180
BM1900	1160	1294	1080	1260	180
WM	1120	1294	1070	1260	190
WM1700	1120	1296	1070	1260	190
WM1900	1140	1271	1090	1260	170

The reference material in table 6 was earlier detailed to be the wrought, high (Nb, B) program material. The results for the low (Nb, B) version of the reference material are included for comparison.

The magnitude of the on-cooling liquation-cracking temperature range is given by the parameter T_P-DRT. Higher values of this parameter denote poorer weldability. The results in table 6 show that the weld and base metal removed from the retired CRF exhibited the poorest weldability based on T_P-DRT. The use of a PWHT with a high solution temperature (1038°C) was seen to slightly improve weldability in both the weld and base metals. PWHT performed with the lower solution treatment temperature did not affect the weldability behavior of the weld metal.

For the wrought program materials, hot-ductility testing results indicate only minor variations as a function of both composition and number of heat treatment cycles. There appears to be a slight decrease in weldability, as indicated by the parameter (T_P-DRT), with increasing niobium and boron content. In general, the wrought program material with the lowest niobium and boron content exhibited the best weldability, particularly in the as-received condition.

Compared to the wrought materials, the cast materials show a more pronounced effect of chemical composition. For the as-received cast program material, the highest NDT, 1160°C, was noted for the low (Nb, B) content and decreased as (Nb, B) content was increased: 1120°C for the medium content and 1105°C for the high content. For a given (Nb, B) content group, the as-received material had the highest NDT; heat treatment cycles tended to lower the NDT, although considerable scatter was noted in the data.

TABLE 7. HOT-DUCTILITY TEST RESULTS FOR PROGRAM HEATS

Material*	NDT (°C)	NST (°C)	DRT (°C)	T_P (°C)	T_P - DRT (°C)
Cast-Low-0	1160	1301	1080	1260	180
Cast-Low-20	1110	1309	1060	1260	200
Cast-Low-40	1120	1299	1070	1260	190
Cast-Medium-0	1120	1293	1080	1260	180
Cast-Medium-5	1110	1292	1080	1260	180
Cast-Medium-20	1120	1299	1020	1255	235
Cast-Medium-40	1105	1304	1050	1255	205
Cast-High-0	1105	1293	1015	1260	245
Cast-High-20	1095	1289	1070	1245	175
Cast-High-40	1085	1289	1040	1230	190
Wrought-Low-0	1200	1311	1150	1260	110
Wrought-Low-20	1160	1306	1120	1260	140
Wrought-Low-40	1160	1304	1140	1260	120
Wrought-Medium-0	1150	1299	1095	1260	165
Wrought-Medium-5	1150	1299	1090	1260	170
Wrought-Medium-20	1150	1294	1110	1260	150
Wrought-Medium-40	1140	1294	1120	1260	140
Wrought-High-0	1150	1283	1090	1260	170
Wrought-High-20	1145	1294	1090	1260	170
Wrought-High-40	1140	1289	1090	1260	170

* Information on composition and heat treatment given below:
Low, Medium, and High refer to Nb and B content in table 5.
Numbers 0, 5, 20, and 40 refer to the number of heat treatment cycles the material received.

For the cast program material with 20 and 40 heat treatment cycles, there is some decrease in the DRT but, more importantly, there is an increase in the number of samples cracking at peak temperature. In the case of the high (Nb, B) content cast material, the on-cooling tests could not be performed using a peak temperature of 1260°C for the 20 and 40 heat treatment cycle conditions. The specimens cracked at peak temperature, presumably because significant liquation occurred in these samples. In the case of the 20-cycle material, the peak temperature had to be lowered to 1245°C; for the 40-cycle material, the peak temperature had to be lowered even further to 1230°C. Obviously, the more heat treatment cycles the material experienced, the greater the amount of liquid formed at peak temperature.

The weldability of the materials as determined by the parameter (T_P-DRT) shows a difference between the weldability of the wrought and cast materials. The values for the wrought material range from 110-170°C and from 180-245°C for the cast materials. The upper limit of the cast material is for the as-received high (Nb, B) material; this value was, however, calculated based on the reduced T_P value. In examining the NST for both the cast and wrought program materials, the low (Nb, B) content materials tended toward the high end of the temperature range.

2.5.7 Varestraint Testing Results.

Table 8 lists the CSR and the cooling time CT data for the program heats. In addition, a series of autogenous GTA welds were produced on varestraint samples for the various program heats; spot varestraint tests were run over these welds to simulate welding over a previous weld repair.

TABLE 8. SPOT VARESTRAINT RESULTS FOR PROGRAM MATERIALS

Material*	CSR (mm)	CT (sec)	Material*	CSR (mm)	CT (sec)
Cast-Low-0	0.6	0.87	Wrought-Low-0	0.49	0.40
Cast-Low-5	0.75	1.05	Wrought -Low-5	0.59	0.54
Cast-Low-20	0.85	0.95	Wrought -Low-20	0.63	0.50
Cast-Low-40	0.84	0.99	Wrought -Low-40	0.49	0.49
Cast-Medium-0	0.70	1.10	Wrought -Medium-0	0.42	0.47
Cast-Medium-5	0.81	1.00	Wrought -Medium-5	0.64	0.60
Cast-Medium-20	1.08	1&05	Wrought -Medium-20	0.63	0.60
Cast-Medium-40	0.78	1.10	Wrought -Medium-40	0.55	0.62
Cast-High-0	0.98	1.10	Wrought -High-0	0.55	0.43
Cast-High-5	1.16	1.20	Wrought -High-5	0.66	0.60
Cast-High-20	1.30	1.00	Wrought -High-20	0.63	0.55
Cast-High-40	1.00	0.97	Wrought -High-40	0.58	0.55
Cast-Low-5-Weld	0.81	0.75	Wrought -Low-5-Weld	0.81	0.54
Cast-Low-20-Weld	0.85	0.95	Wrought -Low-20-Weld	0.71	0.55
Cast-Low-40-Weld	0.65	0.67	Wrought -Low-40-Weld	0.50	0.50
Cast-Medium-5-Weld	0.91	0.84	Wrought -Medium-5-Weld	0.84	0.63
Cast-Medium-20-Weld	0.91	0.95	Wrought -Medium-20-Weld	0.83	0.65
Cast-Medium-40-Weld	0.75	0.82	Wrought -Medium-40-Weld	0.50	0.63
Cast-High-5-Weld	0.98	0.85	Wrought -High-5-Weld	0.79	0.60
Cast-High-20-Weld	1.08	1.00	Wrought -High-20-Weld	0.88	0.65
Cast-High-40-Weld	0.78	0.82	Wrought -High-40-Weld	0.65	0.60

* Information on composition and heat treatment given below:
Low, Medium, and High refer to Nb and B content in table 5.
Numbers 0, 5, 20, and 40 refer to the number of heat treatment cycles the material received.
Weld means that the test was conducted over an autogenous GTA weld.

Spot varestraint testing of the wrought material revealed that the low (Nb, B) content material exhibited better cracking resistance than the medium and high (NB, B) content materials. This was true for both cast and wrought materials. No significant difference in liquation cracking behavior was noted between the medium and high (Nb, B) content materials. The spot varestraint tests conducted on top of the autogeneous welds exhibited similar cracking resistance to the base metal. The 5-cycle heat-treated material exhibited a decrease in cracking resistance as compared to the as-received material. No significant difference in cracking resistance was noted among the 5-, 20-, and 40-cycle heat-treated materials.

Spot varestraint test results indicated that the cast material has less resistance to cracking than the wrought material. The as-received cast material exhibited lower CSR values than the heat-treated material. The CT values for the low (Nb, B) content material were generally lower than for the medium and high materials. Weld metal exhibited better cracking resistance than the base metal.

2.6 SUBTASK III: EVALUATE PREWELD HEAT TREATMENTS TO IMPROVE WELDABILITY.

Field experience in the repair of compressor rear frames indicates a decrease in weldability with increasing numbers of repair events. Similarly, testing of the cast program material shows a tendency toward a decreased weldability after multiple thermal cycle exposures. Laboratory testing also showed that increased niobium and boron contents appear to negatively impact weldability. Microstructural observations noted an increase in the amount of delta phase with both an increasing number of heat treatment cycles and with increasing levels of niobium and boron. As such, it was hypothesized that a heat treatment cycle that dissolved the delta phase could improve weldability.

2.6.1 Determination of Rejuvenation Heat Treatment Temperature.

Cast and wrought program materials received 30-minute heat treatments in order to determine the effect of temperature on hardness, grain size, and microstructure. Heat treatments at several temperatures between 1750 and 2100°F (954 and 1149°C) were conducted in a tube furnace with an argon atmosphere. Results of these heat treatments are shown in figures 71a and 71b. The decrease in hardness above 1825°F (996°C) is pronounced in the wrought material and coincides with the solution of delta phase. A hardness decrease is also noted in the cast material. The grain boundaries in the cast material are pinned by the presence of delta phase, which does not fully dissolve until 2000°F (1093°C). In the wrought material, grain growth begins with the dissolution of delta phase.

Based on observations from the program materials, similar heat treatments were also performed on samples taken from the forward and aft flanges of CF6-6 and CF6-50 CRFs. Heat treatment consisted of heating the samples in an argon-filled furnace tube at a rate of 25°F/minute up to 1000°F (538°C), holding at that temperature for 10 minutes, heating to the desired temperature at a rate of 25°F/minute (14°C/minute), holding at that temperature for 1 hour, and then air cooling. A range of heat treatment temperatures between 1750 and 1900°F (954 and 1038°C) were selected. Hardness and grain size measurements for these tests are depicted in figures 72a and 72b. Wrought material taken from CF6-6 and CF6-50 engines exhibited delta-phase dissolution and initial grain growth after a 1-hour exposure at 1850°F (1010°C).

The goals of the rejuvenation heat treatment were to dissolve delta phase and to limit any resultant grain growth in the wrought material to grain size of ASTM 5-6. The 1850°F rejuvenation temperature was seen to dissolve the delta phase and to result in minimal grain growth in the wrought CF6-6 and CF6-50 materials. The temperature chosen for the rejuvenation treatment was scaled back to 1825°F (996°C), however, to account for possible overshoot in the heat treatment furnace.

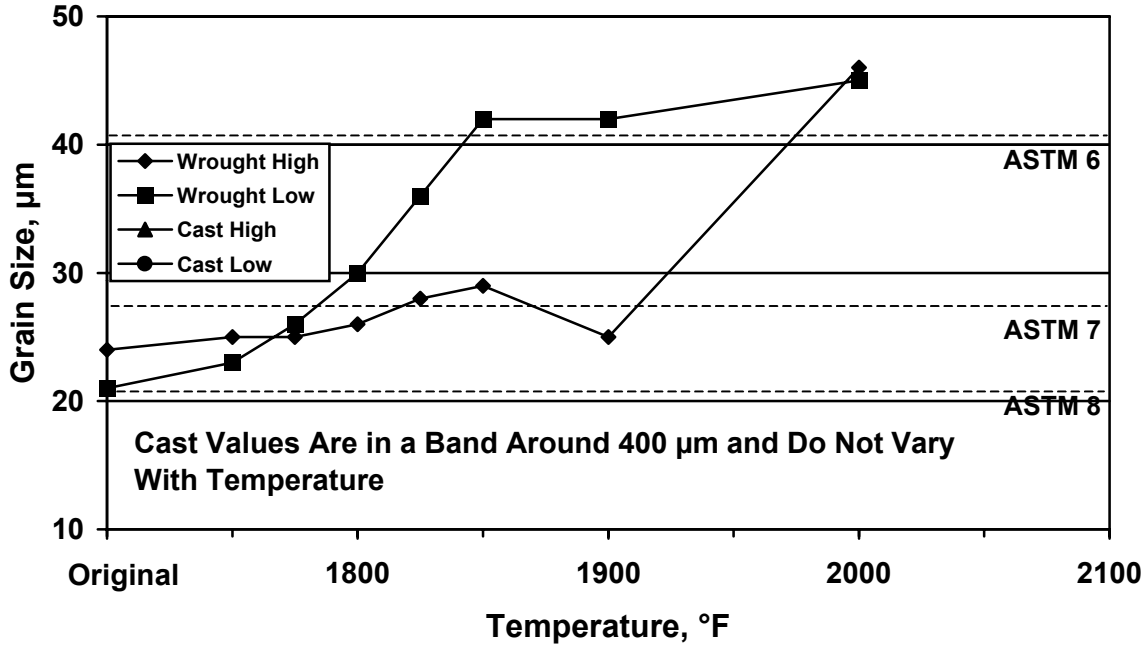

FIGURE 71a. PLOT OF GRAIN SIZE VERSUS 30-MINUTE HEAT TREATMENT TEMPERATURE FOR PROGRAM MATERIALS

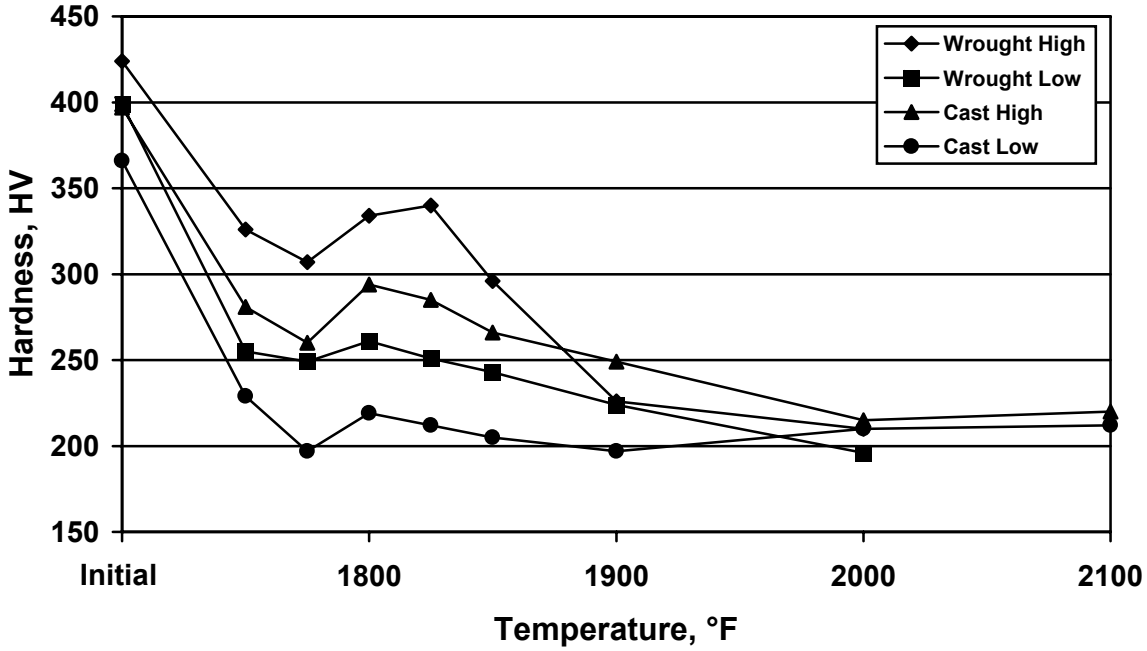

FIGURE 71b. PLOT OF HARDNESS VERSUS 30-MINUTE HEAT TREATMENT TEMPERATURE FOR PROGRAM MATERIALS

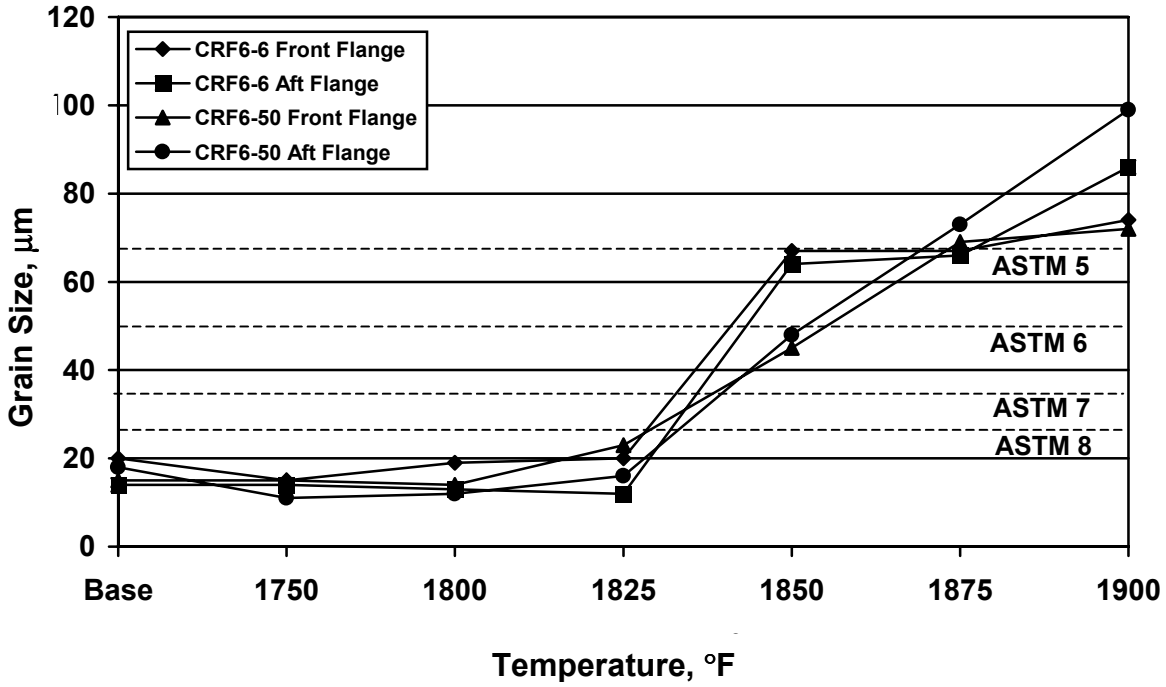

FIGURE 72a. PLOT OF GRAIN SIZE VERSUS 1-HOUR HEAT TREATMENT TEMPERATURE FOR WROUGHT COMPRESSOR REAR FRAME MATERIAL

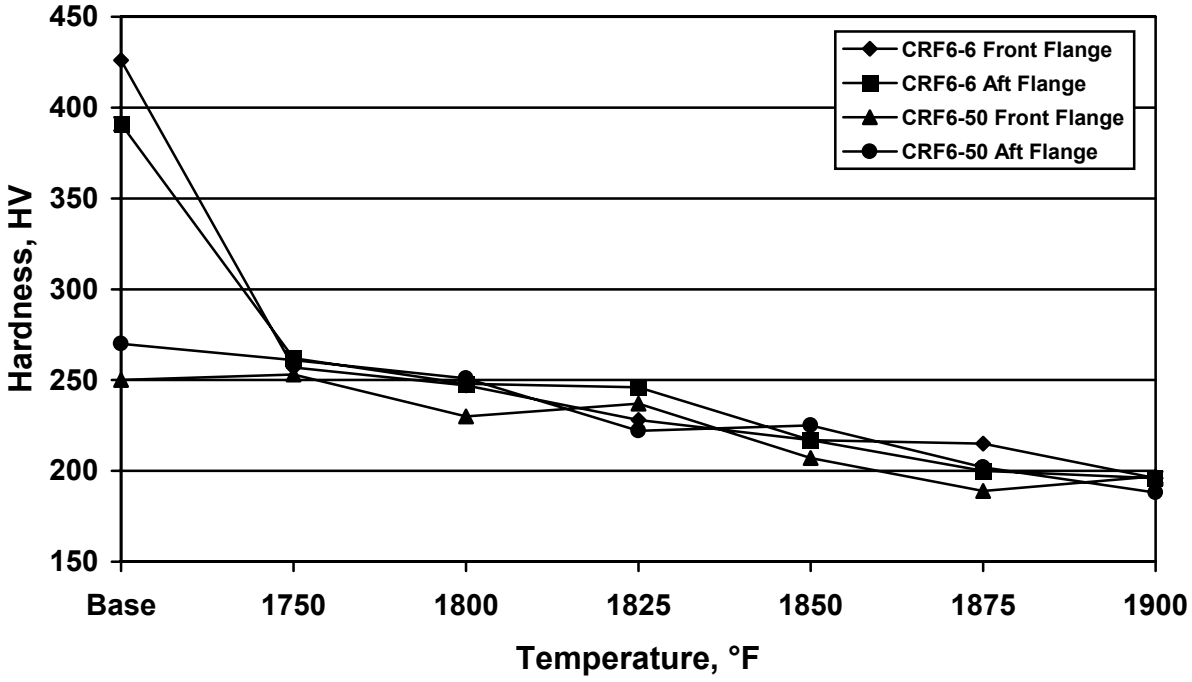

FIGURE 72b. PLOT OF HARDNESS VERSUS 1-HOUR HEAT TREATMENT TEMPERATURE FOR WROUGHT COMPRESSOR REAR FRAME MATERIAL

2.6.2 Rejuvenated Material.

The two materials chosen to receive the rejuvenation heat treatment represented the weldability extremes as determined by hot-ductility and varestraint testing. Cast material with the high niobium and boron content was ranked as having the worst weldability; wrought material with the low niobium and boron content was ranked as having the best weldability. A second, equally important criterion for the selection of the low (Nb, B) wrought material was that it had the greatest potential for grain growth as seen in the heat treatment tests.

These materials received 20- and 40-cycle heat treatments as in the previous program. The heat treatments were followed with a final rejuvenation heat treatment cycle at 1825°F for 1 hour. It should be noted that *these heat treatments were conducted in air, whereas the materials for the previous testing were heat treated in vacuum.* Figures 73a, 73b, 74a, and 74b compare the microstructures of the rejuvenated 40-cycle materials to the standard 40-cycle material. For both the cast and wrought material, the amount of delta phase was greatly reduced.

2.6.3 Varestraint Test Results.

Varestraint testing, similar to that of the initial program, was undertaken for the rejuvenated material. Welding and testing parameters were the same as in the previous testing. The test bars were bent at a rate of 10 ips to a total strain of 4 percent for the cast material and 3 percent for the wrought material.

The results for the high (Nb, B) cast material showed that the weldability response is degraded by the rejuvenation treatment. For the 40-cycle material, the CSR value increased to 1.24 from 0.97 for the nonrejuvenated material. The CT value increased from 1.0 to 1.1 seconds for the 20-cycle material.

For the low (Nb, B) wrought material, the 20 and 40 rejuvenated material response is not significantly different from the nonrejuvenated material. Neither improvement nor degradation of the weldability was noted based on the results of varestraint testing of the wrought material.

2.6.4 Hot-Ductility Test Results.

The hot-ductility test results of the rejuvenated material along with CSR and CT data are listed in table 9. These results exhibited differences when compared to the results of the nonrejuvenated material. In particular, the rejuvenated material exhibited a decrease in nil-strength temperature of ~30°C for the wrought material and ~60°C for the cast material. The nil-ductility temperature obtained from on-heating test results, however, were consistent with those of the nonrejuvenated material.

Because of the decreased nil-strength temperature of the rejuvenated material, the peak temperatures selected for the on-cooling tests had to be decreased in comparison to the nonrejuvenated material. The on-cooling response of the rejuvenated materials was erratic.

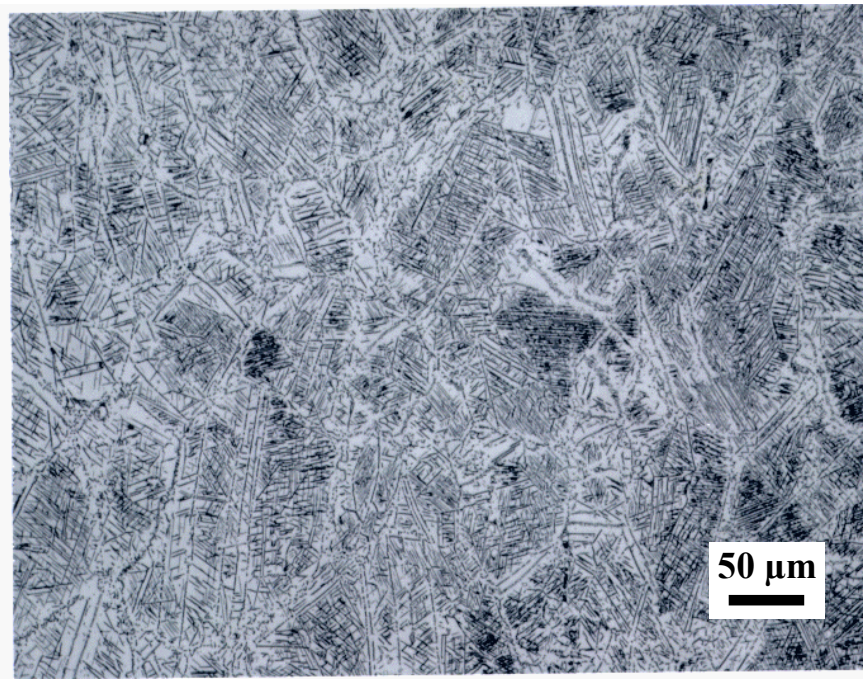

FIGURE 73a. MICROSTRUCTURE OF WROUGHT MATERIAL WITH LOW NIOBIUM AND BORON CONTENT AFTER 40 HEAT TREATMENT CYCLES

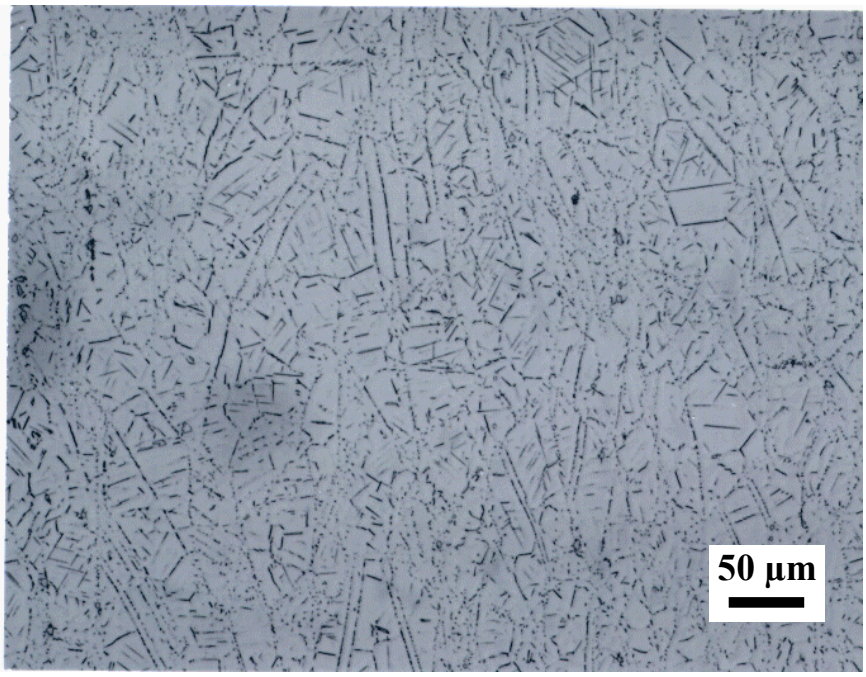

FIGURE 73b. MICROSTRUCTURE OF WROUGHT MATERIAL WITH LOW NIOBIUM AND BORON CONTENT AFTER 40 HEAT TREATMENT CYCLES AND REJUVENATION

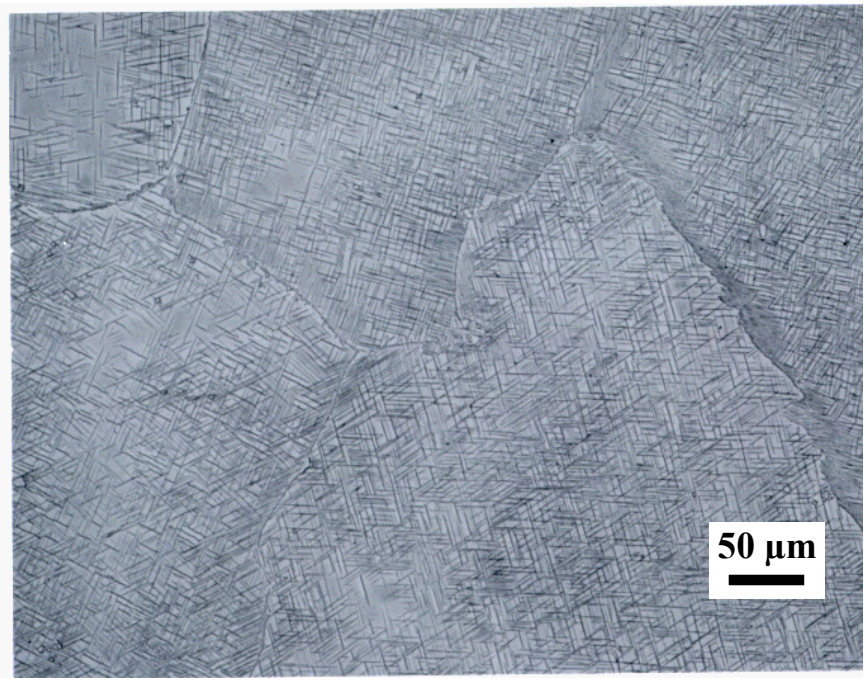

FIGURE 74a. MICROSTRUCTURE OF CAST MATERIAL WITH HIGH NIOBIUM AND BORON CONTENT AFTER 40 HEAT TREATMENT CYCLES

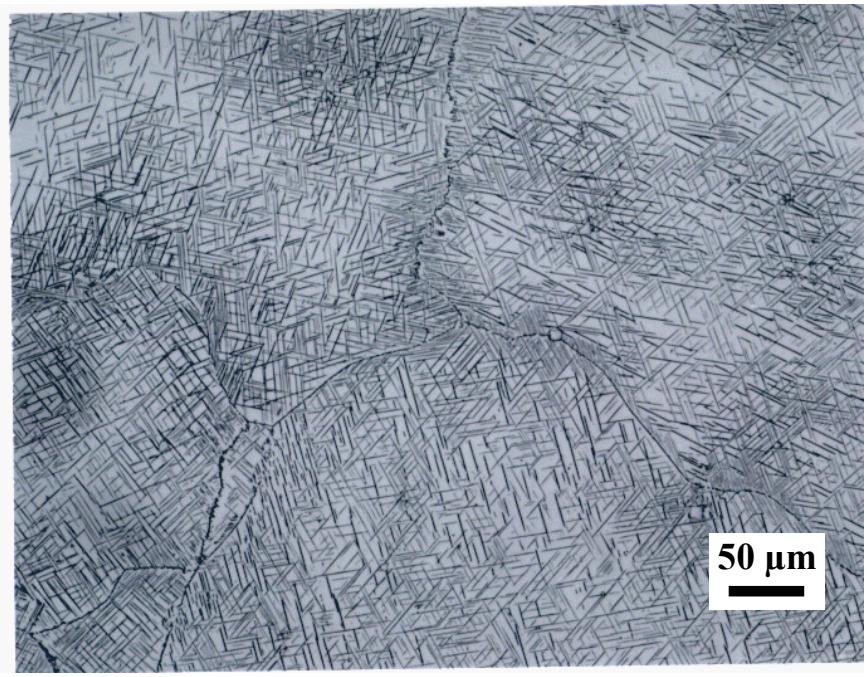

FIGURE 74b. MICROSTRUCTURE OF CAST MATERIAL WITH HIGH NIOBIUM AND BORON CONTENT AFTER 40 HEAT TREATMENT CYCLES AND REJUVENATION

TABLE 9. HOT-DUCTILITY AND SPOT VARESTRAINT RESULTS FOR REJUVENATED MATERIAL

Material	NDT (°C)	NST (°C)	DRT (°C)	T_P (°C)	T_P-DRT (°C)	CSR (mm)	CT (sec)
Cast-20	1100	1237	1055	1185	130	1.05	1.1
Cast-40	1095	1222	1060	1185	125	1.24	1.0
Wrought-20	1190	1281	1160	1240	80	0.55	0.45
Wrought-40	1170	1268	1150	1240	90	0.51	0.50

Figure 75 shows the hot-ductility data for the 40-cycle rejuvenated materials. Scatter in the on-cooling data, as seen in figure 75, made it difficult to determine the DRT. In figure 75, the on-cooling line is drawn as an average between the scattered data. The DRT listed in table 9 is based on this average line.

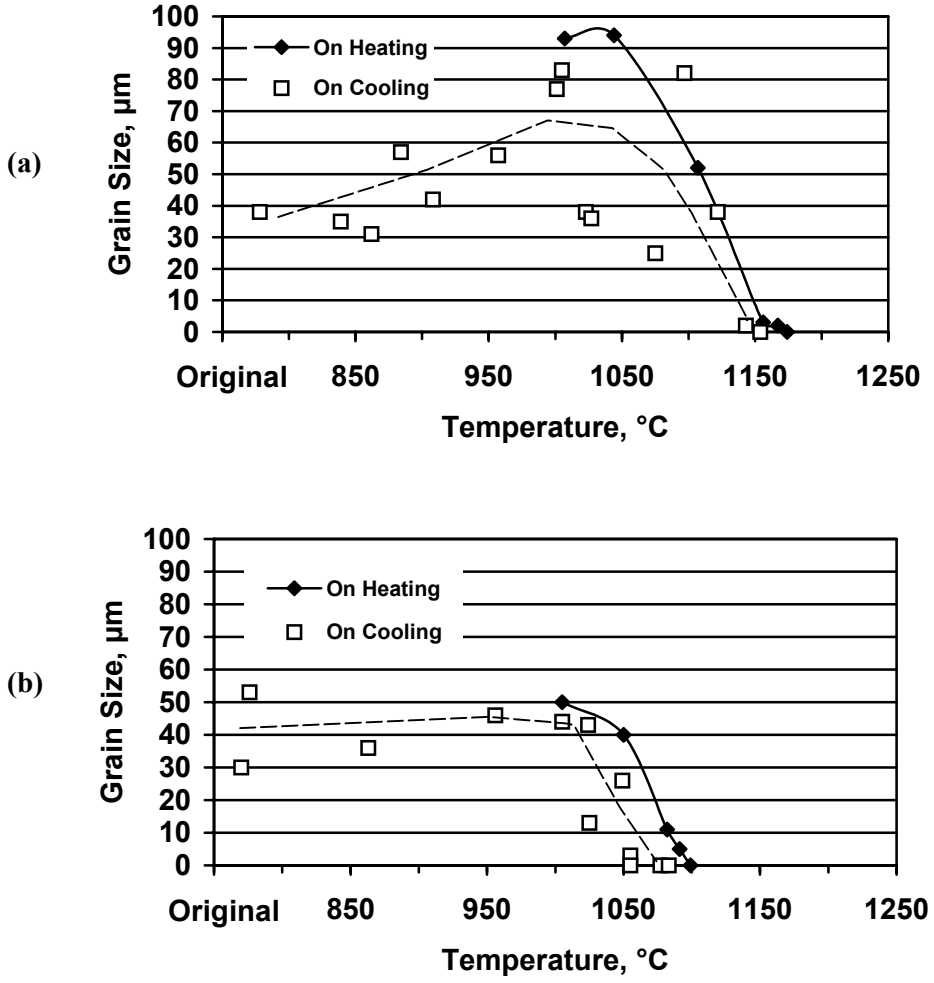

FIGURE 75. HOT-DUCTILITY DATA FOR (a) WROUGHT-LOW-40 REJUVENATED AND (b) CAST-HIGH-40 REJUVENATED PROGRAM MATERIALS

2.7 DISCUSSION OF WELDABILITY RESULTS.

Based on the preliminary metallurgical evaluations of retired CF6-6 and CF6-50 compressors rear frames and discussions with personnel at engine repair facilities, it appeared that a general degradation in repair weldability was associated with the accumulation of heat treatment cycles required by the repair of fatigue cracks in these components. From a metallurgical standpoint, the primary change in the microstructure of both cast and wrought forms of IN718 was the pronounced precipitation of delta phase and the progressive accumulation of this phase as a function of heat treatment cycles. Preliminary weldability testing (figure 62) suggested that liquation cracking susceptibility increased as a function of the number of heat treatment cycles in cast IN718 and supported observations made in the field. As a result, a test matrix was developed that focused on the susceptibility of IN718 to liquation cracking as a function of composition (Nb and B content), product form, and accumulation of delta phase by multiple heat treatments.

2.7.1 Microstructure Evolution.

Virgin-processed IN718, in both cast and wrought form, exhibits a fully austenitic microstructure with a small volume fraction of intermetallic constituents, such as carbides and Laves phase (in cast products only). The standard aging treatments for IN718 result in the submicroscopic precipitation of γ″ (gamma-double prime) or Ni_3Nb. At normal service temperatures (below 1200°F), this microstructure is stable.

When periodic repair welding is required, the weld metal and surrounding HAZ will be softened relative to the surrounding base metal due to the dissolution of γ″. This strength can only be recouped by aging the structure to re-precipitate the γ″. However, to prevent the base metal from being overaged (softened), the entire component is normally subjected to a solution heat treatment prior to aging. In addition, many repair facilities also perform a solution heat treatment prior to welding since this treatment is thought to reduce susceptibility to liquation cracking. Since most of the CRFs contain wrought material whose grain size must be carefully controlled, solution heat treatment temperatures are normally restricted to relatively low temperatures (1700-1750°F) to prevent excessive grain growth. Repeated solution heat treatment in this range is known to promote the formation of delta phase and can result in a high-volume fraction of this phase with accumulated time at temperature.

Since delta phase is essentially Ni_3Nb, increasing the Nb content of the alloy will increase both the rate of formation and the volume fraction. Because of this, the delta phase content of the program heats varied significantly as a function of niobium content (4-5-5.5 wt%) and number of heat treatment cycles (0, 5, 20, and 40).

Delta phase precipitation in the wrought program heats was relatively uniform in the microstructure and was present in high-volume fractions in the high-Nb heat subjected to 40 heat treatment cycles. The microstructure of the wrought program heats after multiple cycles was similar to that observed in actual components. One complicating factor in evaluation of the

wrought program heats was that the virgin-processed material actually contained a significant volume fraction of delta phase.

The microstructure of the cast program heats was relatively free of delta phase in the as-received condition. The multiple heat treatments resulted in delta phase precipitation initially along the cast grain boundaries due to the local Nb segregation in these regions. Delta phase in the low and medium (Nb, B) alloys was concentrated primarily along these boundaries, even after 40 cycles. This microstructure was representative of that observed in cast components removed from the retired CF6-6 and CF6-50 CRFs. The high-Nb program heat exhibited both an inter- and intragranular distribution of delta phase. The volume fraction of delta phase in this heat after both 20 and 40 cycles was considerably higher than that observed in the retired CRFs.

2.7.2 Weldability of Retired Compressor Rear Frame Material.

Table 6 presented the hot-ductility behavior of wrought IN718 base and weld metals from a retired CF6-6 which had a high niobium content (>5 wt%). The cracking susceptibility of these CRF materials, as measured by (T_p-DRT), is significantly higher (80°C) than the virgin-processed low (Nb, B) content heat but only slightly higher (20°C) than virgin-processed high (Nb,B) content heat. Correspondingly, the virgin-processed high (Nb,B) content material exhibited more extensive delta phase precipitation in the as-received condition and, therefore, had a microstructure more similar to the CRF material with multiple repair cycles.

Exposing the CRF material to a 1900°F solution heat treatment and age cycle affected no improvement on the wrought base metal and only a small improvement in the weld metal. In all cases, the relative differences in weldability measured by the value T_p-DRT were small and probably within the standard error of the hot-ductility test. In a broader context, this behavior would suggest a tendency toward liquation cracking susceptibility and a situation where relatively high levels of restraint would be required during welding to promote cracking. Such high restraint would not be present during repair welding of most wrought portions of the CRF and may explain the absence of cracking in the repair simulation that was conducted early in the project on one of the CF6-6 CRFs. Repair welds made in more highly restrained wrought components would potentially be susceptible to cracking. In the situation where cracking may be a problem, the data suggest that lower Nb content would be beneficial.

2.7.3 Weldability of Program Heats.

Both hot-ductility and spot-varestraint testing were used to evaluate the cracking susceptibility of the program heats. The hot-ductility testing was restricted to evaluation of wrought and cast microstructures subjected to as many as 40 heat treatment cycles. The spot-varestraint testing was expanded to include weld metal samples in these materials with similar heat treatment exposure. For convenience, the values of CSR from the spot-varestraint tests and T_p-DRT from the hot-ductility tests are collected in a single table, table 10. These weldability measures should be complimentary and provide a means to compare and contrast weldability behavior.

TABLE 10. CRACK-SUSCEPTIBLE REGION AND T_P-DRT DATA FOR PROGRAM HEATS

Alloy/Cycles	Wrought Alloys		Cast Alloys	
	T_p-DRT	CSR	T_p-DRT*	CSR
Low-0	110	0.49	180	0.60
Low-5	-	0.54	-	1.05
Low-20	140	0.50	200	0.95
Low-40	120	0.49	190	0.99
Medium-0	165	0.47	100	1.10
Medium-5	170	0.60	100	1.00
Medium-20	150	0.60	235	1.05
Medium-40	140	0.62	205	1.10
High-0	170	0.43	245	1.10
High-5	-	0.60	-	1.20
High-20	170	0.55	175	1.00
High-40	170	0.54	190	0.97

* Value based on lower peak temperature as reported in table 7.

The hot-ductility data in table 10 suggest that the wrought alloys were essentially unaffected by multiple thermal cycles. For example, the high (Nb, B) material showed no increase in susceptibility from 0 to 40 cycles as measured by T_p-DRT (170°C). A review of the full hot-ductility data in figure 65 reveals that the other parameters measured in the hot-ductility test show essentially no effect of multiple thermal cycles within each composition range. The CSR values for the weld metal are only slightly higher than those for the base metal as seen in table 8. The CT values, however, are not significantly different from their base metal counterparts. The wrought base material does show lower CSR and CT data for the as-received wrought material for each (Nb, B) level compared to the heat treated material. Overall, increasing the (Nb, B) content is seen to influence weldability in wrought IN718. This effect is best manifested when comparing the hot-ductility data (T_p-DRT) for the low and medium alloys, table 10.

The cast alloys exhibited a higher susceptibility to cracking relative to the wrought alloys for all compositions. This behavior was consistent for both test techniques and confirms actual field experience during repair welding. Using conventional analysis techniques, there appears to be little difference among the cast alloys as a function of composition or number of cycles. The medium and high (Nb, B) alloys did exhibit an unusual degradation in weldability, however. This is reflected in the peak temperature attainable for the on-cooling hot-ductility tests, as reported in table 6. Note that for the medium and high (Nb, B) heats the peak temperature achievable was lower than that for the low (Nb, B) alloys and for all the wrought alloys. Attempts to heat the samples to 1260°C resulted in gross melting of the sample and an inability to determine a DRT. As a result, the peak temperature was reduced until the DRT could be determined. This behavior reflects a degradation in weldability that is not readily reflected using

conventional assessment techniques. It is felt that this degradation is significant, reflecting the effect of both (Nb, B) content and multiple thermal cycles.

Evaluation of the spot-varestraint data for the cast alloys revealed an anomalous response in the medium and high (Nb, B) alloys after 40 heat treatments. For both alloys, there is an increase in CSR with increasing cycles up to 20 and then a decrease at 40 (table 8). A predicted increase in cracking susceptibility is representative of actual field experience and supports the preliminary work presented in figure 62. For example, the percentage increase in CSR for the medium and high (Nb, B) cast alloys after 5 and 20 cycles is 54 percent and 33 percent, respectively, as compared to the 24 percent increase after 30 cycles for the data at 4.4 percent strain reported in table 4. The rationale for the apparent reversal in this trend at 40 cycles in the cast program heats is not clear.

2.7.4 Effect of Rejuvenation Heat Treatments.

The results of weldability testing on rejuvenated cast (high Nb, B) and wrought (low Nb, B) are reported in table 11. Based on heat treatment studies, figures 71a, 71b, 72a, and 72b, the rejuvenation temperature (1825°F) was the crossover for dissolving some delta phase in wrought microstructures while maintaining the grain size. As expected, this heat treatment did not dissolve significant delta phase in the cast microstructure, figures 74a and 74b.

TABLE 11. SUMMARY COMPARISON OF REJUVENATION HEAT TREATMENTS

Material	NST	T_p	T_p-DRT (°C)	CSR (mm)
Cast/20	1289	1245	175	1.30
Cast/20/R	1237	1185	130	1.05
Cast/40	1289	1230	190	1.00
Cast/40/R	1222	1185	125	1.24
Wrought/20	1306	1260	140	0.50
Wrought/20/R	1281	1240	80	0.55
Wrought/40	1304	1260	120	0.49
Wrought/40/R	1268	1240	90	0.51

A comparison between cycled and rejuvenated weldability behavior is summarized in table 11. Unexpectedly, the NST for both cast and wrought rejuvenation treatments was lower than the cycled material. In addition, the peak temperature achievable for on-cooling hot-ductility tests dropped slightly (20°C) for the wrought alloy and dramatically (>60°C) for the cast alloys. This result suggests a reduction rather than an improvement in weldability due to rejuvenation. Unfortunately, because of the curtailment of the program, the root cause for this unexpected behavior could not be investigated further.

3. CONCLUSIONS.

3.1 CRACK GROWTH PREDICTIONS AND VERIFICATION.

a. No limitations were identified with ANSYS to predict K for simple 2D and 3D specimen geometries.

b. Calculated stress intensities for the center cracked panel using ANSYS under plane stress or plane strain matched the theoretical solution for a 2D problem to within 0.35 percent on K.

c. The ANSYS KCALC command calculates K assuming either plane stress or plane strain at the crack tip. Since a typical component with a crack is neither identically plane stress nor plane strain, stress state assumption can lead to inaccurate K predictions. Inaccurate K predictions are most pronounced when plane strain is assumed at the center of relatively thin plates.

d. The amount of plane strain near the crack tip can be quantified with a constraint factor. The constraint factor was taken to be a function of the through-thickness stress normalized by Poisson's ratio and the in-plane stress components for the node ahead of the crack tip. The constraint factor more realistically represents the stress state at the crack tip and can be used with the ANSYS results to calculate K independent of the specimen thickness and stress state.

e. The constraint factor approach predicts average K to within 2.2 percent for a center cracked panel for $0.001 \leq 2a/W \leq 0.5$ with a uniaxial applied load. Applied loads parallel to the crack length impacted calculated K, but this effect was small. Equal biaxial tension to tension/compression altered K by less than 3.5 percent compared to the K-solution for a 1D applied load. This prediction is consistent with multiaxial test data; applied loads parallel to the crack length have little to no affect on measured da/dN and therefore K.

f. The stress intensity for localized initial plasticity followed by elastic cycling was evaluated with an approach that combines a residual stress profile due to initial plasticity followed by subsequent linear elastic cycling. This approach relies on more traditional stress-intensity analysis that can be easily applied to component design without requiring an elastic-plastic/crack tip analysis. Preliminary results for a single 2D geometry identifies how the residual stress approach with ANSYS can accurately predict K_{max} under localized plasticity situations.

3.2 MATERIAL PROPERTY TESTING.

a. A slight crack growth rate acceleration occurred in Regions II and III when new material and weld HAZ areas were exposed to multiple repair thermal cycles. The CGR of high-time field casing material was similar to that of the exposed materials.

b. The crack growth rate of TIG welds was not affected by multiple repair thermal treatments.

c. The 1825°F preweld cycle for weldability rejuvenation did not degrade LCF properties or increase CGR of the wrought (low Nb/B heat) or cast (high Nb/B heat) IN718 materials.

d. Multiple thermal cycles (1700°F) reduced tensile and stress rupture strength but did not affect LCF for wrought IN718 or cast+HIP IN718 materials with various Nb/B chemistries within the specification.

3.3 WELDABILITY IMPROVEMENTS.

a. An increase in the cracking susceptibility after multiple heat treatments during repair events was confirmed by repair facility staff.

b. Examination of retired CF6-6 and CF6-50 components confirmed the presence of significant levels of delta phase in cast, wrought, and weld microstructures.

c. Six types of defects were identified:

- Fatigue cracks associated with stress concentration
- Fatigue cracks associated with weld or casting porosity
- Fatigue cracks associated with a liquation crack
- Liquation cracking in the weld metal
- Liquation cracking in the HAZ adjacent to the weld
- Casting defects (shrinkage pores).

d. Approximately 70 percent of the cracking was associated with either original fabrication welds or repair welds.

e. Weldability decreased as the (Nb, B) content increased for both the cast and wrought materials.

f. Hot-ductility testing revealed no significant effect of thermal cycles in the wrought material.

g. Hot-ductility testing revealed degradation in the medium and high (Nb, B) cast materials after 20 and 40 thermal cycles.

h. Significant levels of delta phase formed in the medium and high (Nb, B) compositions and in the low (Nb, B) composition after 40 thermal cycles.

i. Solution treatment above 1825ºF resulted in rapid dissolution of the delta phase and in an increase in grain size in the wrought materials.

j. A rejuvenation heat treatment of 1825ºF for 1 hour resulted in a significant decrease in delta phase in the wrought low (Nb, B) material but little change in the high (Nb, B) cast material.

k. Rejuvenation at 1825ºF appeared to decrease the weldability based on hot-ductility data.

4. RECOMMENDATIONS.

a. Sufficient work was not completed to be able to recommend whether or not a periodic inspection would be beneficial for the components studied.

b. Current service manual limits, approved repairs, and recommended field management programs need to be followed for combustion casings and compressor rear frames with integral combustion casings.

c. Time and flight cycles should be rigorously tracked on modern engine critical static parts including major pressurized casings and engine mounting components.

d. A change in the solution heat treatment temperature for Inconel 718 parts containing wrought material components with grain size limitations is not recommended. Data indicate that a change to 1825ºF (upper bound to avoid significant wrought material grain growth), in fact, reduces weldability.